Expanding the HP1a-binding consensus and molecular grammar for heterochromatin assembly

Serafin U. Colmenares[1,†], Shingo Tsukamoto[2,†], Collin Hickmann[1], Lucy D. Brennan[1], Mohammad Khavani[2], Mohammad R. K. Mofrad[2,3,*], Gary H. Karpen[1,4,*]

[1]Department of Molecular and Cell Biology, University of California, Berkeley

[2]Molecular Cell Biomechanics Laboratory, Departments of Bioengineering and Mechanical Engineering, University of California, Berkeley

[3]Molecular Biophysics and Integrative BioImaging Division, Lawrence Berkeley National Lab

[4]Department of BioEngineering and BioMedical Sciences, Lawrence Berkeley National Lab

[†]These authors contributed equally to this work.

* Correspondence: gkarpen@berkeley.edu

ABSTRACT

The recruitment of Heterochromatin Protein 1 (HP1) partners is essential for heterochromatin assembly and function, yet our knowledge regarding their organization in heterochromatin remains limited. Here we show that interactors engage the Drosophila HP1 (HP1a) dimer through a degenerate and expanded form of the previously identified PxVxL motif, which we now term HP1a Access Codes (HACs). These HACs reside in disordered regions, possess high conservation among Drosophila homologs, and contain alternating hydrophobic residues nested in a cluster of positively charged amino acids. These findings and molecular dynamics simulations identify key electrostatic interactions that modulate HP1a-binding strength and provide a dramatically improved HP1a-binding consensus motif that can reveal protein partners and the molecular grammar involved in heterochromatin assembly. We propose HP1a acts as a scaffold for other heterochromatin components containing HAC motifs, which in turn may regulate the function and higher order structure of the heterochromatin compartment.

35 **INTRODUCTION**

36

37 Heterochromatin forms an evolutionarily conserved nuclear compartment critical for genome
38 integrity. In humans and Drosophila, heterochromatin houses 25-30% of the genome,
39 respectively, that is primarily composed of repetitive DNA such as transposons and satellite
40 sequences (Hoskins *et al.*, 2007) enriched in gene-poor pericentric and telomeric regions of
41 chromosomes. Important for transposon suppression, chromosome segregation, and telomere
42 protection, heterochromatin displays physical, molecular, and functional attributes distinct
43 from gene-rich euchromatin (Janssen, Colmenares and Karpen, 2018). Constitutively dense
44 through interphase, the heterochromatin compartment is transcriptionally repressive, replicates
45 later in S phase in many organisms, and utilizes alternative DNA repair pathways (Chiolo *et*
46 *al.*, 2011; Janssen, Colmenares and Karpen, 2018).

47

48 Various factors converge in heterochromatin to perform its many functions. Transcriptional
49 repression, as assayed by the insertion of reporter genes or chromosome rearrangements, have
50 been attributed to many heterochromatin factors (HP1a, Su(var)3-9, HP2) (Eissenberg *et al.*,
51 1992; Schotta *et al.*, 2002; Shaffer *et al.*, 2002). Interestingly, hundreds of genes reside in
52 Drosophila heterochromatin, some of which are essential for viability (Weiler and Wakimoto,
53 1995; Dimitri *et al.*, 2003), suggesting the presence of an unknown alternative transcriptional
54 program specific for the heterochromatin landscape. Meanwhile, transcription of repetitive
55 DNA has been shown in many organisms to be instrumental in heterochromatin
56 establishment/maintenance and suppression of transposable elements by providing a non-
57 coding scaffold for small RNAs that recruit heterochromatin complexes (Piwi, Ago2)
58 (Brennecke *et al.*, 2007; Czech *et al.*, 2008). Heterochromatin also employs factors that inhibit

59 replication fork progression and suppress polytenization (Rif1, SuUR) (Makunin *et al.*, 2002;
60 Seller and O'Farrell, 2018), or direct double-strand breaks to the periphery for homologous
61 recombination repair (Smc5/6) (Chiolo *et al.*, 2011). Finally, the heterochromatin subnuclear
62 compartment houses components of sister chromatid cohesion (Dmt) (Yamada *et al.*, 2017)
63 necessary for the coordinated distribution of sister chromatids during mitosis and undergoes
64 dissolution and re-assembly every cell cycle. How such various factors involved in disparate
65 functions are recruited and organized within the same 3-D heterochromatin compartment
66 remains largely unknown.
67
68 Central to heterochromatin organization and function is Heterochromatin Protein 1, or HP1,
69 that specifically binds and propagates the heterochromatic histone mark di- and tri-methylated
70 H3 K9 by recruiting methyltransferases. HP1 also binds multiple proteins, many of which have
71 been shown to require HP1 for enrichment in heterochromatin. HP1 is comprised of two
72 globular structured domains: a chromodomain (CD) that binds methylated H3 K9 (Bannister
73 *et al.*, 2001; Lachner *et al.*, 2001) and a chromoshadow domain (CSD) important for
74 dimerization and protein partner binding (Brasher *et al.*, 2000). Other than short, disordered
75 regions at the flanks of the protein, HP1 also possesses a single unstructured hinge region
76 between the two globular domains that binds nucleic acid (Muchardt *et al.*, 2002). Previously,
77 we and others have shown that the Drosophila homolog HP1a co-purifies with dozens to
78 hundreds of proteins (Alekseyenko *et al.*, 2014; Swenson *et al.*, 2016), and that some partners
79 display a remarkable variation of enrichment patterns, or "subdomains," that indicate the
80 presence of a higher-order structure within heterochromatin (Swenson *et al.*, 2016). Whether
81 the large number of partners utilize individual mechanisms to target HP1a or a common motif
82 to access the heterochromatin domain is an important fundamental question for understanding

83 heterochromatin structure and organization.

84

85 A pentameric HP1-binding motif (PxVxL) was previously identified through a phage display
86 screen to bind the HP1 CSD dimer. Based on the peptide consensus sequence, this pentamer
87 contains alternating hydrophobic amino acids of proline, valine, and leucine that give rise to
88 its name (Smothers and Henikoff, 2000). Structural studies showed that PxVxL peptides bind
89 asymmetrically to a hydrophobic pocket formed by the HP1 CSD dimer, with the central valine
90 occupying the cleft formed by the two CSD C-termini (Thiru *et al.*, 2004). Other domains of
91 HP1, such as the CD and hinge regions, have also been implicated in binding other proteins
92 (Badugu *et al.*, 2005). However, most examples of HP1 partners identified across many species
93 from fission yeast to humans utilize the PxVxL motif, signifying its evolutionary importance
94 (Thiru *et al.*, 2004; Coustham *et al.*, 2006; Honda and Selker, 2008).

95

96 The recent discovery that heterochromatin domains display biophysical properties of
97 biocondensates *in vivo* (Strom *et al.*, 2017) has also prompted a re-evaluation of the PxVxL
98 motif as a potentially important contributor to emergent properties and functions. As
99 biocondensates form membraneless compartments through multivalency and the cumulative
100 weak interactions among components, we propose that HP1 acts as a scaffold that recruits
101 multiple heterochromatin components through the PxVxL motif. In addition, peptides
102 containing PxVxL motifs have been shown to enhance HP1 dimerization (Mendez *et al.*, 2011)
103 and promote or inhibit phase separation *in vitro* and *in silico* (Thiru *et al.*, 2004; Larson *et al.*,
104 2017; Her *et al.*, 2022). Thus, the PxVxL motif may represent not only a common HP1a
105 interaction interface but also a mechanism to modulate local or global HP1a dynamics and

106 condensate composition and biophysical properties.

107

108 Variants of the PxVxL motif, such as LxVxL, LxVxI, and CxVxL, have also been identified
109 (Bassett *et al.*, 2008; Mendez *et al.*, 2011; Mendez, Mandt and Elgin, 2013; Meyer-Nava *et al.*,
110 2020). Interestingly, a non-canonical motif (LxVxI) displayed a higher binding affinity to the
111 HP1a CSD dimer than canonical (PxVxL) and near-canonical (PxVxV) motifs (Mendez *et al.*,
112 2011). The canonical PxVxL motif is also not universally sufficient for binding, as evidenced
113 by mammalian STAM2a, which has a PxVxL motif but fails to bind the CSD (Lechner *et al.*,
114 2005). Furthermore, the HP1a C-terminal extension (CTE) and the flanking residues of the
115 PxVxL motif are implicated in HP1a-partner binding selectivity and interaction strength (Thiru
116 *et al.*, 2004; Mendez *et al.*, 2011; Mendez, Mandt and Elgin, 2013; Liu *et al.*, 2017). Deletion
117 of the last 3 residues on the CTE enhanced HP1a dimerization but severely reduced the binding
118 of PxVxL peptides, whereas chemical shift perturbations were detected at HP1a residues that
119 contact positions beyond the PxVxL pentamer core (Mendez *et al.*, 2011). Altogether, these
120 findings raise questions about the combination of hydrophobic residues sufficient for PxVxL
121 function, and whether additional molecular features exist beyond the pentapeptide motif.

122

123 Here we utilize a combination of evolutionary comparisons, *in vivo* imaging, and full atomistic
124 molecular dynamics (MD) simulations to comprehensively define the molecular signature of
125 the PxVxL motif in Drosophila and determine the specific interactions that regulate HP1a
126 binding. Our analyses show that PxVxL motifs of HP1a-binding partners are highly conserved
127 across Drosophila species, embed in mainly disordered domains of HP1a partner proteins, and
128 are driven by charged residues that we now propose to be a critical component of the molecular

129 grammar for heterochromatin targeting. As a result, we have expanded the number of known
130 functional HP1a-binding sites and provide an improved signature with higher predictive power,
131 which we refer to as the HP1a Access Code, or "HAC". We have also determined that HACs
132 exhibit a range of affinity for HP1a, which are modulated by electrostatic interactions. We
133 propose that HACs embedded in disordered domains are an important part of the molecular
134 language used to assemble the heterochromatin condensate, and that differences in HP1a
135 affinity among protein partners are critical for the composition, ultrastructure, and function of
136 heterochromatin.
137
138 **RESULTS**
139
140 ***Imaging peptide localization in cells identifies new HP1a-binding sequences***
141 Discovery of the foundational HP1a-binding pentamer sequence, PxVxL, showed that it
142 consists of alternating nonpolar residues with the central valine, designated as position 0,
143 binding the junction of two CSD domains in an HP1a dimer (**Figure 1A**). Correspondingly,
144 the proline (P) was designated as position -2 and leucine (L) as position +2, while positions -1
145 and +1 displayed higher variability, and were thus represented as 'x'. Together, the trio of
146 nonpolar residues occupy a hydrophobic pocket formed by the HP1a CSD dimer, as shown by
147 structural studies (Thiru *et al.*, 2004), and is thought to mediate the ability of HP1a to associate
148 with protein complexes.
149
150 HP1a binding sites have been mapped in many proteins, but of those only 6 in Drosophila have
151 been shown to contain functional PxVxL motifs, as demonstrated by disrupting HP1a

152 association through mutation of the central Val residue. These include the SNF2-like chromatin
153 remodeler XNP (Bassett *et al.*, 2008), histone H3 K36 demethylase KDM4A (Lin *et al.*, 2008),
154 zinc finger protein Odj (Kasinathan *et al.*, 2020), structural heterochromatin protein HP2
155 (Stephens *et al.*, 2005), sister chromatid cohesion regulator Dmt (Yamada *et al.*, 2017), and
156 transposon repressor Piwi (Brower-Toland *et al.*, 2007) (**Supplementary Figure 1A**). A
157 sequence alignment showed that while position 0 is consistently valine, the other positions vary
158 between 3 hydrophobic residues (proline, leucine, and cysteine at -2 and leucine, isoleucine,
159 valine at +2) (**Figure 1B**). Using the expanded consensus signature of HP1a-binding domains
160 at positions -2 and +2, we probed the Drosophila proteome, as well as proteins annotated to
161 localize to the nucleus or cytoplasm, for potential HP1a interactors (**Supplementary Figure**
162 **1B**). Not surprisingly, such a small motif identified over 50% of the proteome as HP1a
163 interactors, including more than 50% of proteins annotated as cytoplasmic, where HP1a is not
164 normally found. This led us to investigate whether the consensus sequence and our ability to
165 predict HP1a binding domains can be enhanced. We note, for example, that positively charged
166 residues frequently occupy the -1 and +1 positions along with flanking regions (**Figure 1B**),
167 suggesting that other positions on the HP1a-binding sequence contribute to their function and
168 could improve our understanding of the functional 'HP1a Access Code', hereafter referred to
169 as "HAC."
170
171 In order to discover additional HAC features, we needed to expand the number of sequences
172 that exhibit HP1a association and differentiate them from those that lack such function. We
173 assessed diverse HAC candidate sequences, surveying known HP1a-interacting proteins for a
174 more degenerate pentamer sequence consisting of any hydrophobic amino acid at positions -2
175 and +2, and a central valine or isoleucine. The inclusion of isoleucine is based on sequence

176 alignment of Dmt homologs, some of which were found to contain this residue instead of valine
177 (**Supplementary Figure 2B**). We also focused our search on HP1a interactors that have been
178 partially mapped for HP1a-interacting regions (Pindyurin *et al.*, 2008; Schwendemann *et al.*,
179 2008). Twenty putative HACs were identified in 11 proteins (**Figure 1C**), including HP2 and
180 Odj that were already known to have at least one functional HAC. To test for HAC
181 functionality, we employed an *in vivo*, imaging-based approach to screen 25-amino acid
182 peptides from the HAC candidates for enrichment within the heterochromatin subnuclear
183 compartment, as marked by fluorescently tagged HP1a. Similarly-sized peptides were
184 previously shown to bind HP1a *in vitro* (Mendez *et al.*, 2011), and the relatively short
185 sequences minimize the possibility of including additional domains that may confound results.
186 Thus, this assay indirectly tests HP1a binding through the ability of HAC-containing peptides
187 to localize to the HP1a-rich heterochromatin, but also exposes candidate sequences to
188 physiological conditions not possible with *in vitro* binding assays.
189
190 For our experiment, we tested peptides containing our known and candidate HACs, comprised
191 of the hydrophobic pentameric core containing a PxVxL-like consensus plus 10-amino acid
192 sequences on each flank, by fusing them to a fluorescent tag (mNeonGreen) and a myc nuclear
193 localization signal. Co-transfection into Drosophila S2R+ cells with mScarlet-I-tagged HP1a
194 showed co-enrichment of HP1a with known HACs, indicating that HAC peptides are sufficient
195 to bind HP1a *in vivo* (**Supplementary Figure 1C**). In contrast, expression of the fluorescent
196 tag and the NLS without any HAC peptide failed to concentrate at HP1a-rich nuclear regions.
197 We also mutated the central HAC residue of several peptides, resulting in loss of enrichment
198 in heterochromatin (**Supplementary Figure 1C**). Based on these results, we conclude that the
199 peptide-based imaging approach is sufficient to detect sequences capable of associating with

200 HP1a, as measured by fold-enrichment within the heterochromatin domain over the total
201 nuclear signal.
202
203 Next, we tested putative HACs from several heterochromatin-interacting proteins and
204 identified sequences from SuUR (Pindyurin *et al.*, 2008), Lhr (Brideau and Barbash, 2011),
205 HP4 (Schwendemann *et al.*, 2008), Mu2 (Dronamraju and Mason, 2011), ADD1 (Alekseyenko
206 *et al.*, 2014), Ciz1 (Alekseyenko *et al.*, 2014), HP2 (Stephens *et al.*, 2005), Odj (Kasinathan *et*
207 *al.*, 2020), Mod (Perrin *et al.*, 1998), MED26 (Marr *et al.*, 2014), and Su(var)3-9 (Schotta *et*
208 *al.*, 2002) that did or did not accumulate in heterochromatin (**Figure 1D**). Heterochromatin-
209 enriched peptides measured significantly higher levels of fluorescence intensity at regions of
210 high HP1a enrichment relative to expression of the fluorescent tag without a HAC sequence
211 (**Figure 1E**). This expands the number of known HACs from 6 to 16, while eliminating 10
212 sequences as putative HACs, or at the very least, HACs with HP1a affinities too low to detect
213 with this assay. Image analysis also revealed varying levels of HAC co-enrichment with
214 heterochromatin, with XNP displaying the highest co-enrichment with HP1a, and Piwi
215 exhibiting the lowest. Mutation of the central residue of 4 of these peptides severely impaired
216 heterochromatin localization, confirming that these comprise functional HAC sequences
217 (**Supplementary Figure 1D**). We conclude that the *in vivo* peptide imaging approach can
218 successfully differentiate varying levels of HP1a affinity among HACs, and that motifs
219 resembling a PxVxL are frequently found in many proteins but poorly predict heterochromatin
220 localization.
221
222 Finally, we determined whether the results of our peptide imaging experiment can be
223 recapitulated with full-length proteins. Central residue mutations of HAC sequences in SuUR,

224 Lhr and Mu2 abrogated enrichment to the heterochromatin domain and resulted in lower
225 protein levels (**Supplementary Figure 1E-G**). This indicates that loss of binding with HP1a
226 destabilizes these proteins, as has been shown for other complex-forming proteins (Hsu, Yen
227 and Yeang, 2022). In contrast, corresponding mutations of non-functional sequences displayed
228 no effect on heterochromatin co-localization or protein levels. Meanwhile, mutations in both
229 the HAC and the H3K9me3-binding chromodomain (Wang *et al.*, 2012) were necessary to
230 abolish heterochromatin co-localization of Su(var)3-9 (**Supplementary Figure 1H**),
231 highlighting how other domains also play roles in heterochromatin enrichment. Finally, HP4
232 required the simultaneous mutation of all 3 central HAC residues to fully abrogate the
233 localization of HP4 to heterochromatin (**Supplementary Figure 1I**), confirming their
234 redundant functions to target HP1a. We therefore conclude that new HACs identified by
235 peptide localization correspond to functional heterochromatin localization domains in full-
236 length proteins.

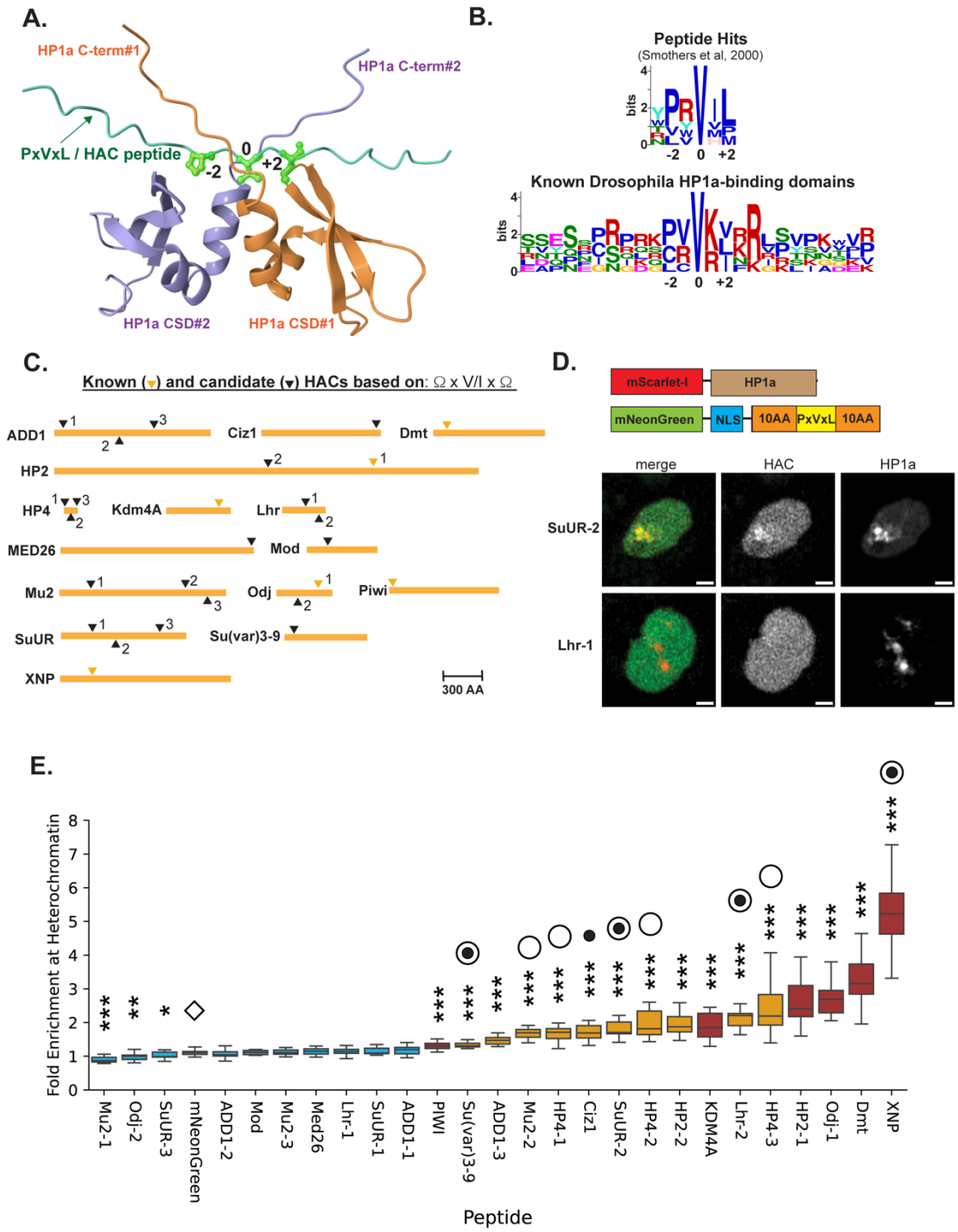

Figure 1 (A) Alphafold-generated model of a HP1a CSD dimer and a peptide containing the PxVxL motif. Sidechains of PxVxL positions -2, 0, and +2 are shown in green. (B) Motif analysis of original peptide sequences identified by phage display (Smothers et al, 2000, top) and the 6 sequences previously identified as HP1a-binding in *Drosophila melanogaster* (bottom). Core PxVxL residues -2, 0, and +2 are marked. (C) Schematic diagram of HP1a-binding proteins and their corresponding known (yellow triangles) or putative (black triangles)

HACs. Numbers indicate positions of putative HACs on full-length proteins from N- to C-terminus, except for known HACs, which are automatically numbered 1. (D) Schematic of expression constructs mScarlet-I-tagged HP1a and mNeonGreen-tagged HACs (top) and representative images of constructs after transient transfection into cultured S2R+ cells (bottom). Scale bars = 1 um. (E) Fold enrichment of known and candidate HACs in heterochromatin are calculated by the ratio of mean intensity in heterochromatin to the mean intensity of the non-nucleolar nucleus. IDs of candidate HACs that fail to enrich in heterochromatin are highlighted in blue; known HACs are marked in red, and candidate HACs that display enrichment in heterochromatin are in orange. Also shown is the heterochromatin enrichment of the mNeonGreen tag, marked with a diamond, which equals about 1 and thus is used as the baseline to test significant enrichment of putative HACs by Student's t-test. *** = p-value<0.001; ** = p-value<0.01; *=p-value<0.05. Determination of which candidate HACs are enriched in heterochromatin was also assessed manually as some candidates that did not visually display heterochromatin enrichment produced higher and lower enrichment values than the mNeonGreen control, likely due to some peptides accumulating at the nucleolus or being excluded from heterochromatin, respectively. HAC peptides tested for central residue mutation effects in this study are marked with dotted circles; HACs shown to be functional in the full-length protein are marked with empty circles.

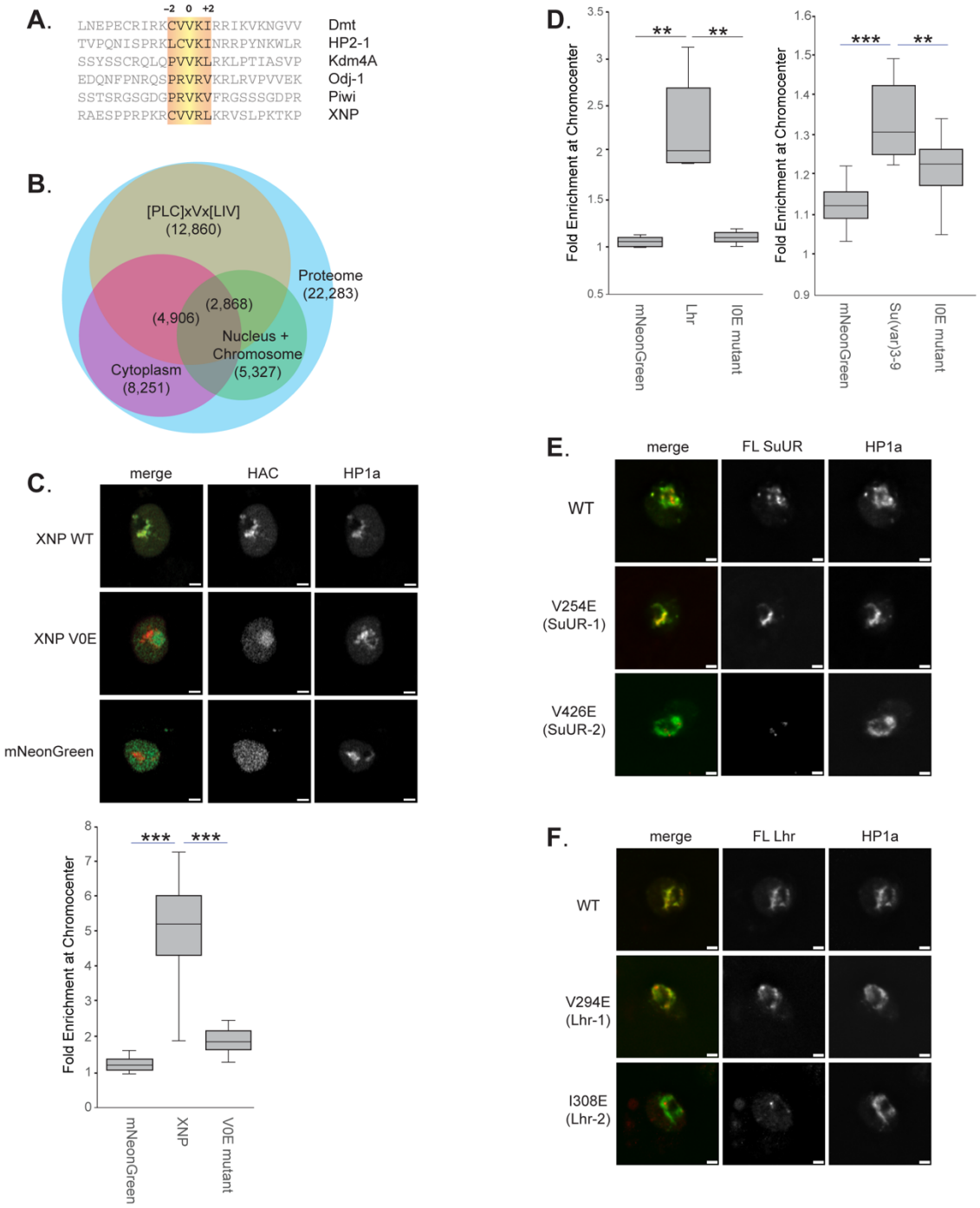
A.
-2 0 +2
LNEPECRIRKCVVKIRRIKVKNGVV Dmt
TVPQNISPRKLCVKINRRPYNKWLR HP2-1
SSYSSCRQLQPVVKLRKLPTIASVP Kdm4A
EDQNFPNRQSPRVRVKRLRVPVVEK Odj-1
SSTSRGSGDGPRVKVFRGSSSGDPR Piwi
RAESPPRPKRCVVRLKRVSLPKTKP XNP
B.
[PLC]xVx[LIV]
(12,860)
Proteome
(22,283)
(2,868)
(4,906)
Nucleus +
Chromosome
(5,327)
Cytoplasm
(8,251)
C.
merge
HAC
HP1a
XNP WT
XNP V0E
mNeonGreen
Fold Enrichment at Chromocenter
***
***
mNeonGreen
XNP
V0E mutant
D.
Fold Enrichment at Chromocenter
**
**
mNeonGreen
Lhr
I0E mutant
***
**
mNeonGreen
Su(var)3-9
I0E mutant
E.
merge
FL SuUR
HP1a
WT
V254E
(SuUR-1)
V426E
(SuUR-2)
F.
merge
FL Lhr
HP1a
WT
V294E
(Lhr-1)
I308E
(Lhr-2)

263

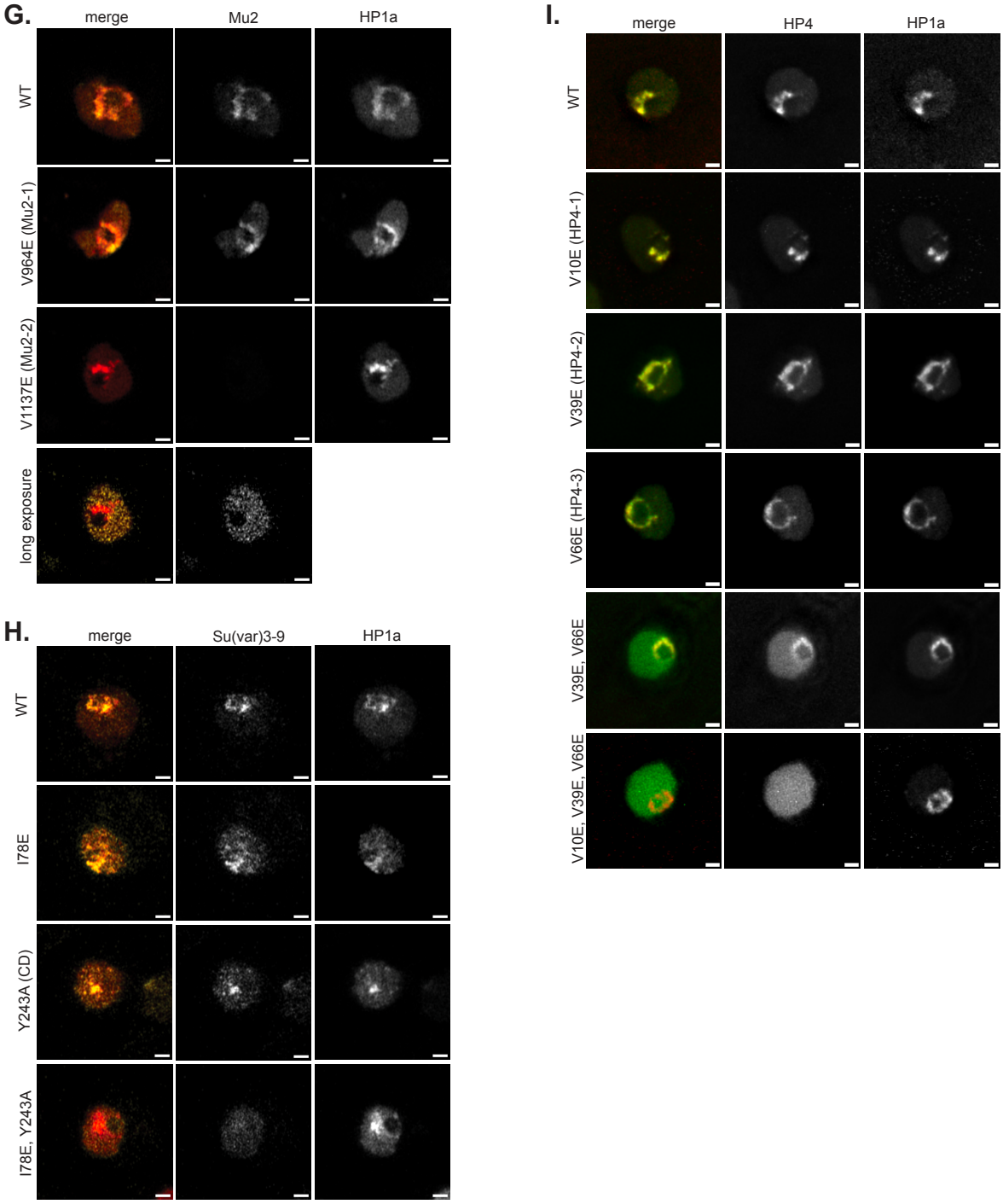

Supplementary Figure 1 (A) Sequence alignment of 6 known PxVxL domains (highlighted in yellow) from published research with positions -2, 0, and +2 marked. (B) Venn diagram of proteins containing degenerate PxVxL consensus and their association with GO-annotations of nucleus/chromosome or cytoplasm components. Number of proteins within each group is shown as well as those containing the motif and annotated to be nuclear/chromosomal or cytoplasmic. (C) Representative images of mNeonGreen-tagged wildtype and mutant XNP HAC peptide in relation to mScarlet-I- tagged HP1a in S2R+ cells (top). Mutant XNP HAC has its central residue mutated from Val to Glu (V0E). Quantitation of fold-enrichment in

273 HP1a-rich heterochromatin condensates by XNP HAC constructs and a control containing only
274 the fluorescent tag (bottom). *** = p-value<0.001; ** = p-value<0.01. (D) Validation of
275 putative Lhr and Su(var)3-9 HACs by mutation of central Ile to Glu (I0E). Representative
276 images of full-length SuUR (E), full-length Lhr (F), and full-length Mu2 (G) with and without
277 V0E mutations at putative HAC sites. A longer exposure for mutant Mu2 is included. (H)
278 Representative images of full-length Su(var)3-9 with or without HAC and chromodomain (CD)
279 mutations. (I) Representative images of full-length HP4 with or without individual or
280 combinatorial HAC mutations. Scale bars = 1 um.

281

282 ***Drosophila HACs are conserved yet embedded in disordered regions.***

283 In order to further define the sequence features that mediate HP1a binding and
284 heterochromatin-targeting, we investigated whether functional HACs are more evolutionarily-
285 conserved compared to non-functional peptides. Sequence alignment of HP1a CSD and C-
286 terminal tails for 12 Drosophila species across 40 million years of evolution show remarkable
287 conservation (91-100% identity in the CSD, 100% in the C-terminal tail) (**Supplementary**
288 **Figure 2A**). Sequence alignments of heterochromatin proteins harboring previously known
289 HACs and their homologs also show a high degree of conservation in terms of containing a
290 degenerate HAC pentamer sequence at the same position in the protein (**Figure 2A left,**
291 **Supplementary Figure 2B**). Kdm4A, Dmt, HP2, and Odj HACs are preserved across all 12
292 Drosophila species, though the Piwi HAC appears to be more recently evolved. Similar results
293 were obtained with our newly identified HACs, with 6 of 10 conserved across Drosophilids
294 (**Figure 2A middle, Supplementary Figure 2B**). In contrast, the non-functional candidate
295 sequences, as a group, were generally less conserved compared to functional ones (mean
296 conservation = 70% vs 87%) (**Figure 2A right, Supplementary Figure 2B**). However, the
297 non-functional candidate sequences with high conservation could be part of other domains.

298

299 The higher degree of conservation among functional HAC sequences suggests that they may
300 also share an ordered structure. However, disorder prediction analysis of the entire protein

sequence using PONDR (Romero *et al.*, 2001) showed that known HACs are either embedded within disordered domains, or in transition regions between ordered and disordered regions (**Figure 2B left**). Similarly, newly identified HACs showed a similar association with disordered regions (**Figure 2B middle**). In contrast, the group of non-functional sequences included both disordered and highly ordered structures (**Figure 2B right**). This indicates that functional HACs, despite their localization in disordered regions, which are often associated with higher mutation rates than globular domains, may be subjected to higher purifying selection for conservation. This also suggests that HACs inherently occur in the more solvent-accessible unstructured regions of proteins to facilitate binding to the HP1a CSD dimer. Overall, our results indicate that high evolutionary conservation and association with disordered domains are two shared features of HACs.

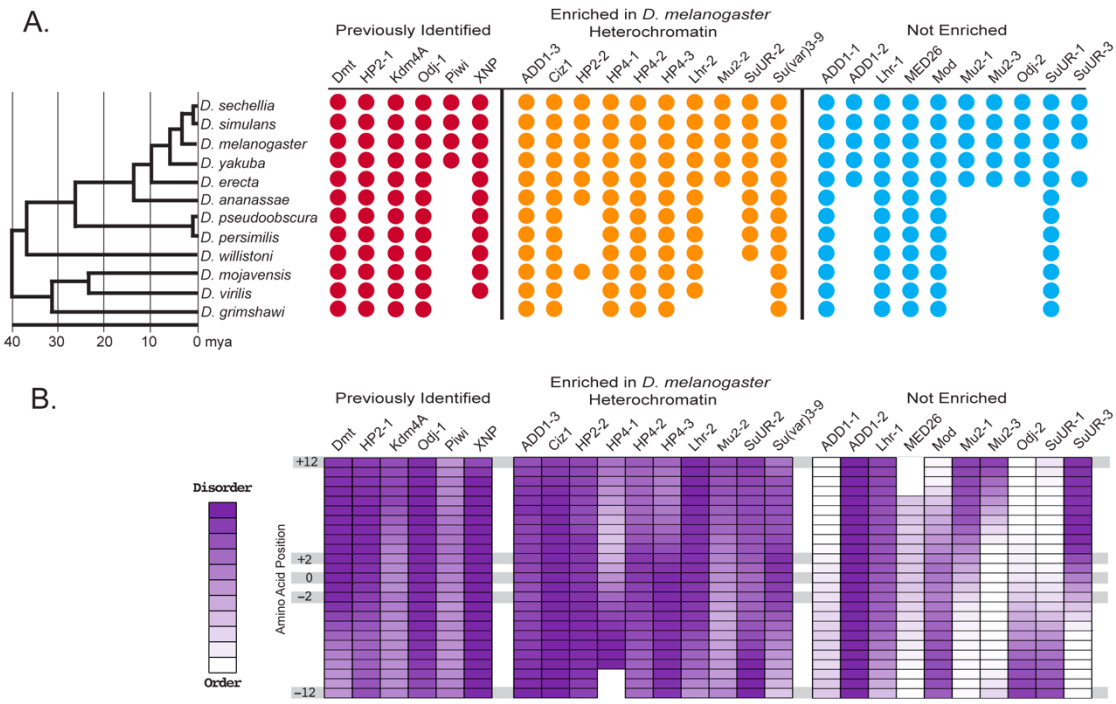

Figure 2 (A) Conservation of HAC sequences tested in this study among Drosophila species spanning up to 40 million years of evolution (tree indicated on the left). Positive identification was assessed by presence of [hydrophobic]x[V/I]x[hydrophobic] pattern after alignment to *D. melanogaster* sequences among previously known HACs (red circles), as well as positively

317 identified HACs (yellow circles) and sequences that did not display HP1a co-enrichment (blue
318 circles) from Figure 1E. (B) Heat map showing disorder prediction per residue of HAC
319 sequences in (A) as obtained from the PONDR-VLXT algorithm. Prediction scores indicate
320 presence of intrinsic disorder (purple) to globular structures (white). Core HAC residues at -
321 12, -2, 0, +2, and +12 positions are indicated.

A.

```
                                Chromoshadow                          Tail
D. sechellia        GLEAEKILGASDNNGRLTFLIQFKGVDQAEMVPSSVANEKIPRMVIHFYEERLSWYSDNED
D. simulans         GLEAEKILGASDNNGRLTFLIQFKGVDQAEMVPSSVANEKIPRMVIHFYEERLSWYSDNED
D. melanogaster     GLEAEKILGASDNNGRLTFLIQFKGVDQAEMVPSSVANEKIPRMVIHFYEERLSWYSDNED
D. yakuba           GLEAEKILGASDNNGRLTFLIQFKGVDQAEMVPSSVANQKIPQMVIHFYEERLSWYSDNED
D. erecta           GLEAEKILGASDNNGRLTFLIQFKGVDQAEMVPSSVANQKIPQMVIHFYEERLSWYSDNED
D. ananassae        GLEAEKILGASDNNGRLTFLIQFKGVDQAEMVPSTVANVKIPQMVIHFYEERLSWYSDNED
D. pseudoobscura    GQEAEKILGASDNNGRLTFLIQFKGVDQAEMVPSSIANLKIPQMVIGFYEERLSWYSDNED
D. persimilis       GQEAEKILGASDNNGRLTFLIQFKGVDQAEMVPSSIANLKIPQMVIGFYEERLSWYSDNED
D. willistoni       GLEAEKILGASDNNGRLTFLIQFKGVDQAEMVLSTVANVKIPQMVIRFYEERLSWYSDNED
D. mojavensis       GLEAEKILGASDNNGRLTFLIQFKGVDQAEMVPSTVANVKIPQMVIRFYEERLSWYSDNED
D. virilis          GLEAEKILGASDNNGRLTFLIQFKGVDQAEMVPSTVANVKIPQMVIRFYEERLSWYSDNED
D. grimshawi        GLEAEKILGASDNNGRLTFLIQFKGVDQAEMVPSTVANLAIPQMVIRFYEERLSWYSDNED
                    * ****************************** *::**   **.*** **************
                    |                                                            |
                   146                                                          206
```

B.

```
HP2:
Drosophila_mojavensis          AAVRPLPPLVPIMPAKLVQKEKDLQLPPQPLPPKLRKLRVRLNRSVIPNWLKSLK-----...PQVKIPIVNSVPL-PVPLPVLEVKP
Drosophila_virilis             TITKAPAPS--IPSEKPMQKPKELQLPSQPLPQKTRKLRVRLNRNMIKNWVLGLQ-----...QLLKAPVVRSMPL-PVPLPVLEVKA
Drosophila_grimshawi           AATATETTKQQCVLPAKHPTTNKLHLEPQLRTPKLRKLHVRLNRNCFKNWLKAHQ-----...----KSVPLPVPLPSL---------
Drosophila_willistoni          RVEVDIPQQ----------------------QVQQNEMQLE--------------------...LVEEVRTIRRCRVRLNLPPQVPPTR
Drosophila_pseudoobscura       AVSSKSQPI---------------------TKPKLRKCLVKINRGVIKKWMEA-------...PVAPVDKSDSVSVSVLAQP------
Drosophila_persimilis          PVSSKSQPI---------------------TKPKLRKCLVKINRGVVKKWMEA-------...PVAPVDKSDSVSVSVLAQP------
Drosophila_ananassae           IATQPAKPV-----------------------QKEKKLCVKINRRAFNKWMEQQQGPQAT...---PAPVPAPQPTASAPDPKAPINP
Drosophila_melanogaster        RSTGNTVPQ----------------------NISPRKLCVKINRRPYNKWLRSTQ--ERN...----AKATLNTALCPSTEKHLPDEP
Drosophila_simulans            HSTGNTVPL----------------------IVNSRKLCVKINRRPYNKWLRSTQ--ERN...----AKTTLKTGICSLTEQHLPDDP
Drosophila_sechellia           HSTGNIVPQ----------------------IVNPRKLCVKINRRPYNKWLRSTQ--ERN...----AKTTLKTGICSLTEQHLPDDP
Drosophila_erecta              HSTGNTVLQ----------------------KAKLRKLCVKINRMPFHKWLRSTQ--E-N...PVLPAKTPLKTAIYPLTENQLPDES
Drosophila_yakuba              RTTGNIVPQ----------------------KAKLRKLCVKMNRRPFNKWLRSTQ--EKN...VSPPAKTALKTAIYPLTEKKLPDET

KDM4A:
Drosophila_pseudoobscura         TSTSSL-RLKQAVVKLRKLPQSAL-----------VS
Drosophila_persimilis            TSTSSL-RLKQAVVKLRKLPQSAM-----------VS
Drosophila_willistoni            SSSSSA-CLKKLVVKVRKLPPRDPEPAAVNSEASAIT
Drosophila_ananassae             SSYSSS-RQLQPVVKIRKLPQKPI-----------VP
Drosophila_yakuba                SSYNSC-RQLQPVVKLRKLPPTAS-----------VP
Drosophila_erecta                SSYNSC-RQLQPVVKLRKLPPTAS-----------VP
Drosophila_melanogaster          SSYSSC-RQLQPVVKLRKLPTIAS-----------VP
Drosophila_sechellia             SSYSSC-RQLQPVVKLRKLPTIAS-----------VP
Drosophila_simulans              SSYSSC-RQLQPVVKLRKLPTIAS-----------VP
Drosophila_grimshawi             SV-----NCKQPVVKLRKLPVATP--LTTQTANPQIE
Drosophila_virilis               SSRSSA-NLKQAVVKLRKLPTVVP---TAESAPVEAA
Drosophila_mojavensis            SSRSSCSNLKQAVVKLRKLPSTVT---------DAQP

XNP:
Drosophila_willistoni          -------------PIRKEKEQASSRENNRTYPTLKRCAVRLQRVKLPLT--------SEP
Drosophila_grimshawi           ------------------------------------AVGTLAAATTETATTEESATAATI
Drosophila_mojavensis          ----------------------------------RRCVVRLKRVKWLTAAPISRETASSA
Drosophila_virilis             --------------------------------LRRCVVRLKRLKLPTA-----SAAEAG
Drosophila_persimilis          RPRRDLTLSKEKHPTKPSATSVLAQQQQQQQHRLKTCLVRVKRIKASEPEPRPSIKEPEP
Drosophila_pseudoobscura       RPRRDSTLSKEKHPPKPSATSVLAQQQQQQQHRLKTCLVRVKRIKASEPEPRPSIKEAEP
Drosophila_ananassae           -------------TLSV-----------------KRCLVRLKRVSL--------------
Drosophila_melanogaster        -------------PPRP-----------------KRCVVRLKRVSL-------------P
Drosophila_simulans            -------------PPRP-----------------KRCVVRLKRVSL-------------A
Drosophila_sechellia           -------------PPRP-----------------KRCVVRLKRVSL-------------P
Drosophila_yakuba              -------------PPRP-----------------KRCVVRLKRVSL-------------T
Drosophila_erecta              -------------PLRP-----------------KRCVVRLKRVSL-------------P

Odj:
Drosophila_willistoni          ----PLTSNYPRVLIKRLPSPVKKI
Drosophila_grimshawi           ----TQSHLSPRVRIMRCRHPSEAL
Drosophila_mojavensis          ----SPRHGSPRVRLLRCRDPNNGR
Drosophila_virilis             ----SSSHLSPRVRLVRCRDPSTPR
Drosophila_persimilis          ----NPRSDYPRVVVKRYRMPVATT
Drosophila_pseudoobscura       ----NPRSDYPRVVVKRYRMPVATT
Drosophila_ananassae           ----KHNMQSPRVRLKRFHLPAKSE
Drosophila_yakuba              EAQKLPNSQSPRVRVKRLRVQEVEK
Drosophila_erecta              EAQQLPNSQSPRVRVKRLRVEEIEK
Drosophila_melanogaster        EDQNFPNRQSPRVRVKRLRVPVVEK
Drosophila_simulans            ETQNLSNSQSPRVRVKRLRVPVVEK
Drosophila_sechellia           ETQNLSNSQSPRVRVKRLRVPVVEK

PIWI:
Drosophila_grimshawi            --DVHQRSGQEPQSKIFRNQSDRHTPGDR----------DRSDVSSSRR-ASTS-----HG
Drosophila_mojavensis           --DISPESVQQPRPKIFRGDGFKSDDRDRSEASSSRGTSRSHAPSTSHAASTSYAATTLHA
Drosophila_virilis              --DRSPRSVQEPRAKVFRDNGPHNR--------------DRSEASRS------Y-----RG
Drosophila_willistoni           S-DEGRKRAEEPSAKFYKCHSDGSDPSRIPPKASSDAQPSSSSSSRGRSFVPNE-----PR
Drosophila_melanogaster         S-STSRGSGDGPRVKVFRG------------------------SSSG------D-----PR
Drosophila_simulans             S-STSRGSGDGPRVKVFRA------------------------SSSG------D-----PR
Drosophila_sechellia            S-STSRGSGDGPRVKVFRA------------------------SSSG------D-----PR
Drosophila_yakuba               P-SNSRGSDDGPRVKVFRG------------------------SSSD------G-----LR
Drosophila_erecta               P-SNSGGSCDGPREKIFRA------------------------SSSD------G-----SR
Drosophila_ananassae            P-STSHEGREEPRAKIFKGPSDPRRE-----------------GSRG------D-----PR
Drosophila_persimilis           PGSSTDEKRDEPRAKVFKGQSEA--------------------STSG--------------
Drosophila_pseudoobscura        PGSSTDEKRDEPRAKVFKGQSEA--------------------STSG--------------

Dmt:
Drosophila_grimshawi           NSQSRYRIRKFVVRIKRIK----------QQETIV
Drosophila_virilis             INQVNC-VRKCYVRLKRLK----------LPTNNA
Drosophila_mojavensis          KRNNLVRVRNCIVRIKRLKLNARDPTTYDVNKTLT
Drosophila_willistoni          VTNQMKSIKKCVVKIKRLK---------NLPKSHT
Drosophila_pseudoobscura       ANLPNATISPFRIRIKKLP----------VPK---
Drosophila_persimilis          ANLPNATISPFRIRIKKLP----------VPK---
Drosophila_ananassae           TPIP---LRKCVVKIRRLR----------VQENTP
Drosophila_melanogaster_Dmt    LNEPECRIRKCVVKIRRIK----------VKNGVV
Drosophila_sechellia           PNVPECRLRKCVVKIRRIK----------VKNSVA
Drosophila_simulans            PNVPECRIRKCVVKIRRIK----------VKNAVA
Drosophila_yakuba              LTEPECRIRKCVVKLKRCK----------VQEGGA
Drosophila_erecta              LTEPERRIRKCVVKIRRIK----------VQKGVG
```

HP4:

```
Drosophila_willistoni          -MSQRSVQNKMKKMVVRIPRHPYLNLHGDHLLQ-----ENRVRKCRVNLERLKMS---PKQ--LKPKHVKVCVCRLPEYFFTERSE
Drosophila_pseudoobscura       ----MTPP-KIKKVVIKIPRHPYFAVQVDQGNM----VEYQLRKCRVNLERLKPPTPFALQLKPKPKRCIVRVARLPD---VAR--
Drosophila_persimilis          ----MTPP-KIKKVVIKIPRHPYFAVQVDQGNM----VEYQLRKCRVNLERLKPPTPFVLQLKPKPKRCIVRVARLPD---VAR--
Drosophila_ananassae           ----MSPKAKKMKMVVKIPRHPYFTVQSDSMQEHMRAVEYQVRKCRVNLERIKSSNAFPLK--PKPKRCIVRVARLPD---VERSE
Drosophila_melanogaster        ----MSP--KTKKMIVKIPRHPYFNVQGERSVE--REVEYQVRKCRVNLERIKSSTPFPLK--PKPKRCIVRVARLPD---VERSE
Drosophila_simulans            ----MSP--KTKKMIVKIPRHPYFNVQGDRSVE--REVEYQVRKCRVNLERIKSSTPFPLK--PKPKRCIVRVARLPD---VERSE
Drosophila_sechellia           ----MSP--KTKKMIVKIPRHPYFNVQGDRSVE--REVEYQVRKCRVNLERIKSSTPFPLK--PKPKRCIVRVARLPD---VERSE
Drosophila_erecta              ----MSP--KTKKMVVKIPRHPYFNVQVERSVE--REVEYQVRKCRVNLERIKSSNPFPLK--PKPKICIVRVARLPD---VERSE
Drosophila_yakuba              ----MLP--KTKKMVVKIPRHPYFNVQGEGSVE--REVEYQVRKCRVNLERIKSSTPFPLK--PKPKRCIVRVARLPD---VERSE
Drosophila_mojavensis          MLTKMSPQNKLKKMIVKLPRHPLIMANSDFVYQ----ECMQIRKCRVNLERIKGQTPFPLK--SKPKRCCVRVARLPD---VERSE
Drosophila_grimshawi           ----MSHQNKIKKMIIKIPRHPFIIDQSNVNYQ----ENISLRKCRVNLERINGQQSFPLK--AKPKRCCVRVARLPN---VERNE
Drosophila_virilis             ----MSPQNKIKKMVIKIPRHPYIIAQGEFDYQ----ERVQIRKCRVNLERMKGQQPFPLK--PKPKRCCVRVARLPN---VERSE
```

Su(var)3-9:

```
Drosophila_grimshawi                VRFKNELERNITIKLERLSESKIQK
Drosophila_mojavensis               VRFKNELERNITIKLERLSEMKIQK
Drosophila_virilis                  VRFKNELERNITIKLERLSEKKIQK
Drosophila_willistoni               VRFKNELERNITIKLERLSEKKIQK
Drosophila_pseudoobscura            VRFKNELERNITIKLERLSEKKIKL
Drosophila_persimilis               VRFKNELERNITIKLERLSEKKIKL
Drosophila_ananassae                VRFKNELERNITIKLERLSEKKIQK
Drosophila_sechellia                VRFKNELERNITIKLERLSEKKIKK
Drosophila_simulans                 VRFKNELERNITIKLERLSEKKIKK
Drosophila_melanogaster             VRFKNELERNITIKLERLSEKKIKN
Drosophila_yakuba                   VRFKNELERNITIKLERLSEKKIEK
Drosophila_erecta                   VRFKNELERNITIKLERLSEKKLKK
```

ADD1:

```
Drosophila_willistoni               KTTNKPNPALLQLEKQRLEELKNSDPKLKMKVVVKLRRAEEDFEVARKWMAQH-HKKHTL
Drosophila_mojavensis               KTTHKPNPALLQLERQRMDEMKRNDSKLKMKPIVRLVRAEEQFEVARKWVEKYGQKKSKV
Drosophila_grimshawi                KMTNKPNPALLHLERQRIEETKRNDAKLKRKFVVKLRRAEKDFDVARKWVEENNKLNNLN
Drosophila_virilis                  KMTNKPNPALLHLERQRMEETKRNDAKLKMKVVVKLRRAEEDFEVARKWMDM--EHAKKL
Drosophila_pseudoobscura            KTTNKPNPALLQLERQRMEEIKHTDAKLKMKVRVVLRRAEEEFEVARKWAKNRDKQN---
Drosophila_persimilis               KTTNKPNPALLQLERQRMEEIKHTDAKLKMKVRVVLRRAEEEFEVARKWAKNRDKQN---
Drosophila_ananassae                KTTNKPNPALLQLERKRMEEMKKSDAKLKMKVVVKLRRAEDEFEVARLWAEENKKRQQDS
Drosophila_melanogaster             KTTNKPNPALLQLERQRMEDMKKSDAKLKMKVMVKLKRAEDEFEVARKWVEDM-KQGQEL
Drosophila_sechellia                KTTNKPNPALLQLERQRMEDMKKSDAKLKMKVMVKLKRAEDEFEVARKWVEDM-KQKQEL
Drosophila_simulans                 KTTNKPNPALLQLERQRMEDMKKSDAKLKMKVMVKLKRAEDEFEVARKWVEDM-KREQEL
Drosophila_yakuba                   KTTNKPNPALLQLERQRMEDMKKFDAKLKMKVMVKLRRAEDEFEVARKWVEECRKKEQEL
Drosophila_erecta                   KTTNKPNPALLQLERQRMEDMKKSDAKLKMKVMVKLKRAEDEFEVARKWVEECRKREQEL
```

Lhr:

```
Drosophila_ananassae           IKSAKYYIKPVRVRLKRLDLDDYIS
Drosophila_melanogaster        LKSAKYYIKRCRIRLKRVEIDDYLP
Drosophila_sechellia           LKSAKYYIKSCRIRVKRVEIDDYLP
Drosophila_simulans            LKSAKYYIKSCRIRLKRVEIDDYLP
Drosophila_yakuba              LKSAKYYIKSCRIRVKRVDFEDLLP
Drosophila_erecta              LKSAKYYIKSCRIRVKRVDFKDYVP
Drosophila_mojavensis          LDSVRLYVKKVRVRVKRLDLADYVR
Drosophila_pseudoobscura       IKSAKYYTKKLIVRVKRIDLDEYLP
Drosophila_persimilis          IKSAKYYTKKLIVRVKRIDLDEYLP
Drosophila_willistoni          IKSAKYYVKKVRVLMKRQNLDDFIP
Drosophila_virilis             LKSAKYYVKKVQVRLKRLDLADYMP
Drosophila_grimshawi           -------------------------
```

Ciz1:

```
Drosophila_melanogaster         KATKPGPASTKRNVLVSVKRTSAAAIKAATKS
Drosophila_simulans             KAAKPGPASTKRNVLVSVKRTSAAAIKAATKS
Drosophila_sechellia            KAAKPGPASTKRNVLVSVKRTSAAAIKAATKS
Drosophila_erecta               KAAKPGPASTKRNVLVSVKRTSAAAIKAATKS
Drosophila_yakuba               KAAKPGPASTKRNVLVSVKRTSAAAIKAATKS
Drosophila_persimilis           KVGKPGPASTKRNVLVNVKRTSAAAIKAATKS
Drosophila_pseudoobscura        KVGKPGPASTKRNVLVNVKRTSAAAIKAATKS
Drosophila_mojavensis           KANRPGPASKKRQVLVSLKRTSAAAIKAATNS
Drosophila_virilis              KANRPGPASTKRQVLVSLKRTSAATIKAATKS
Drosophila_ananassae            KAAKPGPASTKRNVVVSVKRTSNATIKAATKS
Drosophila_grimshawi            ATSRPGPASTKRQVLVNGKRTPAAIIKAATKT
Drosophila_willistoni           KGAKPGPASTKRNVVVNVKRT--VAIKTGNKS
```

323

```
SuUR:

Drosophila_grimshawi        PS-----------------SPSKIFA-RKLNVKINRLHLPKMQKNVLAAISSKIPTNQLTKPAPAPREQPTPLPVKSPVKAKPMPEPN
Drosophila_mojavensis       PNTST--------------ITRKVLNVRL---RRASIQID-----------------------PTNSAKASELPTKAVKASPKKSPNS
Drosophila_virilis          RPTPKIKGKKLNVRLSRVCLPQK----DLNIIAVTNSHKPKEQAATNSHKPKEQASKPGQEVSKKPPEEITPLEIKLLRAKPNNKVKL
Drosophila_willistoni       METVK--------------HPSP----VL---------------------------------A----TRNVNIRLRRT--------
Drosophila_pseudoobscura    DSSRQ--------------KTRS----TP---AAAAVSPT-----------------------EK----TRKVNVRLRRM--------
Drosophila_persimilis       DSSRQ--------------KTRS----TPAAAAAAAVSPT-----------------------EK----TRKVNVRLRRM--------
Drosophila_ananassae        EKVDN--------------NPKP----IT---PPKKVATP-----------------------KK----AMKLNIRLKR---------
Drosophila_melanogaster     ATDNM--------------PPRK----RT---RAATVHLT-----------------------PK----TRRLNVRILRV--------
Drosophila_sechellia        AMDNM--------------PPKK----RT---RAATVHLT-----------------------PK----TRRLNVRILRC--------
Drosophila_simulans         A---M--------------PPRK----RT---RAATVHLT-----------------------PK----TRRLNVRILRC--------
Drosophila_yakuba           ALT-I--------------SPRK----RT---RAATVHFT-----------------------PK----TRRLNVRILRV--------
Drosophila_erecta           GLT-M--------------PPRK----ST---RAATVHFT-----------------------PK----TRRLNVRILRV--------
                                                                 :  .

Mu2:

Drosophila_pseudoobscura    --------KIGNTPEEGVVEKIASKRVGRPRK...NANTSAVAKRRVGRPRKSQTPTEDK
Drosophila_persimilis       --------KIGNTPEEGVVEKIASKRVGRPRK...NANTSAVAKRRVGRPRKSQTPTEDK
Drosophila_grimshawi        -------------------------------...NASSKRAARVR--------------
Drosophila_mojavensis       -------------------------------...KAGSARAATRKSDSAKPTLKNVEDT
Drosophila_virilis          K------------------------------...PAPSLRSFRKSTSKTDLTEETKEDI
Drosophila_willistoni       R-----------------------------S...SEEKDVKGRKLKVNVKNITSQGNKQ
Drosophila_ananassae        TKKAKESSKAEQPKIQKRVTRLNSANESVESH...GSTKLGPRKGSALPGSNEEEPLDAK
Drosophila_melanogaster     V-------KTGGALIKRAVVRISRVSIEQLES...PSSSSAAAKEPNVSTATTR------
Drosophila_simulans         V-------KVTGALIKRAVVRISRVSIEQLEA...PSSSSAAAKGPNVSTATTRATRTTR
Drosophila_sechellia        V-------KAAGALIKRAVVRISRVSIEQLES...PSSSSAAAKGPNVSTAITRTTRTTR
Drosophila_yakuba           V-------KPADALIKRAVVRISRASIENPAS...PSSSTAAAKGPNVS-ATTRAPKTVR
Drosophila_erecta           V-------KPEGAIFKRAVVRISKISIENPES...PSSSSAAAKGPNVS-GTTRTARSAR

HP2:

Drosophila_mojavensis       STC---S------------ ...-------SNSSCRKLRILIK------- ...LEDPTYPSDQSVC---------HDVGDKA
Drosophila_virilis          SSSSSGSSRRKLRILLRKV ...ALEQISVDNPLDNRGDLVVNEDSVDQA ...PTGQV---------------------EVN
Drosophila_grimshawi        ------------------- ...--------------------------- ...--------------------------EKP
Drosophila_willistoni       ------------------- ...EGKISENSTIEKKRLR----------- ...KKGRQNDNESEI------LVQAESTQEIA
Drosophila_pseudoobscura    SEA---TELEGPPSTTPTL ...ESKQTSESNPSSEKSK---EPQPEKQP ...PSVPITPCTAPCRQLRVLMRRTPSSKSSV
Drosophila_persimilis       SEA---TELEGPPSTKPTL ...ESKQTSESNPSSEKSK---EPQPETQP ...PSVPITPCTAPCRQLRVLMRRTPSSKSSV
Drosophila_ananassae        ---------------TPQK ...--------TPSCRKLRILIKRTPNTKY ...ESPDVPPTATEMEEPPQTSLDIKPPDDTE
Drosophila_melanogaster     TKS---SDQTKNSFITPNR ...VQKELRTPTASCRKLRVLIKRTPTSSL ...SLGEVNPDSDPVAAES--VAVLHES-DRD
Drosophila_simulans         TKS---SDQT-NSFITPIR ...EQKELRTPTASCRKLRVLIKRTPTSNL ...SSDEINPDSDPVAAESLTVAILHDS-DRD
Drosophila_sechellia        TKS---SDQT-NSFITPNR ...EQNELRTPTASCRKVRVLIKRTPTSNL ...SSDEINPDSDPVAGESLPVAILHDS-DRD
Drosophila_erecta           TKS---SDQTKNTFITPNR ...LEKELGTPTASCRKLRVLIKRTPTSNL ...SSGEINPESDP---------------DKD
Drosophila_yakuba           TKS---SDQTKNTIITPKK ...IQKELSSPTASCRKLRVLIKRTPTSDL ...SSGVLNPESDPVADL---LPVAVTESDKE
```

Supplementary Figure 2: (A) Sequence alignment of HP1a CSD (highlighted in blue) and CTE (highlighted in yellow) for 12 Drosophila species. Divergent residues are marked in red. (B) Alignments of HP1a-binding proteins containing HACs across 12 Drosophila species. Pentameric core domains of HACs are highlighted in blue; HACs tested to accumulate in heterochromatin are highlighted in red. Some HAC sequences were manually curated as alignments of SuUR, Mu2, and HP2 homologs did not align with the Drosophila melanogaster HAC sequences and may represent paralogous HACs.

The pentameric core requires flanking residues for heterochromatin localization

To identify the amino acids and chemical interactions responsible for binding of HACs with HP1a dimers, we performed full atomistic molecular dynamics (MD) simulations on 25-amino acid HAC sequences containing the hydrophobic core at the center. We confirmed that 15 of the 16 HACs showed high prediction accuracy with pLDDT (predicted Local Distance Difference Test) (**Supplementary Method Table 1**), and the expected positioning of their core

339 region at the center of the CSD dimer in AlphaFold models and throughout the 250 ns MD
340 simulations (**Figure 3A, Supplementary Figure 3A-O**). To investigate whether the core
341 region is sufficient to explain the variable fold-enrichment of HACs in heterochromatin
342 (**Figure 1E**), we compared the root mean square deviation (RMSD) of HAC sequences from -
343 2 to +2 in the last 50 ns of the MD simulations (**Figure 3B)**. Though Piwi, with the lowest fold
344 enrichment score, showed very high fluctuation, the RMSD of the core regions of other
345 peptides showed poor correlation with the ranking of HP1a co-enrichment scores from
346 experimental observations (**Figures 1E, 3B,** $R^2 = 0.07$). To expand and elucidate key residues
347 of HACs, the root mean square fluctuation (RMSF) was calculated for Piwi and XNP, which
348 had the lowest and highest fold enrichment scores from the peptide imaging assay, respectively
349 (**Figure 3C**). XNP showed overall lower RMSF values than Piwi as well as a longer region of
350 low RMSF values (≤RMSF values of the Piwi core region, dotted horizontal lines, **Figure 3C**),
351 consistent with the stronger enrichment of the XNP HAC with HP1a in cells (**Figure 1E**). As
352 expected, the core regions (-2 to +2) exhibited the lowest RMSF values, indicating the part of
353 the HAC with the most stable association with the CSD binding pocket (**Figure 3C**).
354 Interestingly, the proximal flanking sequences on both sides (-7 to -3 and +3 to +7) also showed
355 low RMSF values and no significant difference from the core regions of both XNP and Piwi
356 (**Figure 3C**). While Piwi showed no significant RMSF difference between the proximal
357 flanking sequences and distal flanking sequences (-12 to -8 and +8 to +12), XNP had a
358 significant difference between the proximal and distal flanking sequences (**Figure 3C**). These
359 RMSF results from the MD simulations suggest the potentially crucial role of the proximal
360 flanking regions in determining the strength of the HP1a-peptide interactions and accessibility
361 to heterochromatin.

362

363 We tested different lengths of flanking sequences required for the central core of HACs to
364 maintain heterochromatin enrichment *in vivo*. Lack of any flanking sequences abrogated the
365 ability of three different HACs to localize to heterochromatin at levels indistinguishable from
366 negative controls (**Figure 3D**, **Supplementary Figure 3P and Q**). In contrast, the retention of
367 5 amino acids flanking each side of the central pentamer maintained enrichment with HP1a,
368 indicating that flanking residues are crucial to HAC association with HP1a (**Figure 3D,**
369 **Supplementary Figure 3P**). In conclusion, both MD simulations and *in vivo* peptide
370 localization demonstrate that the traditional PxVxL motif is insufficient for heterochromatin
371 enrichment, and additional residues within 5 amino acids on both sides of the hydrophobic core
372 are required for HAC function.

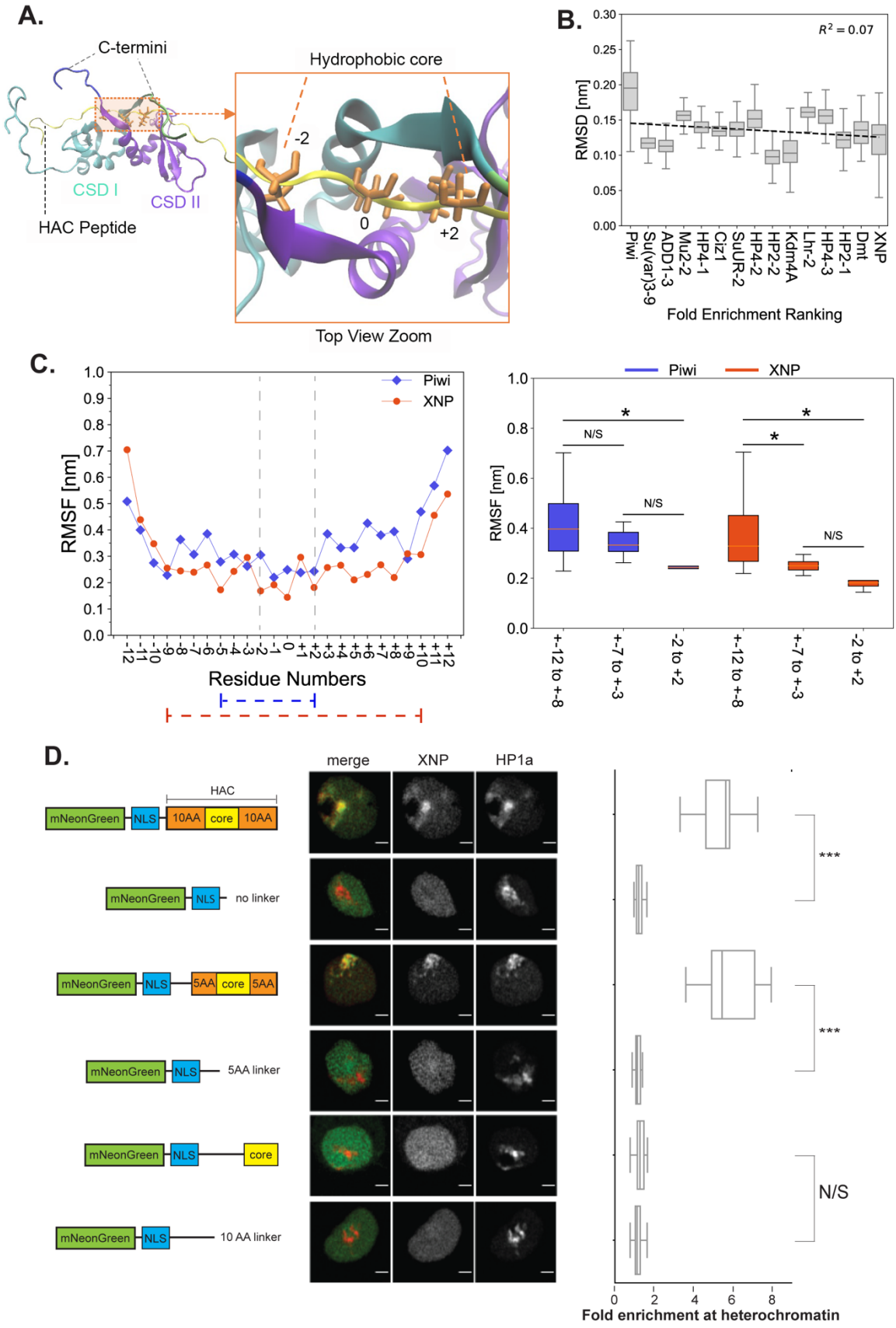
A.
C-termini
Hydrophobic core
CSD I
CSD II
HAC Peptide
-2
0
+2
Top View Zoom
B.
$R^2 = 0.07$
RMSD [nm]
Piwi
Su(var)3-9
ADD1-3
Mu2-2
HP4-1
Ciz1
SuUR-2
HP4-2
HP2-2
Kdm4A
Lhr-2
HP4-3
HP2-1
Dmt
XNP
Fold Enrichment Ranking
C.
Piwi
XNP
RMSF [nm]
Residue Numbers
N/S
*
+-12 to +-8
+-7 to +-3
-2 to +2
D.
HAC
mNeonGreen
NLS
10AA
core
5AA
no linker
5AA linker
10 AA linker
merge
XNP
HP1a
***
N/S
Fold enrichment at heterochromatin

373

Figure 3 (A) Visualization of the CSD dimer with the XNP HAC. Left panel: side view. Right Panel: Zoomed top view. Each CSD monomer is colored cyan and purple with a green and blue colored C-terminal tail, respectively. XNP peptide is colored yellow. Residues of the central hydrophobic core at the -2, 0, and +2 positions (in licorice drawing style) are colored orange. (B) Root mean square deviation (RMSD) ± SD [nm] of the core sequences from -2 to +2 of 15 HACs between 200 to 250 ns of the MD simulations. The peptides are ranked according to the experimental ranking of fold HP1a co-enrichment from Piwi, the lowest, to XNP, the strongest, based on results from Figure 1E. The x-axis values for the linear regression calculation are assigned from 1 (Piwi) to 15 (XNP). The R-squared value is shown on the graph. (C) Left: Root mean square fluctuation (RMSF) [nm] of 25-residue for XNP and Piwi HAC sequences (-12 to +12) between 200 to 250 ns of the MD simulations. The gray dash line at the -2 and +2 is drawn to indicate the core pentamer. The blue and red dashed lines indicate the span of sequences that consecutively display RMSF values less than the combined average of Piwi and XNP = 0.32 nm. Right: Averaged root mean square fluctuation (RMSF) ± SD [nm] of the XNP and Piwi distal flanking sequences (positions -12 to -8 and +8 to +12), proximal flanking sequences (positions -7 to -3 and +3 to +7), and core sequences (positions -2 to +2). Asterisks denote p-values < 0.05 (*) (D) Left: Representative localization images of XNP HAC constructs with different amounts of flanking residues around the hydrophobic core as illustrated in the right panel. As controls, fluorescent tags with different lengths of linker regions were also tested. Right: Quantitation of HP1a co-enrichment at heterochromatin domains for the tested HAC constructs. N/S = not significant; *** = p-value < 0.001.

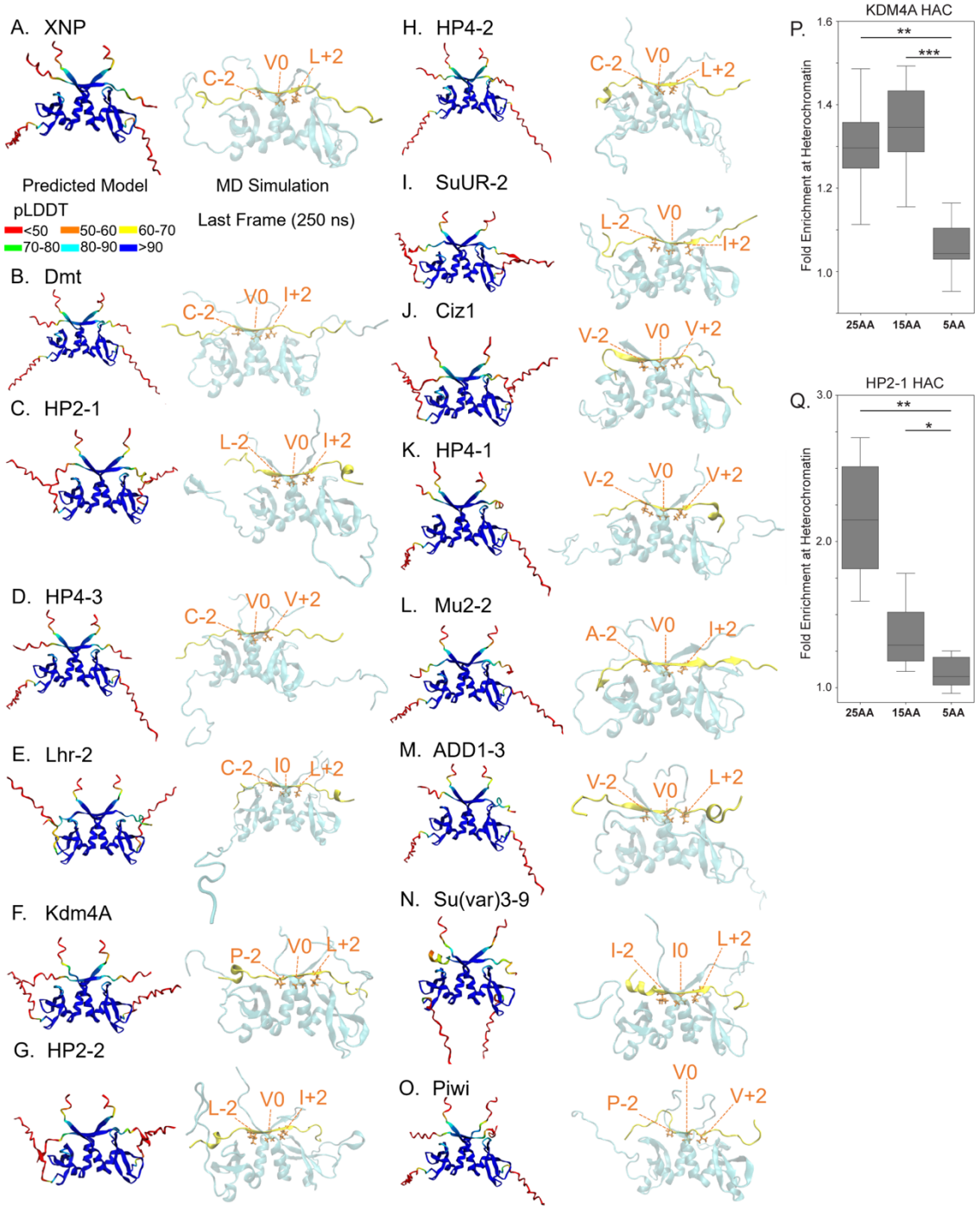

Supplementary Figure 3: (A-O) The Alphafold Multimer-predicted computational model (left) and visualized MD simulation image of the last frame at 250 ns (right) for the CSD dimer and 15 peptides. The Alphafold Multimer-predicted structure is colored based on pLDDT (predicted local distance difference test) scores. Red: pLDDT<50, Orange: 50<pLDDT<60, Yellow: 60<pLDDT<70, Green: 70<pLDDT<80, Skyblue: 80<pLDDT<90, and Blue: 90<pLDDT. CSD homodimer and the peptide are colored cyan and yellow, respectively. Residues at the -2, 0, and +2 positions (in licorice drawing style) are colored orange, with the amino acid code indicated. (P-Q) Quantitation of HP1a co-enrichment at heterochromatin

405 domains for the tested KDM4A and HP2-1 HAC constructs, respectively. 25AA = full-length
406 native sequence containing core region surrounded by 10 residues on each flank; 15AA = core
407 region surrounded by 5 residues on each side; 5AA = core region only. *** = p-value < 0.001;
408 ** = p-value < 0.01; * = p-value < 0.05.

409

410 ***Electrostatic forces surrounding the hydrophobic pocket drive HAC enrichment to***
411 ***heterochromatin***

412 To identify the driving force of the interactions between HACs and HP1a, the types of amino
413 acids in HACs and their molecular properties were analyzed *in silico*. Sequence alignment of
414 all 16 HACs displayed high frequencies of hydrophobic amino acids at positions -7, -5, -1, +5,
415 and +7 in addition to the core hydrophobic residues (-2, 0, and +2) (**Figure 4A**). Amino acids
416 with positively charged side chains (Lys and Arg) are enriched in the flanks and interior of the
417 central hydrophobic core (-4, -3, +1, +3, and +4) when compared to non-HAC peptides (**Figure**
418 **4A, Supplementary Figure 4A**). In contrast, negatively charged residues (Asp and Glu) are
419 relatively under-represented among HAC peptides. The sequence alignment analysis thus
420 suggests that hydrophobic and positively charged amino acids contribute significantly to HP1a
421 interactions at specific positions of HACs.

422

423 We first investigated the effects of the hydrophobic properties of HACs using MD simulations.
424 The hydrophobic pocket formed by the central pentamer of HACs and the HP1 CSD dimer was
425 previously identified to be the main interaction region. The flanking hydrophobic residues,
426 such as -5 and +5, were also thought to contribute to hydrophobic interactions (Thiru *et al.*,
427 2004). We compared the hydrophilic surface area of the HAC sequences from -7 to +7 obtained
428 from the MD analysis with the experimental ranking of HP1a co-enrichment (**Figure 4B, 1E**).
429 Surprisingly, despite some variations, the hydrophilic surface area values did not correlate with

430 the fold enrichment ranking (**Figure 4B, Supplementary Figure 4B,** R^2 = 0.14). The
431 hydrophilic surface area of only the HAC central pentamer from -2 to +2 also showed no
432 correlation with the fold enrichment scores (**Supplementary Figure 4D,** R^2 = 0). Comparing
433 the hydrophilic surface area frequencies of the top two and bottom two ranking peptides
434 showed that Piwi had the highest and lowest hydrophilic surface area in the HAC core pentamer
435 (-2 to +2) and the proximal flanking region (-7 to +7), respectively (**Supplementary Figure**
436 **4C, E**). This indicates that Piwi possesses the lowest hydrophobic interaction between the CSD
437 dimer and the HAC core pentamer, but the highest hydrophobicity between the CSD and the
438 proximal flanking sequence (**Supplementary Figure 4C, E**). However, Su(var)3-9 and Dmt,
439 which had the second lowest and second highest fold enrichment scores, respectively, did not
440 show a corresponding trend of hydrophilic surface area values in relation to Piwi and XNP
441 (**Supplementary Figure 4C, E**).

442

443 To investigate how the hydrophilicity and hydrophobicity of each residue on the HAC peptide
444 participate in the interaction, we visualized the hydrophilic and hydrophobic distribution
445 properties of the HP1a-interacting XNP regions (**Figure 4C**). As expected, there is a
446 hydrophobic pocket between the -2 to +2 amino acid sequences of the HAC and HP1 CSD
447 dimer (**Figure 4C**). On the contrary, the nearby flanking residues tend to have high
448 hydrophilicity rather than hydrophobicity (**Figure 4C**). The hydrophobic pocket of the peptide
449 and **α**-helices of the CSD dimer were surrounded by a high hydrophilic region composed of -
450 4, -3, +1, +3, and +4 positions, indicating the possible existence of other types of interactions
451 that could modulate interactional strength with HP1a. These results also suggest that the
452 hydrophobic interactions of the HACs alone are insufficient to describe the fold enrichment of

453 HAC-containing peptides with HP1a.

454

455 Given the lack of correlation between the hydrophobic properties and strength of HP1a co-
456 localization *in vivo*, we then investigated the electrostatic contributions of the core and flanking
457 amino acids using MD simulations. Electrostatic interactions, which include salt bridges, pi-
458 cation interactions, and hydrogen bonding, represent another key type of interaction in protein
459 structure and binding (Zhou and Pang, 2018). Salt bridge interactions, in particular, are known
460 to be one of the most robust forms of residue-residue interactions (Xie *et al.*, 2015). Salt bridge
461 interactions form when the distance between the side-chain carbonyl oxygen of Asp or Glu and
462 the side-chain nitrogen atoms of Arg, Lys, or His is within 0.4 nm, facilitated by Coulomb
463 attraction with water molecules (Kumar and Nussinov, 2002; Pylaeva, Brehm and Sebastiani,
464 2018). The high hydrophilic and positively charged amino acid-conserved regions were seen
465 at -4, -3, +1, +3, and +4 (**Figure 4A, C**). Therefore, we calculated Coulomb energy levels
466 between the HACs from +4 to +4 and the HP1a CSD dimer with C-terminal tails. Notably,
467 Coulomb energy levels generally decreased among peptides ranked from low to high HP1a co-
468 enrichment, indicating that attractive electrostatic force followed the trend of the *in vivo* fold
469 enrichment ranking (**Figure 4D, Supplementary Figure F**, R^2 = 0.46). Comparing the
470 electrostatic energy of the top two and bottom two ranking peptides similarly showed a
471 correlation between Coulomb energy levels and heterochromatin enrichment (**Supplementary**
472 **Figure G**). The Coulomb energy between the HACs from -7 to +7 and the HP1a CSD dimer
473 with C-terminal tails showed less correlation (**Supplementary Figure H, I**, R^2 = 0.28),
474 implying the -4 to +4 residues of HACs have more important contributions to the fold
475 enrichment scores. The visualization of the electrical charge distribution of the HP1a-

476 interacting XNP regions showed a high charge density at -4, -3, +1, +3, and +4 amino acids
477 outside the hydrophobic pocket of the CSD, but did not show a charge density outside -4 and
478 +4 regions, emphasizing the importance of electrically charged amino acids between -4 and +4
479 in the electrostatic interactions with HP1a (**Figure 4E**).

480

481 Overall, our observations indicate that electrostatic interactions between the HAC residues
482 from -4 to +4 and the HP1a CSD dimer with C-terminal tails are crucial determinants in the
483 binding of HAC-containing peptides with HP1a dimers. Of course, hydrophobic and
484 electrostatic residues beyond the ranges of positions analyzed here may also contribute to HP1a
485 binding, but these positions, such as distant flanking sequences (-12 to -8 and +8 to +12), are
486 more variable in residue content and experience more fluctuation (as shown by RMSF variation
487 in Figure 3).

488

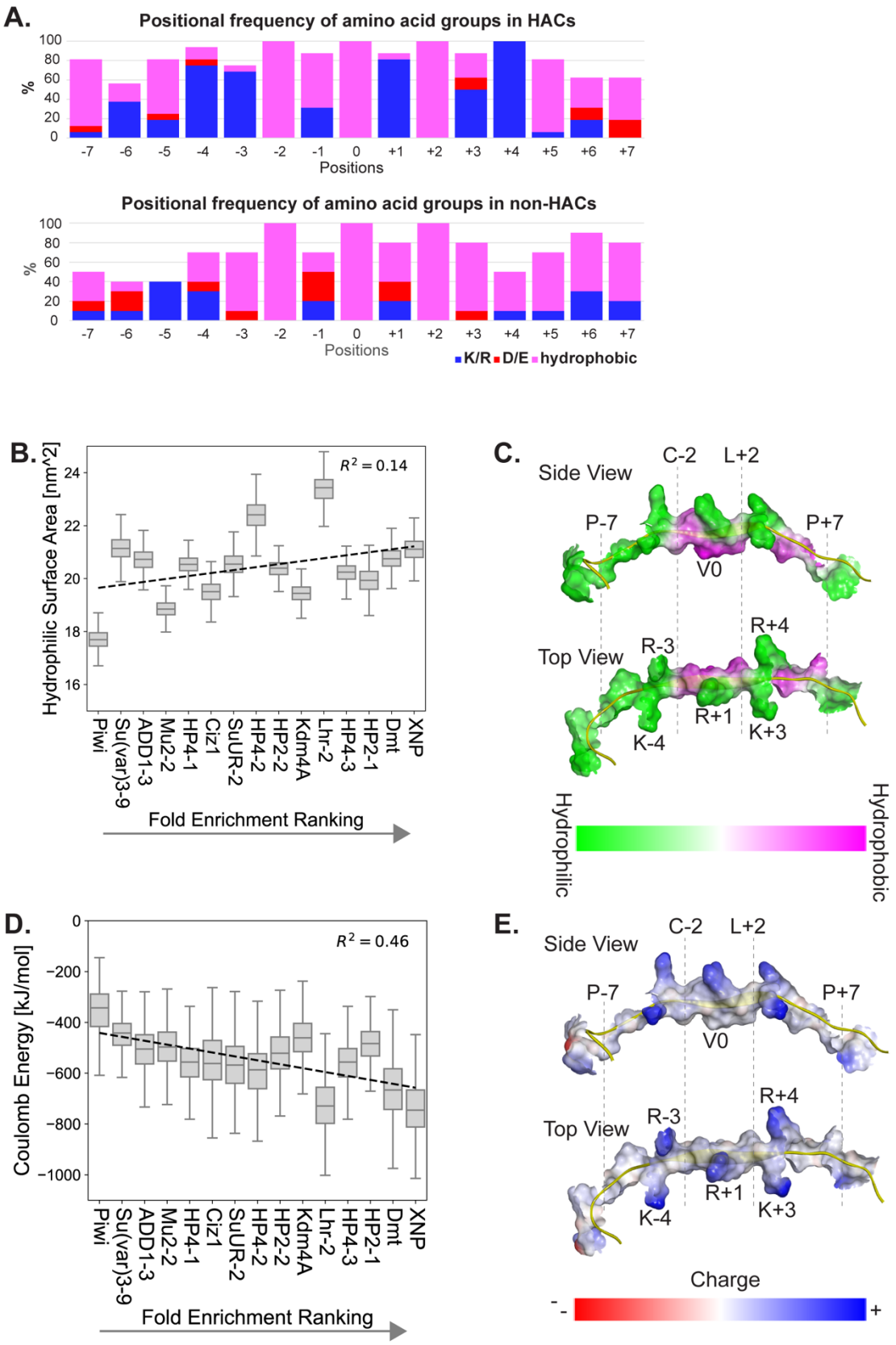
A.
Positional frequency of amino acid groups in HACs
%
Positions
Positional frequency of amino acid groups in non-HACs
K/R D/E hydrophobic
B.
Hydrophilic Surface Area [nm^2]
$R^2 = 0.14$
Piwi
Su(var)3-9
ADD1-3
Mu2-2
HP4-1
Ciz1
SuUR-2
HP4-2
HP2-2
Kdm4A
Lhr-2
HP4-3
HP2-1
Dmt
XNP
Fold Enrichment Ranking
C.
Side View
C-2
L+2
P-7
P+7
V0
Top View
R-3
R+4
R+1
K-4
K+3
Hydrophilic
Hydrophobic
D.
Coulomb Energy [kJ/mol]
$R^2 = 0.46$
Fold Enrichment Ranking
E.
Charge

489

490 **Figure 4** (A) Frequency of occupancy by hydrophobic (pink), positively charged (blue), and
491 negatively charged (red) select groups of amino acids at each position among tested HACs
492 (top) and non-HACs (bottom). Numbering of positions are in relation to the central residue at
493 position 0. (B) Hydrophilic surface area ± SD [nm^2] of sequences from -7 to +7 of 15 HACs
494 between 200 to 250 ns of the MD simulations. The peptides are ranked according to the
495 experimental ranking of fold HP1a co-enrichment from Piwi, the lowest peptide, to XNP, the
496 strongest peptide. The x-axis values for the linear regression calculation are assigned from 1
497 (Piwi) to 15 (XNP). The R-squared value is shown. (C) Visualizations of XNP HAC surface
498 hydrophilicity and hydrophobicity in the side view (above) and the top view (bottom) were
499 calculated using the Discovery Studio software. The hydrophilic to hydrophobic properties are
500 colored from green to pink. XNP backbone is colored yellow. (D) Coulomb energy ± SD
501 [kJ/mol] of 15 HAC sequences from -4 to +4 between 200 to 250 ns of the MD simulations. A
502 ranking similar to that of (A) is used to order the peptides. The R-squared value is shown. (E)
503 Visualization of the XNP HAC surface charge in the side view (above) and the top view
504 (bottom). The negatively to positively charged properties are colored from red to blue. XNP is
505 colored yellow.

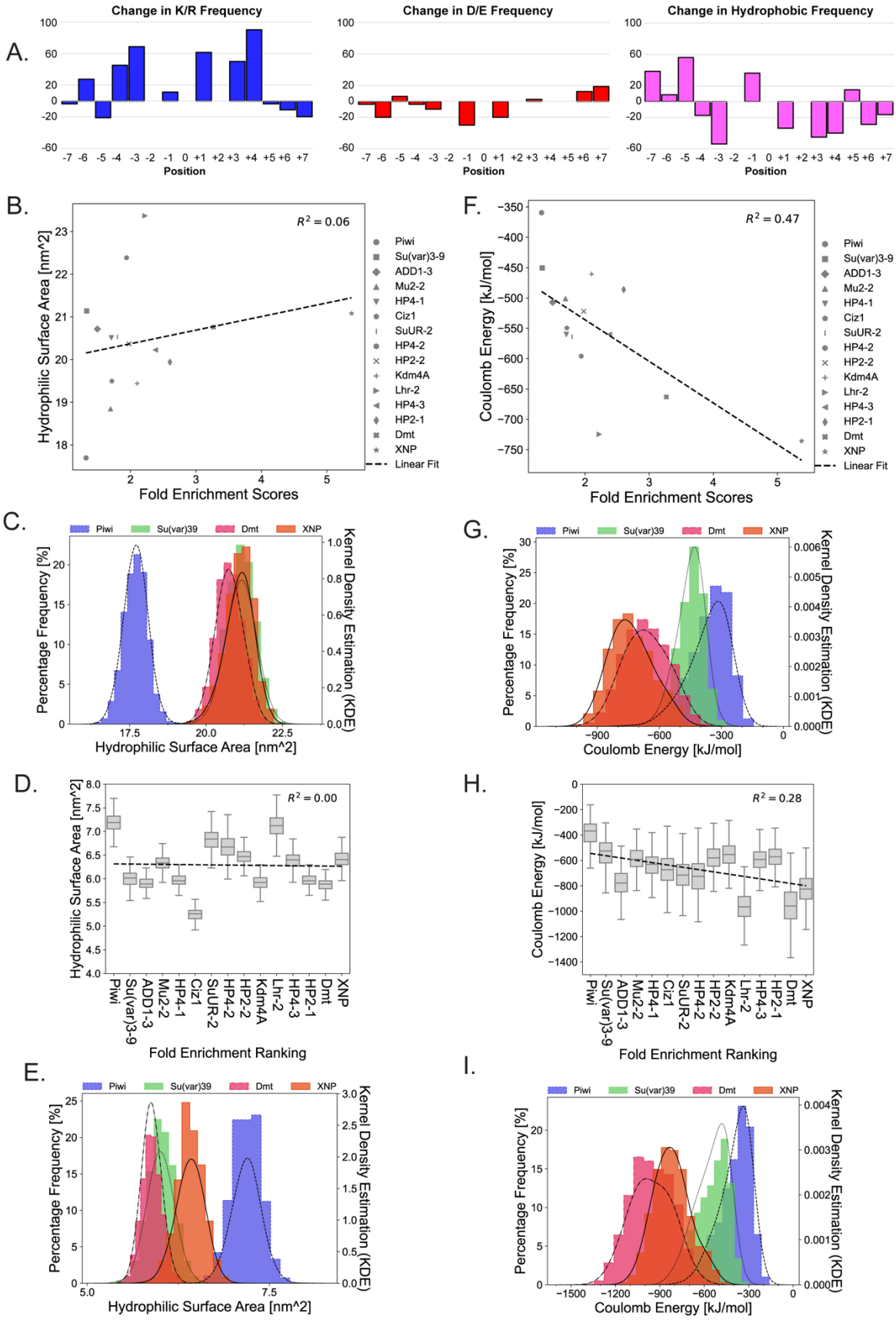
A.
Change in K/R Frequency
Change in D/E Frequency
Change in Hydrophobic Frequency
Position
B.
$R^2 = 0.06$
Hydrophilic Surface Area [nm^2]
Fold Enrichment Scores
F.
$R^2 = 0.47$
Coulomb Energy [kJ/mol]
Fold Enrichment Scores
Piwi
Su(var)3-9
ADD1-3
Mu2-2
HP4-1
Ciz1
SuUR-2
HP4-2
HP2-2
Kdm4A
Lhr-2
HP4-3
HP2-1
Dmt
XNP
Linear Fit
C.
G.
Piwi
Su(var)39
Dmt
XNP
Percentage Frequency [%]
Kernel Density Estimation (KDE)
Hydrophilic Surface Area [nm^2]
Coulomb Energy [kJ/mol]
D.
$R^2 = 0.00$
Hydrophilic Surface Area [nm^2]
Fold Enrichment Ranking
H.
$R^2 = 0.28$
Coulomb Energy [kJ/mol]
Fold Enrichment Ranking
E.
I.

506

507 **Supplementary Figure 4:** (A) Bar graphs showing differences in percent frequency of
508 positively charged residues (left in blue), negatively charged residues (center in red) and
509 hydrophobic residues (right in pink) between HAC peptides and non-HACs. (B) Hydrophilic
510 surface area of sequences from -7 to +7 of 15 HACs between 200 to 250 ns of the MD
511 simulations are plotted according to the fold HP1a co-enrichment values (Figure 1E). The R-
512 squared value is shown. (C) Histogram showing the percentage frequency of hydrophilic
513 surface area for sequences from -7 to +7 of HACs for Piwi, Su(var)3-9, Dmt, and XNP between
514 200 to 250 ns of the MD simulations. Piwi: Blue with a dash line. Su(var)3-9: Green with a
515 dotted line. Dmt: Pink with a dash and dotted line. XNP: Orange with a solid line. Histogram
516 was fitted by kernel density estimation (KDE). (D) Hydrophilic surface area ± SD [nm^2] of
517 sequences from -2 to +2 of 15 HACs between 200 to 250 ns of the MD simulations. The
518 peptides are plotted according to ranking in terms of fold HP1a co-enrichment. The R-squared
519 value is shown. (E) Histogram showing the percentage frequency of hydrophilic surface area
520 for pentameric core sequences from -2 to +2 of HACs for Piwi, Su(var)3-9, Dmt, and XNP
521 between 200 to 250 ns of the MD simulations, using the same format as C. (F) Coulomb energy
522 of 15 HAC sequences from -4 to +4 between 200 to 250 ns of the MD simulations are plotted
523 according to HP1a co-enrichment values. The R-squared value is shown. (G) Histogram
524 showing the percentage frequency of Coulomb energy for 9 residues from -4 to +4 of HACs
525 for Piwi, Su(var)3-9, Dmt, and XNP between 200 to 250 ns of the MD simulations, using the
526 same format as C. (H) Coulomb energy ± SD [kJ/mol] of 15 HAC sequences from -7 to +7
527 between 200 to 250 ns of the MD simulations. The peptides are plotted according to ranking in
528 terms of fold HP1a co-enrichment. The R-squared value is shown. (I) Histogram showing the
529 percentage frequency of Coulomb energy from positions -7 to +7 of Piwi, Su(var)3-9, Dmt,
530 and XNP HACs between 200 to 250 ns of the MD simulations, using the same format as C.

531

532 ***Distinct roles of positively charged amino acids in HAC binding***

533 To reveal the molecular roles of positively charged amino acids in the HAC peptide binding
534 and structure, we analyzed the individual Coulomb energy from positions -7 to +7 for several
535 HACs in association with the HP1a CSD dimer and C-termini in the MD simulations (**Figure**
536 **5A, C**). Three peptides were chosen for the electrostatic analysis: XNP as the strongest
537 interacting peptide, Piwi as the weakest interacting peptide lacking a positively charged amino
538 acid at the +3 position, and Ciz1 as the relatively weak interacting peptide lacking a positive
539 amino acid at the +1 position. **Table 1** shows the quantitative values of Coulomb energy for -
540 7 to +7 sequences of these three peptides. Overall, -4, -3, +3, +4 HAC amino acids had higher

541 attractive Coulomb energy than -7 to -5 and +5 to +7 regions, quantitatively confirming the
542 important contributions of -4 to +4 amino acids suggested in Figure 4.

543

544 The highest attractive energy to the CSD dimer was observed at the +4 position for all three
545 peptides (**Table 1, Figure 5A**), where a salt bridge interaction with Asp157^{II} (of CSD^{II}) was
546 detected (**Figure 5B, Supplementary Figure 5A**). Similarly, the -4 position of the XNP and
547 Ciz1 HACs formed a salt bridge interaction with Asp157^{I}, but was not present for Piwi due to
548 the lack of a positively charged amino acid at the -4 position (**Figure 5A**). All 16 peptides that
549 exhibited heterochromatin enrichment have a positively charged amino acid at the +4 position
550 (**Figure 4A**), suggesting the +4 positively charged amino acid comprises a basic feature of the
551 HAC motif.

552

553 In contrast, the residues with the highest attractive Coulomb energy with the HP1a C-terminus
554 varied among the three peptides (**Table 1**). The Coulomb energy at the +3 position displayed
555 high variance among the three peptides (-164±70.42, -47.39±57.50, and -3.01±5.15 [kJ/mol]
556 for XNP, Ciz1, and Piwi, respectively). Unlike the other two, Piwi lacks a positively charged
557 amino acid at the +3 position. Interestingly, there is also a discrepancy between XNP and Ciz1,
558 even though both XNP and Ciz1 have lysine at the +3 position. Molecular interaction analysis
559 showed that the Arg+3 of XNP formed a salt bridge or H-bond with HP1a Glu205^{I} or Asp203^{I}
560 (**Figure 5D, Supplementary Figure 5B**). However, Arg+3 of Ciz1 did not form such
561 interactions and instead had an unfavorable interaction with HP1a Arg197^{II} (**Figure 5D, F,**
562 **Supplementary Figure 5C**). This difference is attributed to interactions between +1 of the
563 HACs and Arg197^{II} of the CSD: Arg+1 of XNP formed a maximum of three H-bonds with

564 Arg197^{II}, including its side chain (**Figure 5E, Supplementary 5C**), while Ser+1 of Ciz1 had
565 only one H-bond with the carboxylic acid group of Arg197^{II}, leading to a repulsive interaction
566 between the Arg197^{II} side chains and Lys+3, and a H-bond between Arg197^{II} and Glu205^{I}
567 (**Figure 5F, Supplementary 5C**). These results indicate that Arg+1 plays an important role in
568 both the H-bond interaction with Arg197^{II} and the maintenance of the electrostatic force field
569 to develop the salt bridge and H-bond among +3, Asp203^{I}, and Glu203^{I}. We therefore tested
570 the effects of a Ser+1Arg Ciz1 mutation *in vivo* to determine if increasing electrostatic
571 interactions at this position will enhance HP1a co-enrichment. The Ciz1 mutant modestly
572 improved the fold enrichment score compared to a wildtype Ciz1 HAC, indicating the
573 deterministic effect of +1 in controlling the strength of the HP1a and HAC peptide interaction
574 (**Figure 5G, Supplementary Figure 5D**).

575

576 As previously noted, Piwi lacks a positively charged amino acid at +3, but our analysis showed
577 that the Lys+1 side chain can form an H-bond with Ser199^{I} or salt bridge interaction with
578 Asp203^{II} (**Figure 5H, Supplementary Figure 5E**). A positively charged amino acid at position
579 +1 may therefore compensate for the lack of a positively charge at +3 by forming a salt bridge
580 or hydrogen bond to attain sufficient HP1a interaction strength. There are likely many other
581 compensatory mechanisms for different HACs, as positively charged residues occupy variable
582 positions within and surrounding the hydrophobic core (**Supplementary Figure 5F**).

583

584 To validate the computational theory of the electrostatic effects of positive amino acids on
585 HAC peptide and HP1 interactions, we performed single and combinatorial amino acid
586 mutation experiments with XNP, which had the highest Coulomb energy for the C-terminus

587 and CSD dimer (**Table 1, Figure 5A, C**). First, single mutation experiments showed that
588 Arg+1Ala and Arg+4Ala mutations significantly decreased the fold enrichment in
589 heterochromatin (**Figure 5I, Supplementary Figure 5G**). Although high electrostatic energy
590 was observed for Arg+3 in the MD simulation, the Arg+3Ala mutation did not show a
591 significant difference in HP1a co-enrichment. The compensatory mechanism of the Piwi Arg+1
592 side chain for the lack of a positively charged amino acid at +3 (**Figure 5H**) might explain the
593 lack of effect of Arg+3Ala in the XNP experiment. Nevertheless, the double mutations of
594 Lys+3 and Arg+4, as well as double mutations of Lys-4 and Arg-3, greatly diminished XNP
595 HAC enrichment in heterochromatin compared to the single mutants. Furthermore, a quadruple
596 mutation of -4, -3, +3, and +4 nearly abrogated all enrichment, suggesting the basic residues
597 act cooperatively to stabilize HAC enrichment to heterochromatin (**Figure 5I, Supplementary**
598 **Figure 5H**). These results show that positively charged amino acids immediately flanking the
599 pentameric core are essential for HAC function. Further, they suggest that the interaction
600 strength between the HAC and HP1a can be controlled by selecting appropriate mutations of
601 positively charged amino acids in the HAC sequence.

602

603 To obtain a comprehensive view of the molecular forces that govern HAC binding to HP1a,
604 we analyzed the XNP HAC for electrostatic and hydrophobic interactions in simulations
605 (**Figure 5J, Supplementary Figure 5I**). Limiting the scope of analysis to between HAC
606 residues -7 and +7, we identified salt bridges forming at positions -4, +3, and +4 with both the
607 CSD and C-terminal tail, as previously discussed. We also detected pi-cation interactions at
608 the basic positions -4, +1, and +4 with the hydrophobic pocket residues of the CSD dimer.
609 Meanwhile, hydrophobic interactions were predicted at positions -5, -2, -1, 0, +2, and +5,

consistent with previous studies. Hydrogen bonds were also formed by both nonpolar and basic amino acids at 9 of the 15 residues analyzed. Of important note is the hydrogen bonding detected at position -2 unique to cysteine, due to its polar, hydrophobic sidechain. This confers an extra electrostatic interaction absent from other hydrophobic residues that occupy that position in other HACs, and thus provides higher affinity for HP1a. We predict that other HACs follow a general pattern of molecular interactions contained in this XNP map, though alternative interactions are likely to occur due to the positional variations of basic and hydrophobic residues of other HACs that impact HP1a affinity.

Table 1 Sequences and coulomb energy ± SD [kJ/mol] among the CSD dimer or CTE and -7 to +7 residues of XNP, Ciz1, and Piwi. The highest coulomb energy among the -7 to +7 is highlighted in red.

Residue	XNP	Ciz1	Piwi	CSD_XNP	CSD_Ciz1	CSD_Piwi	C-terminus_XNP	C-terminus_Ciz1	C-terminus_Piwi
-7	P	S	G	-1.02 ± 4.99	0.17 ± 0.89	-7.34 ± 8.71	-0.04 ± 0.13	-2.79 ± 9.95	0.02 ± 2.09
-6	R	T	S	-9.27 ± 11.92	-1.94 ± 6.99	-0.89 ± 2.73	-46.09 ± 62.83	-20.22 ± 19.17	-5.35 ± 13.21
-5	P	K	G	-5.45 ± 2.38	-2.55 ± 4.81	0.09 ± 0.55	0.60 ± 1.37	-41.43 ± 39.44	-0.10 ± 1.04
-4	K	R	D	-105.93 ± 48.80	-90.84 ± 59.05	1.06 ± 5.62	-49.02 ± 59.89	-40.17 ± 16.80	0.00 ± 7.94
-3	R	N	G	-4.58 ± 5.44	-8.29 ± 2.93	1.32 ± 4.32	-50.86 ± 45.06	-59.87 ± 18.65	0.23 ± 0.22
-2	C	V	P	-59.14 ± 10.41	-14.00 ± 3.01	-14.79 ± 9.36	-0.84 ± 1.17	-0.58 ± 2.31	-0.01 ± 0.05
-1	V	L	R	-41.48 ± 9.21	-38.41 ± 7.45	-41.34 ± 12.06	-0.35 ± 0.75	-0.33 ± 0.62	-32.02 ± 43.60
0	V	V	V	-34.87 ± 7.38	-34.82 ± 9.73	-32.84 ± 9.36	-0.13 ± 0.27	-0.02 ± 0.03	0.04 ± 0.05
+1	R	S	K	-66.45 ± 25.07	-27.53 ± 9.84	-60.91 ± 32.91	2.45 ± 6.20	-0.19 ± 1.72	-32.08 ± 50.42
+2	L	V	V	-20.24 ± 5.45	-15.57 ± 5.31	-18.88 ± 7.60	-13.30 ± 4.62	-14.29 ± 4.19	-16.89 ± 4.62
+3	K	K	F	7.16 ± 5.26	4.82 ± 4.27	-21.33 ± 5.79	-161.04 ± 70.42	-47.46 ± 57.53	-3.01 ± 5.15
+4	R	R	R	-133.15 ± 21.40	-132.20 ± 21.07	-81.99 ± 52.34	-3.96 ± 9.15	-29.54 ± 23.95	-6.04 ± 11.63
+5	V	T	G	-16.68 ± 5.73	-18.45 ± 8.98	-15.14 ± 6.16	-0.05 ± 1.17	-12.96 ± 23.31	0.04 ± 0.38
+6	S	S	S	-0.93 ± 1.01	-0.69 ± 2.24	-1.21 ± 3.60	-6.33 ± 14.80	-18.59 ± 30.59	-0.11 ± 0.86
+7	L	A	S	1.49 ± 0.99	-0.37 ± 2.36	-1.34 ± 6.45	0.83 ± 2.43	-0.28 ± 1.13	-0.01 ± 0.23

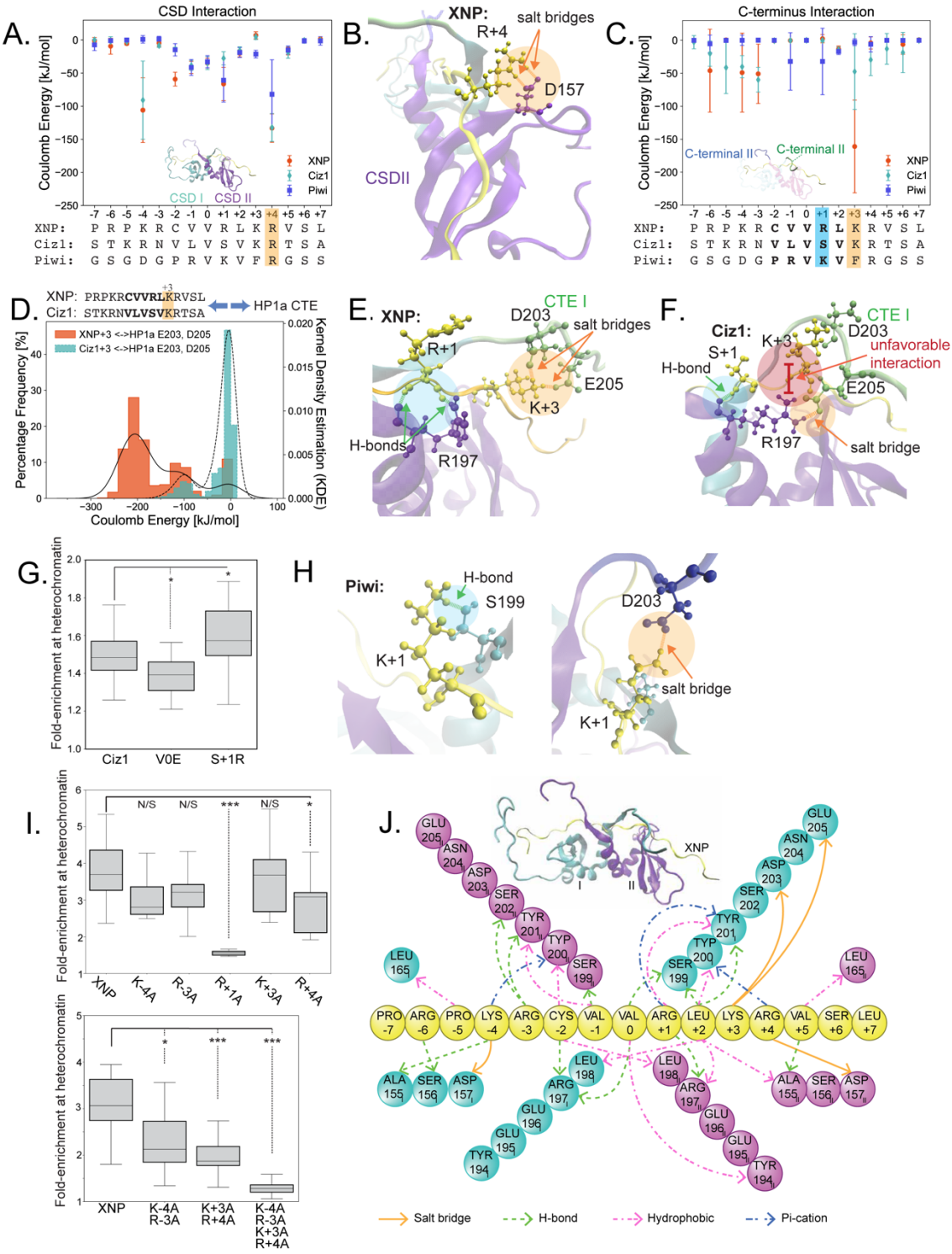

Figure 5: (A) Coulomb energy ± SD [kJ/mol] between the CSD dimer and -7 to +7 residues of XNP, Ciz1, and Piwi. Orange circle: XNP, Cyan diamond: Ciz1, and Blue square: Piwi. (B) Visualization of the salt bridge interaction between Arg+4 and Asp157^{II}. Arg+4 and Asp157^{II} in the Corey-Pauling-Koltun (CPK) drawing style are colored yellow and purple, respectively.

(C) Coulomb energy ± SD [kJ/mol] between the HP1a C-terminal tails and -7 to +7 residues of XNP, Ciz1, and Piwi. Orange circle: XNP, Cyan diamond: Ciz1, and Blue square: Piwi. (D) Histograms showing the percentage frequency of Coulomb energy between HP1a $Asp203^{I}/Glu205^{I}$ and +3 of XNP and Ciz1 between 200 to 250 ns of the MD simulations. The histogram was fitted by kernel density estimation (KDE). XNP: Orange with a solid line. Ciz1: Cyan with a dashed line. (E) Visualizations of XNP and (F) Ciz1 with blue, orange, and red circles with arrows indicating a hydrogen bond, salt bridge, and unfavorable interactions, respectively. (G) Quantification of HP1a co-enrichment of Ciz1 HAC and mutations either disabling the central valine or adding a positive charge at the +1 position. (H) Visualization of H-bond interaction between Piwi Lys+1 and $Ser199^{I}$ (left) and salt bridge interaction between Piwi Lys+1 and $Asp203^{II}$ (right). H-bond and salt bridge are highlighted in green and orange, respectively. (I) Quantification of HP1a co-enrichment of XNP HACs with single alanine substitutions at positions -4, -3, +1, +3, or +4 (top) or double substitutions at positions -4 and -3 or +3 and +4 or quadruple substitutions at all positions (bottom). Asterisks denote p-values < 0.05 (*), <0.01 (**), <0.001 (***). (J) 2D molecular interactional map of HP1a CSD dimer with C-terminal tails and XNP HAC. Each CSD monomer is colored cyan and purple, respectively. XNP is colored yellow. Orange, green, pink, and blue dashed lines represent a salt bridge interaction, hydrogen bond, hydrophobic interaction, and pi-cation interaction.

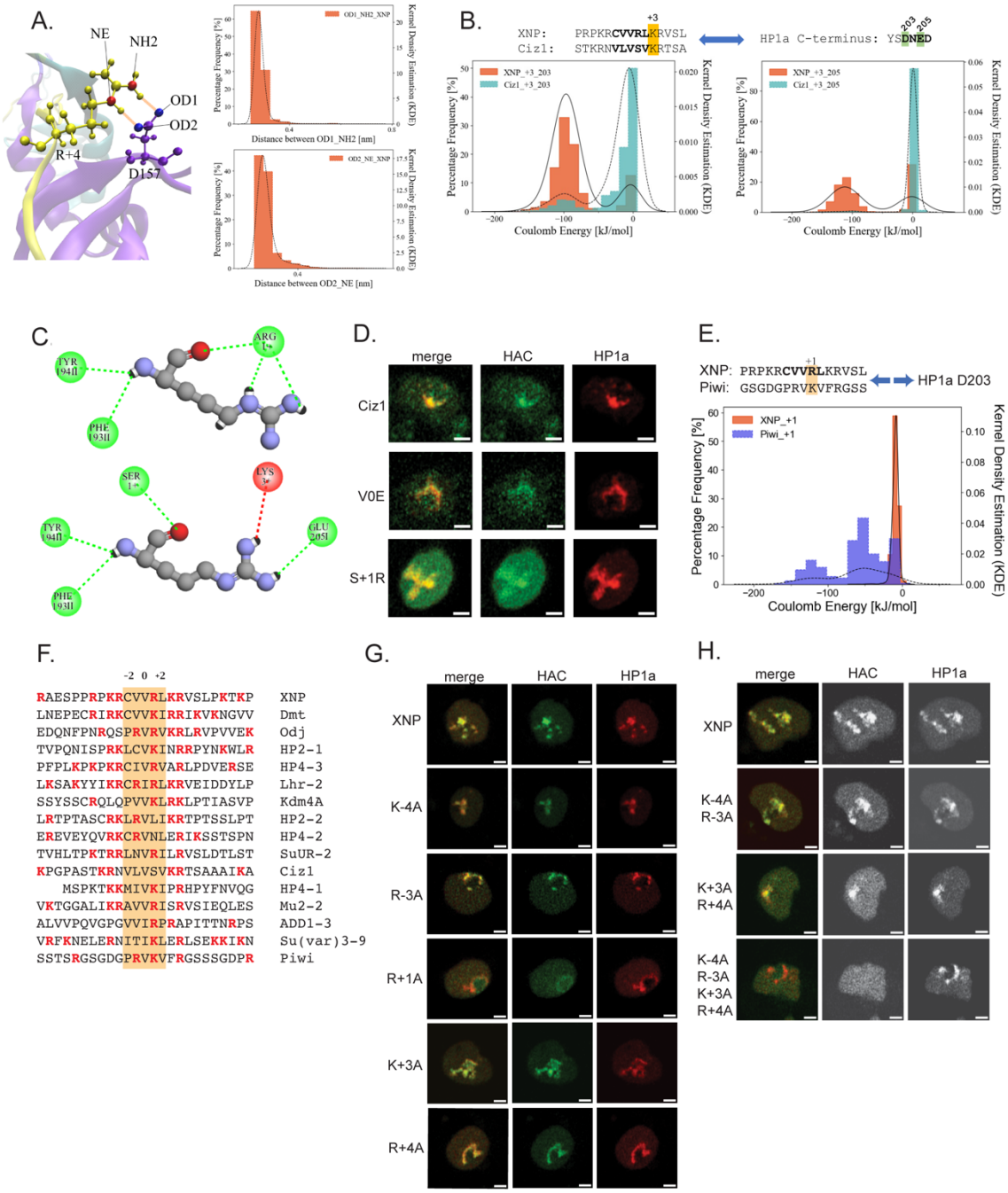
A.
NE
NH2
OD1
OD2
R+4
D157
OD1_NH2_XNP
Distance between OD1_NH2 [nm]
OD2_NE_XNP
Distance between OD2_NE [nm]
Percentage Frequency [%]
Kernel Density Estimation (KDE)
B.
XNP: PRPKRCVVRLKRVSL
Ciz1: STKRNVLVSVKRTSA
+3
HP1a C-terminus: YSDNED
203
205
XNP_+3_203
Ciz1_+3_203
XNP_+3_205
Ciz1_+3_205
Coulomb Energy [kJ/mol]
C.
ARG
TYR 194H
PHE 193H
SER
LYS
GLU 205I
D.
merge
HAC
HP1a
Ciz1
V0E
S+1R
E.
XNP: PRPKRCVVRLKRVSL
Piwi: GSGDGPRVKVFRGSS
HP1a D203
+1
XNP_+1
Piwi_+1
F.
-2 0 +2
RAESPPRPKRCVVRLKRVSLPKTKP XNP
LNEPECRIRKCVVKIRRIKVKNGVV Dmt
EDQNFPNRQSPRVRVKRLRVPVVEK Odj
TVPQNISPRKLCVKINRRPYNKWLR HP2-1
PFPLKPKPKRCIVRVARLPDVERSE HP4-3
LKSAKYYIKRCRIRLKRVEIDDYLP Lhr-2
SSYSSCRQLQPVVKLRKLPTIASVP Kdm4A
LRTPTASCRKLRVLIKRTPTSSLPT HP2-2
EREVEYQVRKCRVNLERIKSSTSPN HP4-2
TVHLTPKTRRLNVRILRVSLDTLST SuUR-2
KPGPASTKRNVLVSVKRTSAAAIKA Ciz1
MSPKTKKMIVKIPRHPYFNVQG HP4-1
VKTGGALIKRAVVRISRVSIEQLES Mu2-2
ALVVPQVGPGVVIRPRAPITTNRPS ADD1-3
VRFKNELERNITIKLERLSEKKIKN Su(var)3-9
SSTSRGSGDGPRVKVFRGSSSGDPR Piwi
G.
XNP
K-4A
R-3A
R+1A
K+3A
R+4A
H.
K-4A
R-3A
K+3A
R+4A
K-4A
R-3A
K+3A
R+4A

646

I.

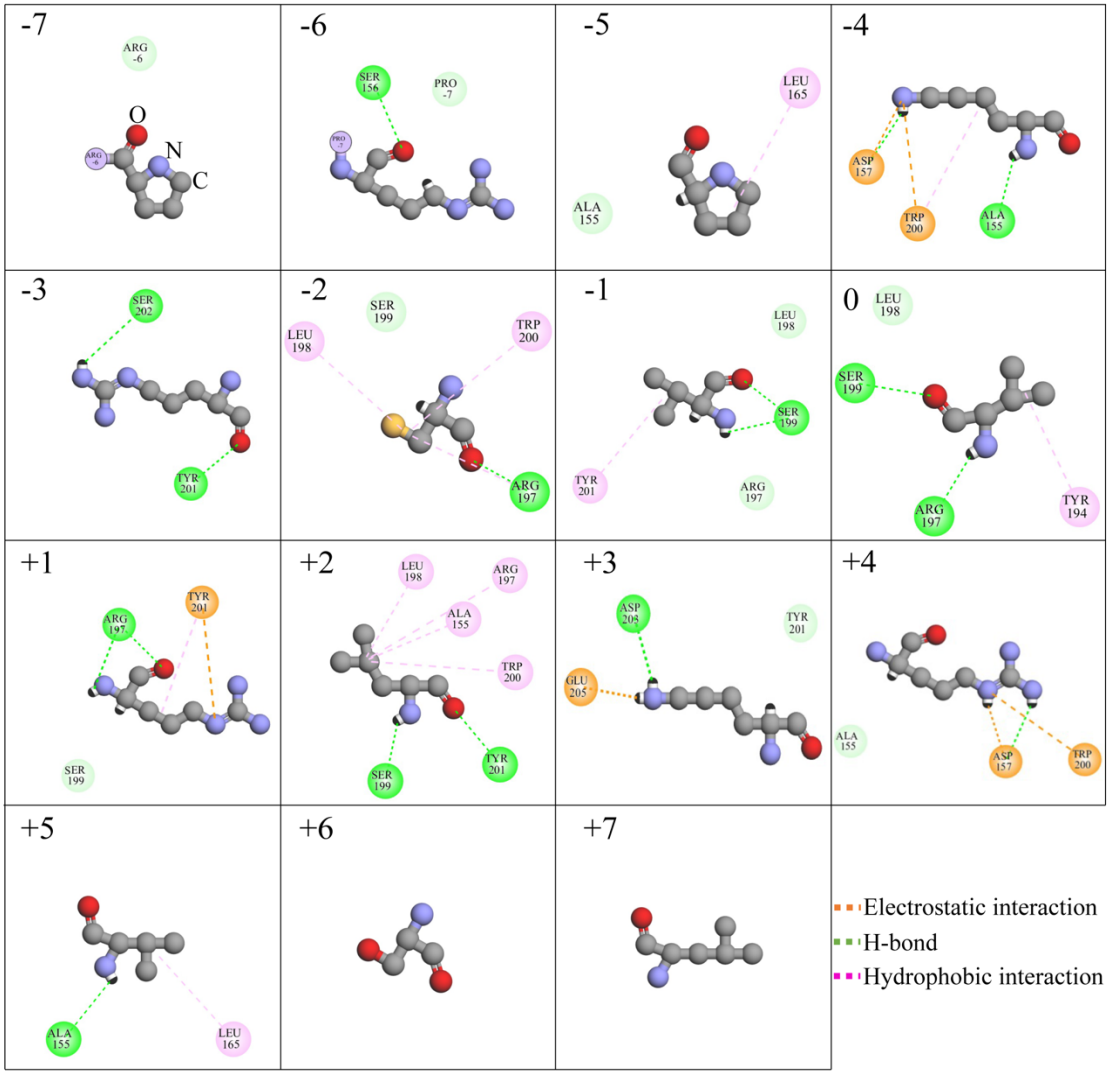

Supplementary Figure 5: (A) Visualization of salt bridge interactions between XNP HAC Arg+4 and Glu157 of HP1a CSDII (left). Histograms of the percentage frequency of salt bridge formation between the guanidinium and a guanidino group of the XNP HAC Arg+4 sidechain and 2 O atoms of HP1a Glu157^{II} (right). (B) Histograms showing the percentage frequency of the salt bridges between Asp203^{I} and +3 (left) and between Glu205^{I} and +3 (right) of XNP as orange with a solid line, and of Ciz1 as cyan with a dashed line, between 200 to 250 ns of the MD simulations. (C) Interaction models of HP1a Arg197 showing 3 hydrogen bonds forming with Arg+1 of the XNP HAC (top), and a single hydrogen bond forming between Ser+1 plus charge repulsion with Lys+3 of the Ciz1 HAC (bottom). (D) Representative images of Ciz1 HAC and mutations either disabling central valine or adding a positive charge at the +1 position. (E) Histogram showing the percentage frequency of the Coulomb energy between Asp203^{II} or Ser199^{I} and +1 of XNP as orange with a solid line and Piwi as blue with a dashed line, between 200 to 250 ns of the MD simulations. All histograms were fitted by kernel density

661 estimation (KDE). (F) Alignment of all 16 HACs with pentameric core highlighted in yellow
662 and marked with -2, 0, and +2 positions, and positively charged residues marked in red. (G)
663 Representative images of mNeonGreen-tagged XNP HACs with single alanine substitutions at
664 positions -4, -3, +1, +3, or +4 co-transfected with mScarlet-I-tagged HP1a (H) Representative
665 images of XNP HACs containing combinations of alanine mutations at either -4 and -3, +3 and
666 +4, or all four positions. (I) Interactional profiles of XNP from -7 to +7 generated by Discovery
667 Studio. Orange, green, and pink dashed lines represent an electrostatic interaction, hydrogen
668 bond, and hydrophobic interaction. Grey, blue, and red atoms of amino acid structures indicate
669 carbon, nitrogen, and oxygen, respectively.
670
671 ***Generation of an improved HAC molecular signature using homolog analysis***

672 Our discovery of new HAC sequences, coupled with their high conservation between
673 Drosophila species, amount to 173 peptide sequences that could be used to improve our
674 understanding of the HAC molecular signature. Color-coded sequence alignment stacks of
675 HACs and their homologs between hydrophobic, positively charged, and negatively charged
676 residues reveal high conservation within each group of HAC homologs (**Figure 6A** and
677 **Supplementary Figure 6A**). This suggests that HAC organization for each protein possesses
678 specific features that contribute to its affinity for HP1a. For example, HACs containing a
679 proline at -2 position often lack positively charged residues at the -3 and -4 positions, which
680 may indicate a proline-imparted kinked structure that prohibits positively charged residues at
681 those positions or render them unnecessary. We also identified rare, new residues at key
682 positions such as leucine or asparagine at position +4, of *D. willistoni* HP2-1 and Mu2-3,
683 respectively, capable of supporting HP1a co-enrichment (**Supplementary Figure 6B**), despite
684 the other 171 sequences containing positively charged residues at that position.
685
686 To identify unifying features of HACs, the occupancy of the same groups of amino acids were
687 quantified for each position (**Figure 6B**). Aside from the expected 100% occupancy of
688 nonpolar residues at positions -2, 0, and +2, there is nearly 80% occupancy at position +5 and
689 about 60% at positions -7, -5, -1, and +7. This indicates that hydrophobic forces in the flanking

690 regions of some HAC pentamers also contribute to functional HP1a binding directly or
691 indirectly. Consistent with our analysis in previous figures, positively charged residues
692 predominate at positions -6, -4, -3, +1, +3, and +4, which also correspond to a dearth of
693 negatively charged residues. We hypothesize that the less frequent but conserved occupations
694 of negatively charged residues in the flanking regions among specific HAC homologs reflect
695 mechanisms to partially destabilize HP1a affinity and/or utilize alternative mechanisms of
696 binding HP1a at those positions. This domination of HAC organization by nonpolar and basic
697 residues is highlighted by the corresponding dramatic drop of amino acid heterogeneity
698 between positions -6 and +6 (**Supplementary Figure 6C**). Finally, HAC organization across
699 various Drosophila species is also marked by association with intrinsically disordered regions
700 (**Figure 6C**), indicating that properties of these regions contribute to HAC function or that
701 HAC sequences impart disorder to the surrounding protein structure.
702
703 To summarize our findings, conservation analysis of Drosophila homolog sequences revealed
704 evolutionary positional bias for nonpolar and basic residues that correspond to various
705 molecular interactions with the HP1a dimer (**Figure 5I**). We refine the original Drosophila
706 HAC signature to consist of nearly any hydrophobic residue at -2, an invariant valine or
707 isoleucine at the central position, and nearly any aliphatic amino acid at +2. Expanding this
708 molecular signature, we also identify a nearly invariant basic residue at +4 (**Figure 6D**). We
709 also observe basic residues to be favored at -4, -3, +1, and +3, while hydrophobic interactions
710 are favored at positions -7, -5, -1, +5, and +7. However, due to the relative heterogeneity of
711 residues found at these positions, they likely modulate HP1a interactions, as we showed
712 previously for positions +1 and +3. Instead, we propose an enrichment of 3-6 basic residues
713 between positions -4 to +4 as a key signature of HACs (**Figure 6D**). Additionally, no acidic

714 residues are found at -6, -3, -1, +1 and +5, and no aromatic residues are located at -4 and +6,

715 suggesting these are detrimental to HAC function.

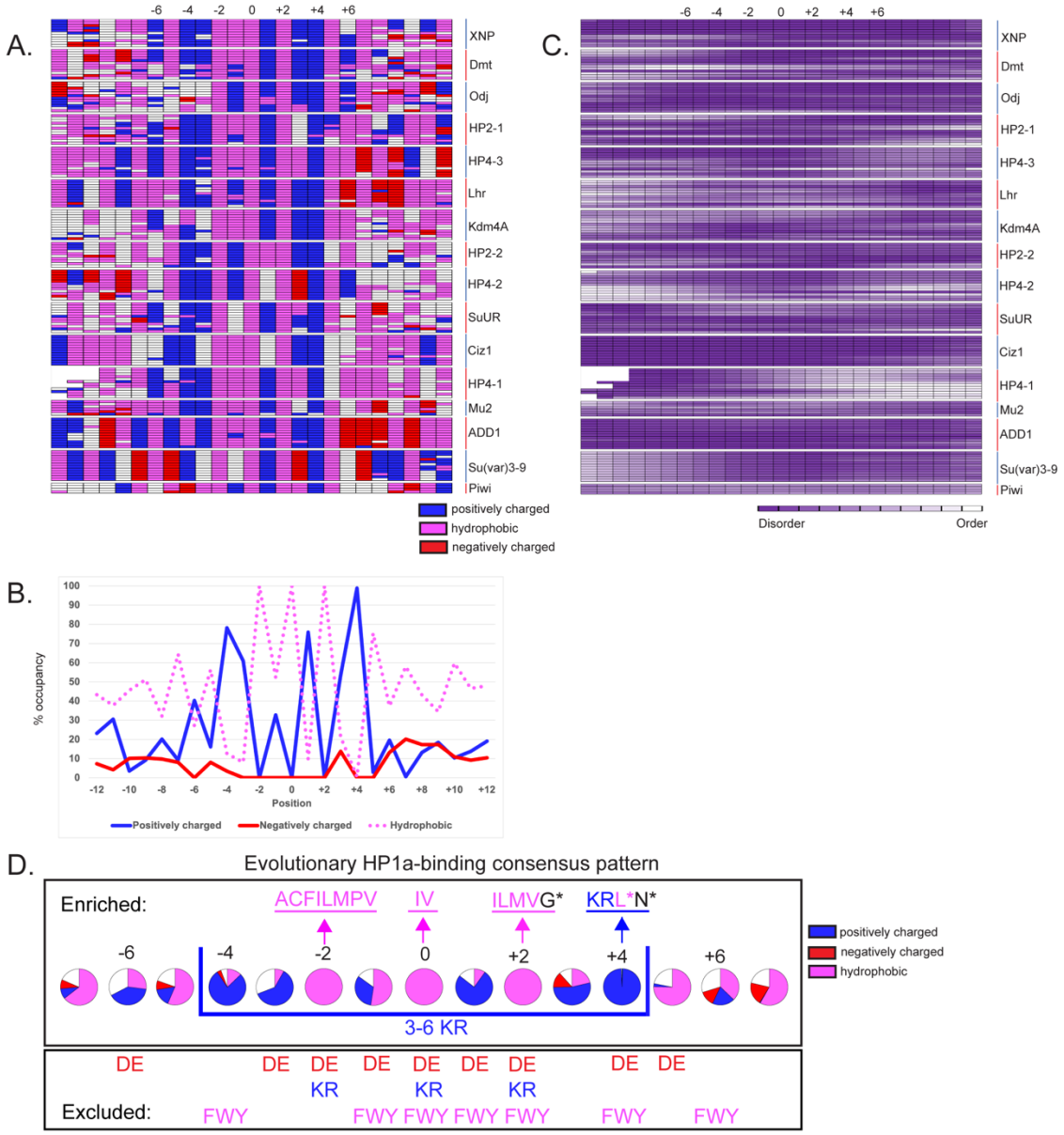

716

717 **Figure 6** (A) Compilation of alignments for each HAC homolog across Drosophila evolution
718 showing positioning of basic (red), hydrophobic (blue), and acidic (green) residues. Position
719 numbers are indicated on the top and gene names are provided on the right of each stack of
720 alignments. (B) Percent occupancy of basic (red), hydrophobic (dotted), and acidic (green)
721 residues is calculated across Drosophila evolution for each position in all HACs. (C)
722 Compilation of disorder prediction scores are shown for each position across evolution for each
723 HAC. (D) Diagram of the evolutionarily conserved HAC molecular signature shows amino

acids compatible for specific positions (top row), incompatible amino acids (second row), sidechain group bias (third row).

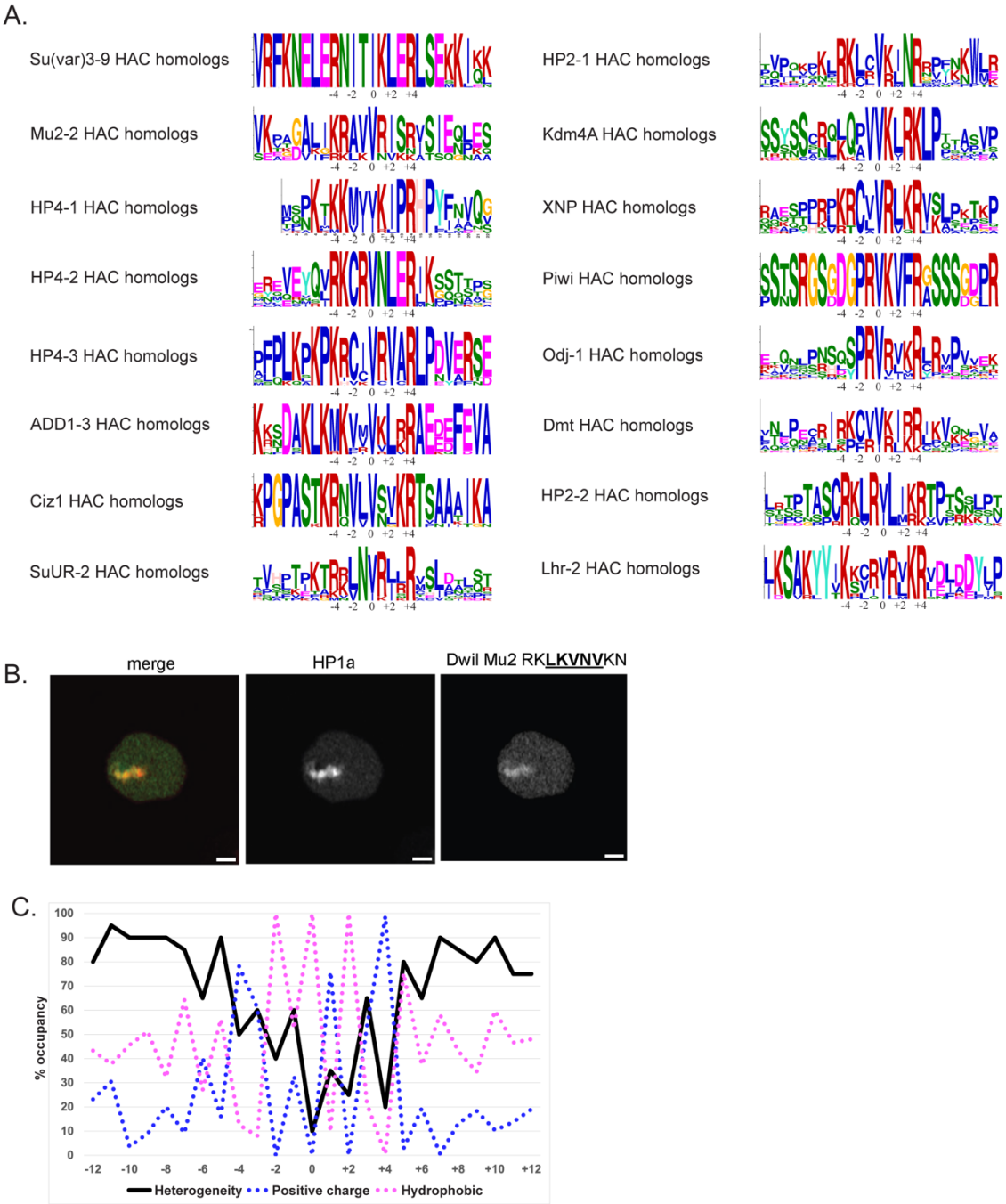

Supplementary Figure 6. (A) HAC sequence pileup using MEME Suite 5.5.7 showing high conservation of specific residues among each group of homologs. (B) Imaging panels showing enrichment of putative Mu2 HAC from *Drosophila willistoni* containing a unique Asn+4. Scale bar = 1 um. (C) Positional bias for basic (red dots) and hydrophobic (blue dots) residues across Drosophila evolution of HACs is contrasted with the heterogeneity of amino acids (purple) for

732 each position.
733
734 Previously, we showed that the PxVxL motif based on known HP1a-binding sites is found in
735 nearly half of all proteins, including those annotated to be in the nucleus or chromosomes
736 **(Supplementary Figure 1B)**. In contrast, the updated HAC molecular signature reduces the
737 number of potential candidates over 10-fold, even without accounting for disorder content
738 **(Figure 7A)**. GO analysis of the proteins that contain sequences matching the updated HAC
739 signature yielded heterochromatin and chromocenter as the top annotations (**Figure 7B**). In
740 contrast, these categories were not significantly represented among the protein hits for the
741 PxVxL motif search, indicating that our updated HAC signature vastly improves the prediction
742 of HP1a-binding motifs.
743
744 To test the ability of the updated HAC signature to identify *bona fide* HP1a binding sites, we
745 used a known HP1a interactor with no known binding sites, HP5, as a test case (**Figure 7C**).
746 We identified two sequences in HP5 that matched our updated HAC signature (marked in pink),
747 whereas 6 other sequences fit a more inclusive search comprised of a hydrophobic-x-valine-x-
748 aliphatic signature (marked in yellow). HP5 was then subjected to a systematic fragment
749 analysis to identify functional HP1a-binding regions in an unbiased manner, using imaging for
750 HP1a co-localization as the readout (**Figure 7C**). Our results showed that only fragments
751 containing the two binding sites predicted by our updated signature co-localized with
752 heterochromatin **(Figure 7D),** suggesting these sequences are *bona fide* HP1a-binding sites.
753 Imaging analysis of 25-mer peptides harboring these putative HACs displayed remarkably high
754 enrichment at HP1a domains **(Figure 7D)**. Whereas individual mutations of the central residues
755 of these two HACs (V159E or V294E) did not impact association of full-length HP5-PA with
756 heterochromatin **(Supplementary Figure 7)**, a double mutation (V159E and V294E)

757 dramatically reduced HP5 expression and abrogated all association with heterochromatin (see
758 longer exposure). Therefore, our results indicate that HP5 is completely dependent on the
759 predicted HAC motifs for associating with the HP1a condensate (**Supplementary Figure 7**).
760 In conclusion, we propose that this updated signature, when combined with disorder prediction
761 and conservation analysis, will be invaluable for identifying other HP1a interactors and
762 regulators of the heterochromatin biocondensate.

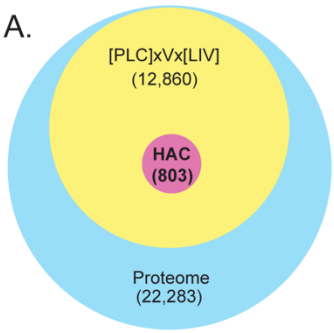

B.

GO Analysis

	HAC (803) FE	HAC (803) raw P-val	HAC (803) FDR	[PLC]xVx[LIV] (12,860)
Cellular component:				
chromocenter	9.76	4.34E-06	7.04E-04	N/S
heterochromatin	7.06	2.42E-08	1.04E-05	N/S
Biological process:				
regulatory ncRNA-mediated heterochromatin function	11.45	4.57E-05	4.80E-02	N/S

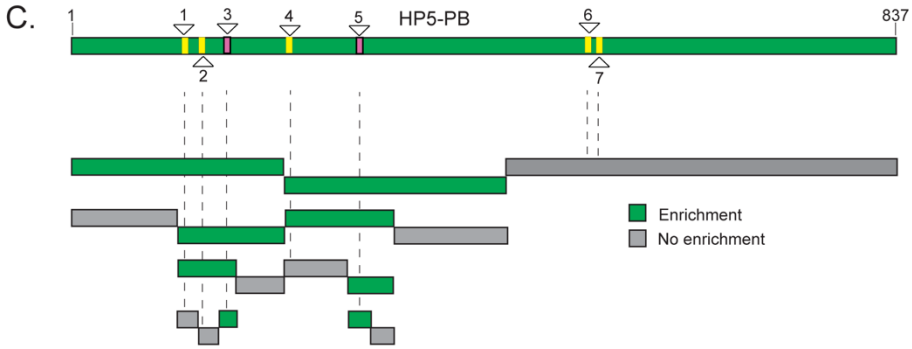

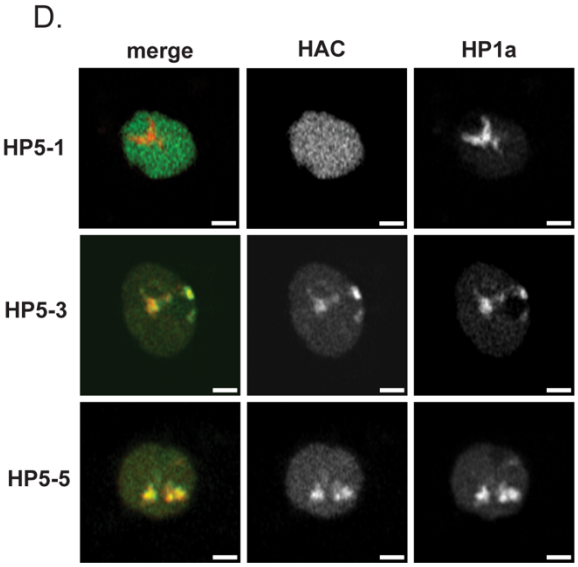

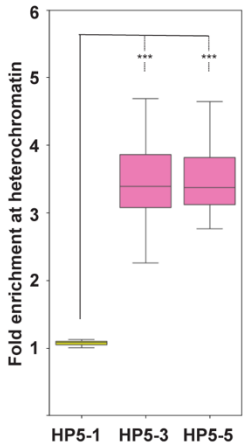

Figure 7: (A) Venn diagram showing the number of proteins harboring a PxVxL motif as defined by the indicated molecular signature versus those with the updated HAC signature. Compare with Supplementary Figure 1B. (B) GO analysis results showing the top annotations of "heterochromatin" and "chromocenter" among proteins containing the updated HAC signature, but not among proteins harboring the degenerate PxVxL motif; FE = fold enrichment above expected results, FDR = false discovery rate, N/S = not significant. (C) Diagram of HP5 isoform PB with locations of putative HP1a-binding sites based on either the PxVxL motif of hydrophobic-x-Val-x-hydrophobic (in pink) or the new HAC signature (in yellow) described in Figure 6B. Green rectangles indicate intact gene or fragments that show co-localization with HP1a in S2R+ cells after transient transfection; gray rectangles indicate lack of co-localization.

774 (D) Representative images showing enrichment of HAC candidate peptides at HP1a-enriched
775 heterochromatin (left). Quantification of HP1a co-enrichment of candidate HP5 HAC peptides
776 (right). Scale bars = 2 microns.

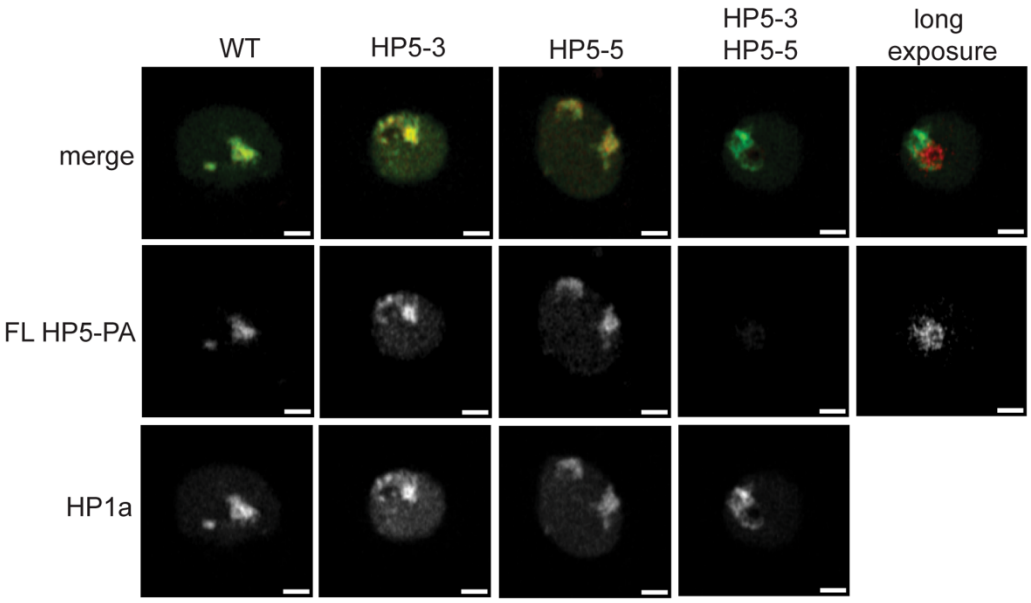

777
778 **Supplementary Figure 7.** Representative images showing enrichment of wildtype or mutant
779 full-length HP5-PA isoform at HP1a biocondensates. A longer exposure of the HP5 double
780 mutant was necessary to visualize the loss of HP1a co-enrichment and accumulation at
781 nucleoli. Scale bars = 2 microns.
782

783 **DISCUSSION:**

784

785 The HAC motif provides a widespread and evolutionarily conserved mechanism for HP1a
786 binding and targeting of the heterochromatin domain. The results of this investigation expand
787 our understanding of this HP1a-binding motif by exposing (1) the range of degeneracy of the
788 core hydrophobic sequences that insert into the CSD dimer cleft, (2) the requirement of basic
789 residues to stabilize HP1a association in Drosophila, and (3) the molecular interactions that
790 modulate HAC affinity with the HP1a CSD and C-terminal tail. This led to expansion and
791 modification of the original pentameric PxVxL motif into a larger consensus region **(Figure**
792 **6D)** consisting of 3-6 positively charged residues that interlace and surround a core of three

793 alternating hydrophobic residues containing a central valine or isoleucine. This 9-mer basic
794 consensus pattern is further flanked by a moderate frequency of both hydrophobic and
795 positively charged residues, as well as low frequency of negatively charged and aromatic
796 residues, over a 15-mer span that, altogether, generate the molecular interface for binding to
797 the HP1a CSD dimer and CTE.
798
799 The HAC signature was determined through positional analysis of 6 previously identified
800 PxVxL sequences in *Drosophila melanogaster*, 10 more sequences identified from HP1a-
801 binding proteins through this study, and 157 sequences acquired from alignments of HP1a
802 partner homologs in 11 other Drosophila species. We note that though most of the HAC
803 homologs were untested in the peptide imaging assay, the positional and sequence conservation
804 between most HAC homologs were readily distinguished in alignments, suggesting that
805 protein-specific molecular interactions between HAC and HP1a are preserved between species.
806 For example, the Su(var)3-9 HAC is 100% identical over its 15-mer length among 12 species
807 of Drosophila, and the HP2-1 HAC is distinctive for containing a highly conserved Asn at the
808 +3 position (**Supplementary Figure 6A**). We also validated the HP1a co-enrichment of 4 HAC
809 homologs that represent some of the more divergent sequences (**Supplementary Figure 6B**).
810 Finally, the HAC-interacting residues of the HP1a CSDs and C-termini are preserved among
811 all Drosophila species included in this study (**Supplementary Figure 8A**). For these reasons,
812 we conclude that HAC homologs represent functionally conserved HP1a-binding domains that
813 greatly inform the HAC consensus signature. We do note that the high similarities in amino
814 acid sequences within each group of HAC homologs cause overrepresentation of specific
815 residues in the consensus analysis. Therefore, a more refined signature could be achieved
816 through the inclusion of more homologs from other Drosophila species or discovery of more

817 HACs in other HP1a-binding proteins.

818

819 Another predominant feature of HACs is their location within or in proximity to intrinsically
820 disordered regions of proteins. Disorder prediction was conducted using the widely used
821 PONDR VL-XT algorithm that integrates three neural networks trained on long (40+ residues),
822 N-terminal, and C-terminal disordered regions of X-ray crystallographic data (Li *et al.*, 1999;
823 Romero *et al.*, 2001). Though we cannot rule out the possibility that some HACs are located
824 on exposed surfaces of globular secondary structures, we hypothesize that HAC association
825 with intrinsically disordered domains confers flexibility and accessibility (Holehouse and
826 Kragelund, 2024) that may be important for targeting the CSD dimer. The AlphaFold-Multimer
827 model for the non-functional HAC candidate ADD1-1, which is predicted to contain a highly
828 ordered structure, fails to position the central hydrophobic core of ADD1-1 at the center of the
829 HP1a CSD dimer (**Supplementary Figure 8B**), despite containing a canonical motif (PxVxL).
830 The binding region exhibited lower prediction confidence (pLDDT < 50) than functional
831 peptides that contain highly disordered regions (pLDDT scores > 90). These structural
832 prediction results suggest that the flexibility of the peptide, attributed to its disordered regions,
833 may be necessary for proper fitting within the HP1a CSD dimer. We also detect the
834 conservation of disorder correlation among putative HACs of other Drosophila species. HACs
835 may therefore represent short linear motifs (SLiMs) or molecular recognition features (MoRFs)
836 within disordered regions that mediate diverse functions (Hsu *et al.*, 2013). Unlike well-defined
837 globular structures, SLiMs and MoRFs possess weaker conservation due to the higher mutation
838 rates found in disordered regions. Nevertheless, we identified positional biases in the
839 surrounding residues of the central hydrophobic core of HACs that contribute to HAC binding
840 with HP1a (**Figure 6D**). Aside from the functional role of flanking basic residues in modulating

841 interactional strength with HP1a, we also observed a strong bias against acidic and aromatic
842 residues when basic ones are absent, suggesting that their presence at these positions interfere
843 with HAC function. Additionally, the location of HACs at highly mutable disordered domains
844 and at paralogous locations in some protein homologs indicates that HACs may undergo
845 relatively rapid evolutionary selection but become stably inherited once established. Our
846 findings highlight the functional importance of intrinsically disordered domains as sites for
847 protein targeting and the evolution of HACs.
848
849 Our findings also expand the molecular signature of the original PxVxL motif that forms the
850 hydrophobic core of functional HACs. Though a trio of alternating hydrophobic residues is the
851 classical feature of the PxVxL motif, there is currently confusion regarding the types of
852 hydrophobic residues that can occupy each position in the motif, and whether this pentamer is
853 sufficient for HP1a binding (Lechner *et al.*, 2005; Meyer-Nava *et al.*, 2020). Our search for the
854 HAC molecular signature uncovers the range of amino acids that occupy each position of the
855 hydrophobic core residues. Expectedly, we identified mostly valines at the central position of
856 HACs, extending the previous structural prediction that only valine can be accommodated by
857 the hydrophobic pocket of the Drosophila HP1a CSD dimer (Thiru *et al.*, 2004). However, we
858 also identified isoleucines at the central positions of Su(var)3-9 and Lhr HACs of Drosophila
859 melanogaster, as well as in HACs of other homologs. Mutation of the central valine residue to
860 glutamate or alanine has previously been shown to eliminate HP1a binding, and we
861 demonstrate that mutation of a central isoleucine of a HAC similarly abrogates heterochromatin
862 targeting (**Supplementary Figure 1C**). Meanwhile, we identify that the -2 position utilizes a
863 much wider variety of hydrophobic residues, including polar cysteines, bulky phenylalanines,
864 and conformationally rigid prolines. Conservation analysis of HACs across Drosophila

865 evolution suggests that only the smallest and largest sidechain volumes of hydrophobic
866 residues are excluded at the -2 position, namely glycine, tyrosine, and tryptophan. Additionally,
867 our MD simulation shows that the sulfur in the cysteine sidechain at this position provides an
868 additional hydrogen bond that may enhance HP1a binding. In contrast, we identify only small
869 hydrophobic residues such as leucine, valine, and isoleucine to occupy the +2 position, though
870 alignment analysis also identifies rare homologs containing glycine and methionine instead.
871 This suggests that the +2 position is more sterically restrictive to larger hydrophobic residues
872 compared to the -2 position. Altogether, this trio of residues comprise an asymmetric
873 hydrophobic plug that is essential to recognize the conformation of the CSD dimer pocket, but
874 which we also show is insufficient to target heterochromatin effectively *in vivo*. Our HAC
875 fragment analysis (**Figure 3**) not only showed that the hydrophobic pentamer is insufficient for
876 heterochromatin targeting, but also that the flanking 5 residues on each side of the pentamer
877 are crucial for stable HAC association with heterochromatin.
878
879 Finally, we determined that electrostatic interactions are required for effective HAC-HP1a
880 dimer binding, in addition to hydrophobic interactions. Despite clear exceptions, it is
881 remarkable that there is a clear correlation between predicted Coulombic energy and measured
882 fold-enrichment (**Figure 4D**), given the higher complexity of *in vivo* conditions and potential
883 contributions from other factors not included in the simulations. In fact, the exceptions are
884 informative about potential complexities in HP1-partner interactions. For example, Lhr-2 has
885 larger attractive Coulomb energy (**Figure 4D**) but also greater hydrophilic surface areas than
886 higher-ranked HP2-1 and HP4-3 peptides (**Figure 4B, Supplementary Figure 4D**). This
887 suggests Lhr-2 contains a less stable hydrophobic pocket that could weaken HP1a interactions,
888 despite its high electrostatic energy. Meanwhile, other exceptions, such as HP2-1, HP4-3, and

889 Kdm4A, show high fold enrichment values despite lower Coulomb energy compared to other
890 HACs (**Figure 4D**). HP2-1 possesses L-2, V0, and I+2, the top three amino acids on the
891 hydropathy index (Kyte and Doolittle, 1982), whereas HP4-3 exhibits high hydrophobicity at
892 L+5, and Kdm4A displays significant hydrophobicity at the flanking region, specifically at L-
893 4 and L+5 (**Supplementary Figure 8C**). These peptides likely engage in more hydrophobic-
894 driven interactions that compensate for their lower electrostatic energy. We should also note
895 that electrostatic and hydrophobic interactions can negatively affect each other and be
896 competitive (Dzubiella and Hansen, 2003, 2004; Wang, Friesner and Berne, 2010). For
897 example, the Dmt HAC had weaker attractive Coulomb energy at the +1 and +4 positions than
898 XNP and Piwi, likely due to the presence of isoleucine, which has the highest hydropathy index
899 (Kyte and Doolittle, 1982), at the adjacent +2 and +5 positions (**Supplementary Figure 8D**).
900 Electrostatic interactions from the +1 and +4 positively charged amino acids are key
901 contributors to the HAC and CSD interaction (**Figure 5**). These results suggest that HAC
902 peptides and CSD dimer interactions are mediated by both hydrophobic and electrostatic
903 interactions, and that maintaining a moderate balance between hydrophobicity and charge is
904 crucial to prevent competition between these types of interactions. Therefore, the contributions
905 of electrostatic and hydrophobic interactions vary between HACs, and such structural
906 flexibility could provide the variations in HP1a affinity that are important for each
907 heterochromatin protein function.
908
909 Conservation analysis and MD simulations both indicate that positions -4, -3, -1, +1, +3, and
910 +4 contain a strong bias for basic residues (lysine or arginine) that make electrostatic
911 interactions with the HP1a CSD and C-terminal tail. In particular, we showed that the positively
912 charged amino acids ±4 form a salt bridge interaction with Asp157 (**Figure 5A, B**). The

913 positively charged amino acid at +1 plays an important role in maintaining the electrostatic
914 force field by forming an H-bond with Arg197 of the CSD dimer and enabling the +3 positively
915 charged amino acid to form salt bridges with Asp203 and Glu205 of the CSD (**Figure 5C, D,**
916 and **E**). Additionally, we identified compensatory mechanisms when specific electrostatic
917 interactions are absent at a given locus (+1, +3) (**Figure 5D, F**). The high conservation of
918 positive charges in Drosophila HACs is made possible by the absolute conservation of
919 interacting residues in Drosophila HP1a homologs, namely Asp157 of the CSD and Asp203
920 and Glu205 of the C-terminal tail (**Supplementary Figure 8A**). Acidic residues at positions
921 157 and 203 are also observed in HP1a homologs of humans, frogs, and fish, suggesting that
922 HACs of these organisms also utilize basic residues for targeting heterochromatin
923 (**Supplementary Figure 8E**). We note that, though HP1 C-terminal tails between these
924 homologs are highly variable in length and sequence, they nevertheless are highly enriched for
925 acidic residues that may partner with different positions of HACs for electrostatic interactions.
926 We therefore propose that the inclusion of 3-6 basic residues within HAC positions -4 to +4 is
927 an integral part of the HAC molecular signature in Drosophila HP1a, which may vary in content
928 and position in non-Drosophila HACs.

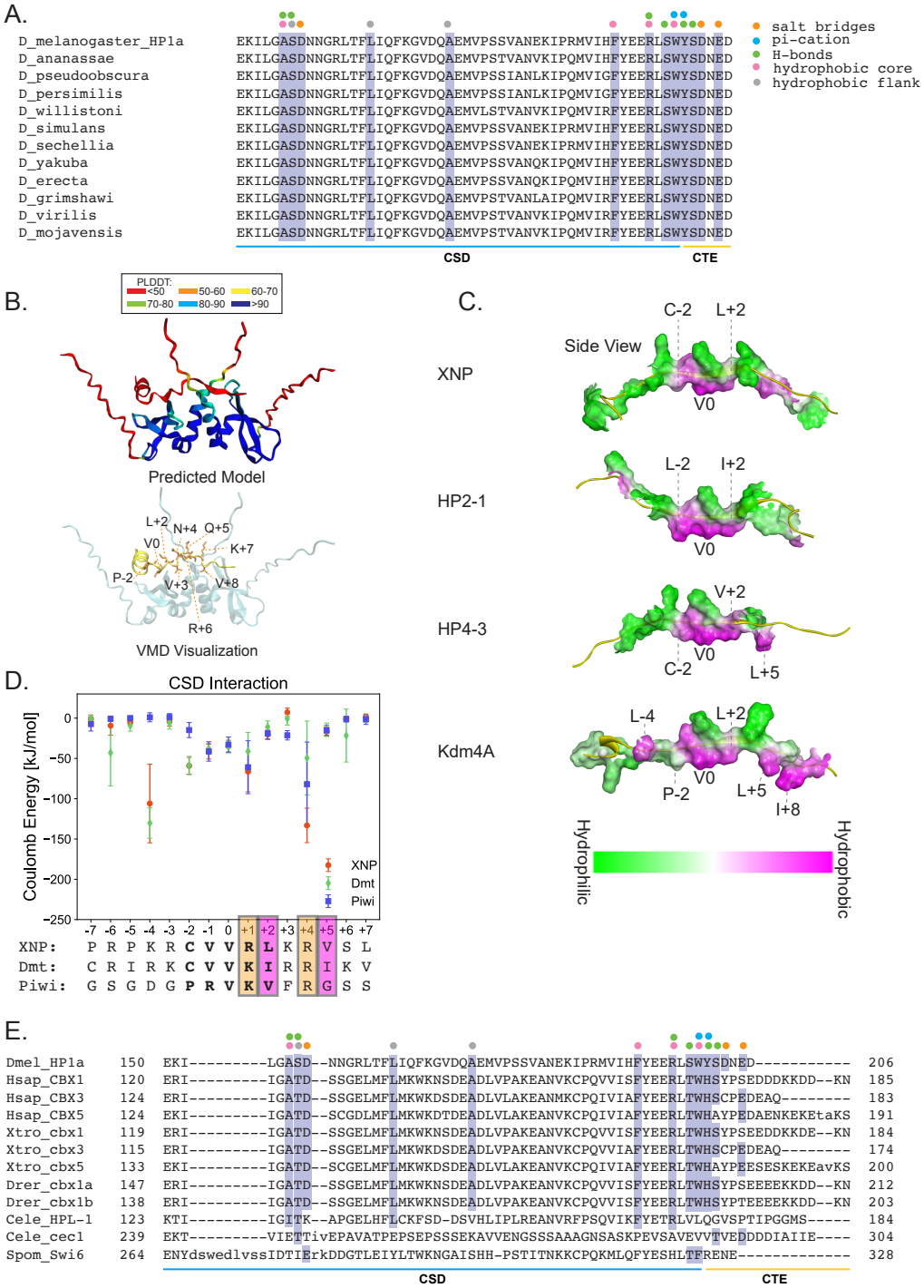

Supplementary Figure 8: (A) Alignment of CSD and C-terminal tails of *D. melanogaster* HP1a homologs with other Drosophila species. Salt bridge-forming residues are marked with orange dots, pi-cation residues in blue, hydrogen bonds in green. Residues that interact with the hydrophobic core of HACs are marked with pink dots, whereas those that interact with flanking hydrophobic residues are marked with purple dots. Conservation is marked with purple highlight. HP1a CSD and CTE regions are marked with blue and yellow lines, respectively. (B) The Alphafold Multimer-predicted computational model (top) and VMD-visualized image of the model for the CSD dimer with C-terminal tails and ADD1-1 (bottom). The Alphafold Multimer-predicted structure is colored based on pLDDT (predicted local

939 distance difference test) scores. Red: pLDDT<50, Orange: 50<pLDDT<60, Yellow:
940 60<pLDDT<70, Green: 70<pLDDT<80, Skyblue: 80<pLDDT<90, and Blue: 90<pLDDT.
941 CSD homodimer and the ADD1-1 are colored cyan and yellow, respectively. Residues at the -
942 2, 0, +2, +3, +4, +5, +6, +7, and +8 positions (in licorice drawing style) are colored orange,
943 with the amino acid code indicated. (C) Visualization of surface hydrophilicity and
944 hydrophobicity of XNP, H2-1, HP4-3, and Kdm4A in the side view were calculated using the
945 Discovery Studio software. The hydrophilic to hydrophobic properties are colored from blue
946 to brown. Each peptide is colored yellow. (D) Coulomb energy ± SD [kJ/mol] among the CSD
947 dimer and -7 to +7 residues of XNP, Dmt, and Piwi. Orange circle: XNP, Green diamond: Dmt,
948 and Blue square: Piwi. Electrostatic sequences at +1 and +4 are highlighted in orange;
949 hydrophobic sequences at +2 and +5 are highlighted in pink. (E) Alignment of CSD and C-
950 terminal tails of *D. melanogaster* HP1a with homologs from other species, including Homo
951 sapiens, Xenopus, zebrafish, worm, and yeast, using a similar format as shown in (A).

952

953 Variations in the number and positions of basic residues in different HACs indicate that they
954 act to modulate HP1a interactional strength. Though it is possible that there are HACs with
955 fewer basic residues, we predict that these will exhibit a much lower affinity for HP1a and
956 cannot be detected by our live imaging assay. Identification of an even more refined molecular
957 signature may also be achieved with a wider conservation analysis beyond the 12 Drosophila
958 species used here and more MD analysis for other types of peptides. To closely examine the
959 molecular interactions of a HAC, we used the highest-enriching sequence of XNP to be a model
960 peptide, by combining visualizations of interactions for residues from -7 to +7 with statistical
961 observations of the MD simulations (**Figure 5I** and **Supplementary Figure 5I**). The last frame
962 was initially used to make the interaction map, which was then adjusted by comparing it with
963 the statistical results, such as Coulomb energy, to obtain a more accurate interpretation. Based
964 on the interaction map, conservation analysis, and Coulomb energy, we can infer that the HAC
965 positions between -4 and +4 form the strongest molecular interactions, extending the
966 previously recognized 5-mer signature of PxVxL. As shown in **Figure 5I**, each amino acid has
967 distinct roles in the interactions between the peptide and the CSD dimer+CTE, and these roles
968 can change depending on the neighboring sequences. We note, for example, that homologs of

969 each HAC tend to possess additional conserved molecular features within their group that are
970 beyond the HAC consensus sequence (**Supplementary Figure 6A**), pointing to protein-
971 specific HP1a interfaces. A more comprehensive mutational study of such protein-specific
972 residues could uncover additional mechanisms of peptide interaction. Alternatively, factors
973 other than hydrophobicity and electrostatic forces could also be contributing to HAC-HP1a
974 interactions, such as post-translational modifications of peptides or HP1a.
975
976 But why would an affinity hierarchy exist for protein interactions with HP1a? HAC structures
977 likely reflect the specific requirements of heterochromatin proteins to achieve different levels
978 of enrichment or mixing in heterochromatin. For example, rare proteins may contain high-
979 affinity HACs for efficient targeting, whereas more abundant proteins, or those containing
980 additional domains that interact with other heterochromatin factors, will not require such high
981 affinity. Alternatively, structurally important heterochromatin proteins likely contain HACs
982 that stably associate with HP1a, whereas enzymes or proteins that only interface transiently
983 with heterochromatin may require lower affinities. For example, HP5 with its two strong HACs
984 could form highly stable heterochromatin structures or even crosslink two HP1a dimers,
985 whereas the Su(var)3-9 methyltransferase likely requires only transient association with HP1a
986 as its chromodomain is expected to bind H3K9me2/3 in heterochromatin (Müller *et al.*, 2016).
987 HAC affinities could therefore facilitate how HP1a organizes heterochromatin architecture by
988 directing the activity of multiple complexes to execute diverse functions in this complex,
989 dynamic biocondensate.
990
991 A hallmark of biocondensates is the accumulation of multivalent interactions between their
992 constituents to drive partitioning from the surrounding environment (Banani *et al.*, 2017). In

993 heterochromatin, this is achieved by the relatively abundant HP1 protein that centrally
994 organizes the accumulation of other structural condensate proteins through its abilities to bind
995 the heterochromatin-specific histone mark H3K9me2/3, homodimerize, and recognize HACs
996 (Janssen, Colmenares and Karpen, 2018). This inherent demixing ability also effectively
997 diminishes, if not outright excludes, other nuclear proteins from the condensate (Banani *et al.*,
998 2017). Nevertheless, the underlying heterochromatic DNA polymer is not precluded from pan-
999 nuclear processes such as transcription, replication, and repair. Therefore, heterochromatin
1000 must either (1) employ dedicated factors to carry out such functions, (2) recruit factors from
1001 such processes to access the interior, (3) transiently or locally dismantle the condensate for said
1002 processes to proceed, or 4) a combination of these mechanisms. HACs can provide the means
1003 to carry out at least the first two potential mechanisms, though controlled destabilization of
1004 heterochromatin may also utilize an activatable HP1a-interacting protein. The HAC-containing
1005 proteins SuUR and Mu2 appear to represent such factors that regulate DNA replication and
1006 repair in heterochromatin, respectively, as SuUR is known to suppress polytenization of
1007 heterochromatic domains (Belyaeva *et al.*, 2006) and Mu2 is an early DNA damage marker
1008 that recruits downstream repair proteins (Dronamraju and Mason, 2009).
1009
1010 HACs contribute to the multivalency of heterochromatin by facilitating the mixing of HP1a
1011 with multiple proteins. Conversely, HP1a CSD dimerization is enhanced through binding
1012 HACs, as has been previously shown with HP2-1 and Piwi peptides (Mendez *et al.*, 2011).
1013 Whether higher HP1a affinity correlates with enhanced dimerization is currently unknown, but
1014 HACs with different binding strengths, in combination with properties of linked domains in
1015 full length versions, could regulate heterochromatin condensate formation, dissolution, and/or
1016 material properties. Interestingly, mammalian HP1 phase separation properties were shown to

1017 be differentially regulated by 2 different PxVxL-containing peptides, further indicating that
1018 HAC-binding alters the biophysical properties of HP1 directly (Larson *et al.*, 2017). Our results
1019 also indicate that HACs show enrichment throughout the heterochromatin domain, even though
1020 the full-length proteins encoding certain HACs, such as SuUR and XNP, normally display
1021 smaller subdomains of enrichment within heterochromatin (Swenson *et al.*, 2016). Subdomain
1022 formation within heterochromatin must therefore be mediated by the concerted action of HACs
1023 and other types of interaction domains present in full length proteins. One possible mechanism
1024 is that such proteins utilize HACs to gain access to the heterochromatin interior and then,
1025 through strong self-interacting domains or protein partners, form subdomain condensates
1026 within heterochromatin. Through a similar pairing of self-interacting domains and particularly
1027 weak affinity HACs, other nuclear bodies, such as those that facilitate transcription, replication,
1028 and repair, may also gain access to the heterochromatin periphery that, upon activation, seed
1029 the formation of complexes to carry out functions (Rajshekar *et al.*, 2023).
1030
1031 We foresee that our improvements in identifying HAC molecular signatures will help identify
1032 such 'seed' components for various nuclear processes, as well as focus attention on intrinsically
1033 disordered regions of various proteins to contain access codes to different biocondensates in
1034 the nucleus (King *et al.*, 2024). Whether all condensates contain short linear motifs to facilitate
1035 the targeting of their components is not known, but our experimental and computational
1036 approaches could provide a framework to identify molecular grammar utilized by other types
1037 of biocondensates. Based on our findings with HACs, we propose that affinity hierarchies by
1038 short disordered motifs may comprise a general mechanism by which various biocondensates
1039 coordinate structural and transient components, as well as access shared nuclear components
1040 and even interface with other condensates.

1041

1042 **ONLINE METHODS**

1043

1044 **Plasmid Construction**

1045 Oligonucleotides of putative HAC sequences (IDT) were cloned into a pCOPIA vector
1046 containing a N-terminal mNeonGreen fluorescent tag and a myc nuclear localization signal.
1047 HACs used for testing variable lengths of flanking sequence contained GGGSG in place of
1048 sequences -12 to -8 and lacked positions +8 to +12, or GGGSGGSGGG in place of -12 to -3
1049 and lacked positions +3 to +12. Corresponding control constructs contained GGGSG or
1050 GGGSGGSGGG after the mNeonGreen tag and myc NLS. Full-length genes for HP1a, XNP,
1051 SuUR, Lhr, Su(var)3-9, HP4, Mu2, and HP5, along with HP5 gene fragments, were cloned into
1052 pCOPIA vectors containing N-terminal mCherry, mScarlet-1, mCitrine, or mGFP fluorescent
1053 tags as described previously (Colmenares *et al.*, 2017). Mutants for HACs and full-length genes
1054 were generated using a one-step directed mutagenesis protocol (Liu and Naismith, 2008).

1055

1056 **Bioinformatics**

1057 25-amino acid sequences containing a central pattern of hydrophobic-x-Val/Ile-x-hydrophobic
1058 consensus were identified as putative HACs using custom Perl scripts. Hydrophobic residues
1059 included Ala, Cys, Phe, Ile, Leu, Met, Pro, Val, Trp, and Tyr, whereas x = any amino acid.
1060 Homologs of *Drosophila melanogaster* protein sequences were obtained using standard NCBI
1061 protein-protein BLAST by retrieval of sequences with the highest homology scores for each of
1062 the other 11 species of Drosophila (taxid:7215), using the non-redundant protein database.
1063 Conservation of putative HACs was determined by testing whether the same consensus pattern
1064 is detected to align with the putative *Drosophila melanogaster* HAC sequence after multiple

1065 sequence alignment of full-length homologous proteins with Clustal Omega (Madeira *et al.*,
1066 2024). Initially, only sequences containing a hydrophobic-x-Val/Ile-x-hydrophobic pattern that
1067 spatially aligned with the putative Drosophila melanogaster HAC, as determined by Clustal
1068 Omega with default settings, were scored positively to be conserved (see Supplementary Figure
1069 2) and are shown on Figure 2. However, re-analysis of HP1a-binding protein homologs for the
1070 final HAC consensus motif (see below) revealed additional putative HAC sequences in other
1071 parts of SuUR, Mu2, and HP2 homologs that do not align with the Drosophila melanogaster
1072 HAC and may represent paralogous HACs. These additional sequences were included in the
1073 analysis for Figure 6 and Supplementary Figure 6. Disorder prediction was analyzed using
1074 PONDR-VLXT (Romero *et al.*, 2001). Positional frequency of each amino acid was analyzed
1075 among groups of HACs using custom Perl scripts. The final HAC consensus used for motif
1076 search from positions -7 to +7 are as follows: [^WF] [^DEW] [^WY] [^STFWY] [^DEFW]
1077 [FPLICVMA] [^DEFWY] [VI] [^DEFWY] [LIVGM] [^WY] [KRLN] [^DEW] [^FWY],
1078 where brackets contain all possible amino acids at each position, or all the excluded amino
1079 acids if marked with "^."
1080

1081 **Tissue culture manipulation and image acquisition**

1082 S2R+ embryonic tissue culture cells were maintained in Schneider's medium (Thermo) with
1083 10% fetal bovine serum (Gemini) and 1% antibiotic-antimycotic (Gibco) at 25°C. Transient
1084 co-transfections with mNeonGreen-tagged constructs and mScarlet-I-tagged HP1a were
1085 conducted using the TransIT-2020 reagent (Mirus). Cells were mounted 72 hours later on
1086 chambered coverslip slides (Ibidi) and live imaging was performed using a Zeiss LSM880
1087 Airyscan microscope with 63X oil immersion objective at room temperature. A mNeonGreen
1088 tag containing only a myc NLS was co-transfected with mScarlet-I-HP1a as a negative control.

1089 Transient co-transfections of fluorescently-tagged full-length HP1a-interacting proteins with
1090 HP1a were similarly conducted and images were collected using an Applied Precision
1091 Deltavision microscope or a Zeiss LSM880 Airyscan microscope with 63X oil immersion
1092 objective. All results are based from at least two biological replicates.
1093

1094 **Image analysis**

1095 Raw images from the Zeiss Airyscan were processed using ZEN black edition software,
1096 whereas Deltavision images were processed using SoftWoRx. All representative manuscript
1097 images were formatted using Fiji software. To calculate heterochromatin enrichment, 3-D
1098 Airyscan images of HP1a were segmented into nucleus, chromocenter, and nucleolus volume
1099 masks by manually setting the intensity thresholds in Arivis Vision4D software. A low
1100 intensity threshold setting selected the nucleus, a high setting was used to segment the
1101 chromocenter, while the negative space lacking HP1a signal adjacent to the chromocenter was
1102 isolated by the subtraction of HP1a nuclear masks with holes from those without holes. The
1103 nucleolar mask was dilated 3-4 pixels to avoid potentially measuring nucleolar intensity signal
1104 of mNeonGreen, which sometimes accumulated in the nucleolus in certain constructs,
1105 including the negative control. The mean chromocenter signal intensity of mNeonGreen was
1106 therefore measured only in chromocenter regions that did not overlap the dilated nucleolar
1107 volume, and its chromocenter enrichment was calculated by dividing the mean chromocenter
1108 intensity with the mean nuclear intensity. 10-36 nuclei were measured for each construct tested
1109 from 2 biological replicates. Student's t test, assuming two-sample tails and unequal variance,
1110 was calculated.
1111

1112 **Alphafold Multimer-predicted computational model**

1113 AlphaFold-Multimer (Evans *et al.*, 2022) was employed to develop the computational models
1114 of the HAC peptide and HP1a CSD dimer with C-terminal tails. The sequences for the
1115 Drosophila HP1a CSD dimer with C-terminal tails and flanking residues, sourced from the
1116 protein database (PDB ID: 3P7J) (Mendez *et al.*, 2011), served as inputs for AlphaFold-
1117 Multimer computational model predictions:
1118 MKKHHHHHHEQDTIPVSGSTGFDRGLEAEKILGASDNNGRLTFLIQFKGVDQAEMV
1119 PSSVANEKIPRMVIHFYEERLSWYSDNEDKK. The 16 heterochromatin-enriched peptides
1120 identified by our experiments (**Figure 1E**) were selected for computational modeling to
1121 investigate the key features of the HP1a-peptide binding. The 25-amino-acid sequences for all
1122 16 peptides are shown in Supplementary Method Table 1. The "pdb100" was used for the
1123 template mode. The model type was set to "alphafold2_mmultimer_v3". The highest-ranked
1124 model for each peptide, based on pLDDT (predicted Local Distance Difference Test) scores,
1125 was used for the following computational analysis. All predicted models, except for Odj-1,
1126 showed high pLDDT (predicted Local Distance Difference Test, scaled 0-100) and pTM
1127 (predicted Template Modelling, scaled 0-1) scores, representing confidence in the local and
1128 overall structure of the complex, respectively (**Supplementary Method Table 1**). The 15 out
1129 of 16 peptide models positioned their central core region at the center of the CSD dimer (**Figure**
1130 **3A, Supplementary Figure 3A-O**). While the disordered edge regions of the complex showed
1131 low prediction accuracy, the key binding sites between the peptide and CSD dimer had very
1132 high confidence with over 90 pLDDT scores (**Supplementary Figure 3A-O**). Odj-1 was the
1133 only model that mispositioned the peptide and had low prediction accuracy even in the binding
1134 sites with 60-80 pLDDT scores. Due to its low prediction confidence, the Odj-1 model was
1135 excluded from further computational analysis. The 15 peptide models, except for Odj-1, were
1136 used for the following molecular dynamics simulation analysis.

Supplementary Method Table 1: The 25-amino-acid sequences of 16 heterochromatin-enriched peptides, with the central valine (V) designated as position 0. The table also includes AlphaFold-Multimer prediction scores: pLDDT (predicted Local Distance Difference Test, scaled from 0 to 100) and pTM (predicted Template Modelling, scaled from 0 to 1) were shown.

	Amino Acid Sequences																									Prediction Scores	
Peptide Name	-12	-11	-10	-9	-8	-7	-6	-5	-4	-3	-2	-1	0	1	2	3	4	5	6	7	8	9	10	11	12	pLDDT	pTM
XNP	R	A	E	S	P	P	R	P	K	R	C	V	V	R	L	K	R	V	S	L	P	K	T	K	P	76.7	0.706
Dmt	L	N	E	P	E	C	R	I	R	K	C	V	V	K	I	R	R	I	K	V	K	N	G	V	V	75.9	0.696
Odj-1	E	D	Q	N	F	P	N	R	Q	S	P	R	V	R	V	K	R	L	R	V	P	V	V	E	K	72	0.655
HP2-1	T	V	P	Q	N	I	S	P	R	K	L	C	V	K	I	N	R	R	P	Y	N	K	W	L	R	77.3	0.729
HP4-3	P	F	P	L	K	P	K	P	K	R	C	I	V	R	V	A	R	L	P	D	V	E	R	S	E	76.2	0.705
Lhr-2	L	K	S	A	K	Y	Y	I	K	R	C	R	I	R	L	K	R	V	E	I	D	D	Y	L	P	80.1	0.761
Kdm4A	S	S	Y	S	S	C	R	Q	L	Q	P	V	V	K	L	R	K	L	P	T	I	A	S	V	P	75.7	0.714
HP2-2	L	R	T	P	T	A	S	C	R	K	L	R	V	L	I	K	R	T	P	T	S	S	L	S	L	77.1	0.732
HP4-2	E	R	E	V	E	Y	Q	V	R	K	C	R	V	N	L	E	R	I	K	S	S	T	S	P	N	75.6	0.687
SuUR-2	T	V	H	L	T	P	K	T	R	R	L	N	V	R	I	L	R	V	S	L	D	T	L	S	T	77.6	0.735
Ciz1	K	P	G	P	A	S	T	K	R	N	V	L	V	S	V	K	R	T	S	A	A	A	I	K	A	75.4	0.719
HP4-1				M	S	P	K	T	K	K	M	I	V	K	I	P	R	H	P	Y	F	N	V	Q	G	78.6	0.727
Mu2-2	V	K	T	G	G	A	L	I	K	R	A	V	V	R	I	S	R	V	S	I	E	Q	L	E	S	77.8	0.732
ADD1-3	K	K	S	D	A	K	L	K	M	K	V	M	V	K	L	K	R	A	E	D	E	F	E	V	A	79.4	0.741
Su(var)3-9	V	R	F	K	N	E	L	E	R	N	I	T	I	K	L	E	R	L	S	E	K	K	I	K	N	78.2	0.74
Piwi	S	S	T	S	R	G	S	G	D	G	P	R	V	K	V	F	R	G	S	S	S	G	D	P	R	75.4	0.688

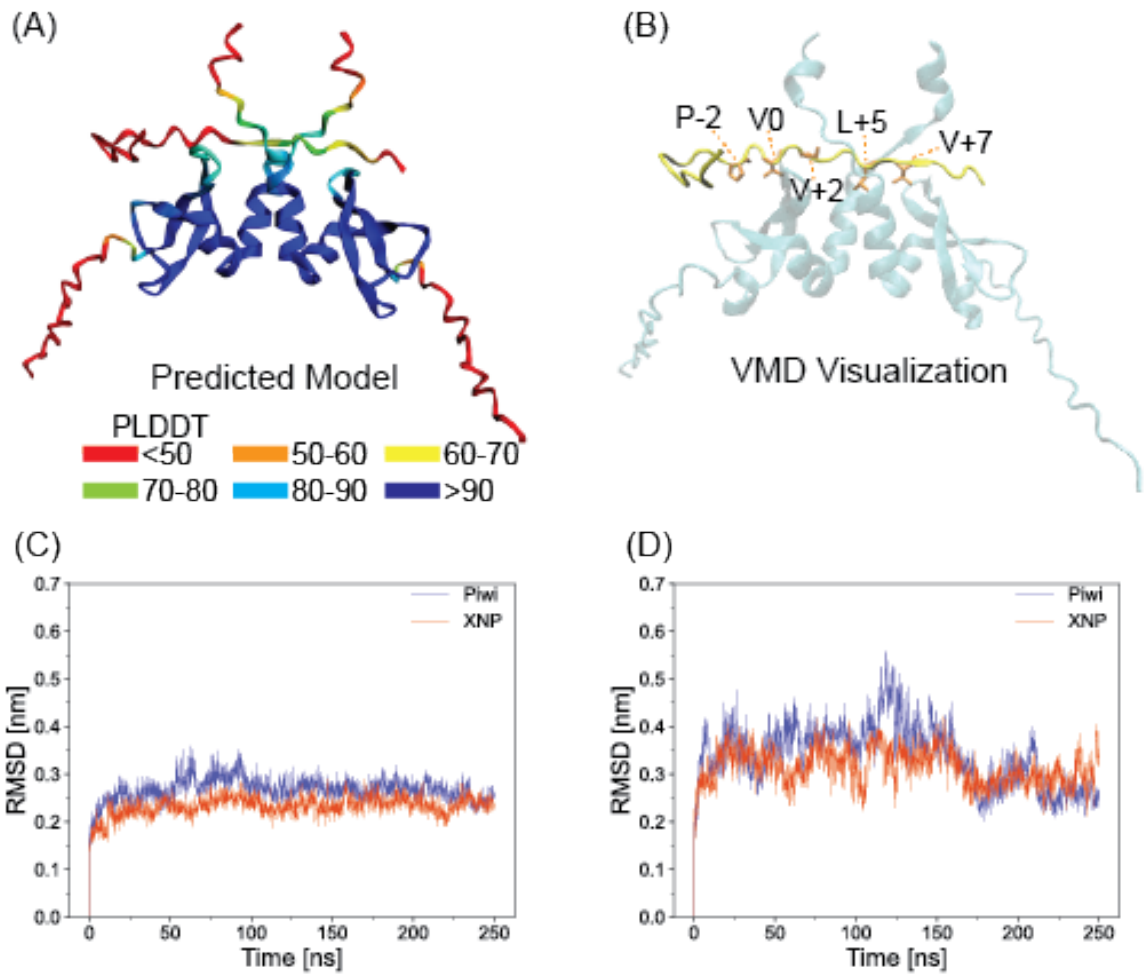

Supplementary Method Figure 1: (A) The Alphafold Multimer-predicted computational model and (B) visualized image of the model for the CSD dimer with C-terminal tails and Odj-1. The Alphafold Multimer-predicted structure is colored based on pLDDT (predicted local distance difference test) scores. Red: pLDDT<50, Orange: 50<pLDDT<60, Yellow: 60<pLDDT<70, Green: 70<pLDDT<80, Skyblue: 80<pLDDT<90, and Blue: 90<pLDDT. CSD homodimer and the Odj-1 are colored cyan and yellow, respectively. Residues at the -2, 0, +2, +5, and +7 positions (in licorice drawing style) are colored orange, with the amino acid code indicated. (C and D) Root mean square deviation (RMSD) of (C) the HP1a CSD dimer (amino acids 141-201) in Piwi and XNP peptide models and (D) the HAC peptides of Piwi and XNP from -7 to +7 amino acids throughout the 250 ns simulations.

Molecular dynamics simulation

GROMACS 2020.4 software package (Pronk *et al.*, 2013; Abraham *et al.*, 2015; Páll *et al.*, 2015; Lindahl *et al.*, 2020) was used for the all-atom molecular dynamics (MD) simulation

1158 with the CHARMM36 force field (Best *et al.*, 2012; Huang and Alexander D MacKerell, 2013).
1159 The developed model of the HAC peptide and HP1a CSD dimer with C-terminal tails was
1160 inserted into a cube box (13*13*13 nm^3) with periodic boundary conditions applied in all three
1161 directions. The CHARMM-modified TIP3P water model was employed to solvate the system
1162 (Boonstra, Onck and van der Giessen, 2016). The sodium and chloride counter ions were added
1163 to the system to obtain the 150 mM concentration of NaCl, a condition where chromatin is
1164 known to be aggregated (Huang and Cole, 1984; Shakya *et al.*, 2020). Energy minimization
1165 was conducted for 50,000 steps with an energy tolerance of 1000 $kJ \cdot mol^{-1} nm^{-1}$ to eliminate no
1166 steric clashes and ensure proper geometry of the system. The target temperature and
1167 equilibration of the solvent and ions in the system were achieved by employing NVT
1168 (isothermal-isochoric) and NPT (isothermal-isobaric) ensembles, each for 5 ns with a time step
1169 of 1 fs, with V-rescale thermostat at a constant temperature of 298 K. The Parrinello-Rahman
1170 barostat was used during NPT ensembles to maintain a pressure of 1 atm. The damping
1171 parameters were set to 0.1 ps for the V-rescale thermostat and 2 ps for the Parrinello-Rahman
1172 barostat. The heavy atom's positions of the protein were constrained during NVT and NPT
1173 equilibration to prevent the additional variable of structural changes in the protein.
1174 Subsequently, protein relaxation was employed for 250 ns (with 2 fs time steps) as the product
1175 step without any position restraints in the equilibrated system. The MD simulations were
1176 performed using NVIDIA V100 SMX2 GPU at the San Diego Supercomputer Center. The
1177 particle mesh Ewald method was used for long-range electrostatic interactions. The 1.0 nm
1178 cutoff was used for short-range electrostatic and van der Waals interactions.
1179

1180 **Analysis of Molecular Dynamics Simulations**

1181 The trajectory files saved every 10 ps were used for the analyses. The HP1a CSD dimer (amino
1182 acids 141-201) in Piwi and XNP peptide models was stable throughout the 250 ns simulations
1183 (**Supplementary Method Figure 1C**). The HAC peptides of Piwi and XNP from -7 to +7
1184 amino acids reached a stable state after around 175 ns (**Supplementary Method Figure 1D**).
1185 Data from 200 ns to 250 ns after reaching the stable state was used for computational analysis.
1186 The simulation was visualized using VMD software (Humphrey, Dalke and Schulten, 1996).
1187 All analyzed results were plotted using Python.

1188 Root Mean Square Deviation (RMSD): RMSD of the HAC central pentamer from -2 to +2 for
1189 the last 50 ns was calculated using "gmx rms" GROMACS tool built-in function.

1190 Root Mean Square Fluctuation (RMSF): RMSF of the XNP and Piwi of 25-residue HAC
1191 sequences (-12 to +12) for the last 50 ns was calculated using "gmx rmsf" GROMACS tool
1192 built-in function. Averaged RMSF of the distal flanking 10 sequences (-12 to -8 and +8 to +12),
1193 nearby flanking 10 sequences (-7 to -3 and +3 to +7), and central 5 sequences (-2 to +2) for
1194 XNP and Piwi was calculated, respectively. Tukey test was employed to compare differences
1195 between multiple groups (p-values < 0.05).

1196 Hydrophobic and charge distribution: The hydrophilic and hydrophobic distribution and
1197 electrical charge distribution of the HP1a-interacting XNP regions were visualized using
1198 BIOVIA Discovery Studio (Dassault Systèmes, USA) (*Discovery Studio*, 2023).

1199 Hydrophilic surface area: The hydrophilic surface area of the HAC central pentamer (-2 to +2)
1200 and the pentamer with nearby flanking (-7 to +7) were computed for the last 50 ns of the MD
1201 simulations using "gmx sasa" GROMACS tool built-in function for oxygen and nitrogen
1202 atoms.

1203 Coulomb energy: The short-range Coulomb energy between the HAC peptide and HP1a CSD
1204 dimer with C-terminal tails with a 1.0 nm cutoff distance was calculated for the last 50 ns of
1205 the MD simulations using "gmx energy" GROMACS tool built-in function. The Coulomb
1206 energy for each individual residue was calculated in the same manner. The frequencies of the
1207 coulombic energy with kernel density estimation were plotted using Python.

1208 BIOVIA (*Discovery Studio*, 2023) visualization of hydrophilicity/hydrophobicity and surface
1209 charge distributions: The hydrophobicity on the peptide is derived from the Kyte-Doolittle
1210 scale. For the charge calculation, partial charges assigned to each surface atom are used. The
1211 algorithm details can be found in BIOVIO Discovery Studio (*Discovery Studio*, 2023).

1212 VMD (Humphrey, Dalke and Schulten, 1996) visualization of hydrogen bonds (H-bonds) and
1213 salt bridge interactions: H-bonds were colored in green when the distance between the possible
1214 acceptor (OH and NH groups) and donor (O and N atoms) pair was within 0.35 nm, and the
1215 angle between the hydrogen, oxygen, and nitrogen was below 30°. Salt bridge interactions were
1216 colored in orange when the distance between the side-chain carbonyl oxygen of Asp or Glu
1217 and the side-chain nitrogen atoms of Arg, Lys, or His is within 0.4 nm.

1218 2D molecular interaction map: The 2D molecular interactional map of XNP and HP1a CSD
1219 dimer with C-terminal tails was created using Adobe Illustrator (Adobe Inc., USA) (*Vector*
1220 *Graphics Software – Adobe Illustrator*, no date) based on the 2D diagrams for each residue
1221 analyzed by BIOVIA Discovery Studio (Dassault Systèmes, USA) (*Discovery Studio*, 2023).

1222

1223 **Acknowledgements:**
1224 Many thanks to members of the Karpen lab and Dr. Grace Y.C. Lee for their valuable feedback.

1225 We thank Dr. Ksenia V Krasileva and Dr. Daniil M. Prigozhint for their helpful discussion
1226 regarding AlphaFold-Multimer modeling, the Japan Student Services Organization (JASSO)
1227 Student Exchange Support Program (Graduate Scholarship for Degree Seeking Students), the
1228 SAITAMA GO GLOBAL STUDENT scholarship, and the Hearts To Humanity Eternal
1229 (H2H8) graduate research grant for supporting Shingo Tsukamoto's doctoral studies. This
1230 research used resources of the Advanced Cyberinfrastructure Coordination Ecosystem:
1231 Services & Support (ACCESS) super-computing facilities, supported by the National Science
1232 Foundation (NSF) Grant No. BIO230220. The Karpen lab is supported by the National
1233 Institutes of Health (R35GM139653).

1234

1235 **References.**

1236 Abraham, M.J. *et al.* (2015) 'GROMACS: High performance molecular simulations through
1237 multi-level parallelism from laptops to supercomputers', *SoftwareX*, 1–2, pp. 19–25. Available
1238 at: https://doi.org/10.1016/j.softx.2015.06.001.

1239 Alekseyenko, A.A. *et al.* (2014) 'Heterochromatin-associated interactions of Drosophila HP1a
1240 with dADD1, HIPP1, and repetitive RNAs', *Genes & Development*, 28(13), pp. 1445–1460.
1241 Available at: https://doi.org/10.1101/gad.241950.114.

1242 Badugu, R. *et al.* (2005) 'Mutations in the heterochromatin protein 1 (HP1) hinge domain
1243 affect HP1 protein interactions and chromosomal distribution', *Chromosoma*. Available at:
1244 https://doi.org/10.1007/s00412-004-0324-2.

1245 Banani, S.F. *et al.* (2017) 'Biomolecular condensates: organizers of cellular biochemistry',
1246 *Nature Reviews. Molecular Cell Biology*, 18(5), pp. 285–298. Available at:
1247 https://doi.org/10.1038/nrm.2017.7.

1248 Bannister, A.J. *et al.* (2001) 'Selective recognition of methylated lysine 9 on histone H3 by the
1249 HP1 chromo domain.', *Nature*. Available at: https://doi.org/10.1038/35065138.

1250 Bassett, A.R. *et al.* (2008) 'The chromatin remodelling factor dATRX is involved in
1251 heterochromatin formation', *PLoS ONE*. Available at:
1252 https://doi.org/10.1371/journal.pone.0002099.

Belyaeva, E.S. *et al.* (2006) 'DNA underreplication in intercalary heterochromatin regions in polytene chromosomes of Drosophila melanogaster correlates with the formation of partial chromosomal aberrations and ectopic pairing', *Chromosoma*. Available at: https://doi.org/10.1007/s00412-006-0063-7.

Best, R.B. *et al.* (2012) 'Optimization of the additive CHARMM all-atom protein force field targeting improved sampling of the backbone ϕ, ψ and side-chain $\chi(1)$ and $\chi(2)$ dihedral angles', *Journal of Chemical Theory and Computation*, 8(9), pp. 3257–3273. Available at: https://doi.org/10.1021/ct300400x.

Boonstra, S., Onck, P.R. and van der Giessen, E. (2016) 'CHARMM TIP3P Water Model Suppresses Peptide Folding by Solvating the Unfolded State', *The Journal of Physical Chemistry B*, 120(15), pp. 3692–3698. Available at: https://doi.org/10.1021/acs.jpcb.6b01316.

Brasher, S.V. *et al.* (2000) 'The structure of mouse HP1 suggests a unique mode of single peptide recognition by the shadow chromo domain dimer', *The EMBO journal*, 19(7), pp. 1587–1597. Available at: https://doi.org/10.1093/emboj/19.7.1587.

Brennecke, J. *et al.* (2007) 'Discrete small RNA-generating loci as master regulators of transposon activity in Drosophila', *Cell*, 128(6), pp. 1089–1103. Available at: https://doi.org/10.1016/j.cell.2007.01.043.

Brideau, N.J. and Barbash, D.A. (2011) 'Functional conservation of the Drosophila hybrid incompatibility gene Lhr', *BMC Evolutionary Biology*, 11(1), p. 57. Available at: https://doi.org/10.1186/1471-2148-11-57.

Brower-Toland, B. *et al.* (2007) 'Drosophila PIWI associates with chromatin and interacts directly with HP1a', *Genes & Development*, 21(18), pp. 2300–2311. Available at: https://doi.org/10.1101/gad.1564307.

Chiolo, I. *et al.* (2011) 'Double-Strand Breaks in Heterochromatin Move Outside of a Dynamic HP1a Domain to Complete Recombinational Repair', *Cell*. Available at: https://doi.org/10.1016/j.cell.2011.02.012.

Colmenares, S.U. *et al.* (2017) 'Drosophila Histone Demethylase KDM4A Has Enzymatic and Non-enzymatic Roles in Controlling Heterochromatin Integrity', *Developmental Cell*, 42(2), pp. 156-169.e5. Available at: https://doi.org/10.1016/j.devcel.2017.06.014.

Coustham, V. *et al.* (2006) 'The *C. elegans* HP1 homologue HPL-2 and the LIN-13 zinc finger protein form a complex implicated in vulval development', *Developmental Biology*, 297(2), pp. 308–322. Available at: https://doi.org/10.1016/j.ydbio.2006.04.474.

Czech, B. *et al.* (2008) 'An endogenous small interfering RNA pathway in Drosophila', *Nature*,

453(7196), p. 798. Available at: https://doi.org/10.1038/nature07007.

Dimitri, P. *et al.* (2003) 'Vital genes in the heterochromatin of chromosomes 2 and 3 of Drosophila melanogaster', *Genetica*.

Discovery Studio (2023) *Dassault Systèmes*. Available at: https://www.3ds.com/products/biovia/discovery-studio (Accessed: 23 October 2024).

Dronamraju, R. and Mason, J.M. (2009) 'Recognition of double strand breaks by a mutator protein (MU2) in Drosophila melanogaster', *PLoS Genet*. Available at: https://doi.org/10.1371/journal.pgen.1000473.

Dronamraju, R. and Mason, J.M. (2011) 'MU2 and HP1a regulate the recognition of double strand breaks in Drosophila melanogaster', *PLoS One*. Available at: https://doi.org/10.1371/journal.pone.0025439.

Dzubiella, J. and Hansen, J.-P. (2003) 'Reduction of the hydrophobic attraction between charged solutes in water', *The Journal of Chemical Physics*, 119(23), pp. 12049–12052. Available at: https://doi.org/10.1063/1.1632902.

Dzubiella, J. and Hansen, J.-P. (2004) 'Competition of hydrophobic and Coulombic interactions between nanosized solutes', *The Journal of Chemical Physics*, 121(11), pp. 5514–5530. Available at: https://doi.org/10.1063/1.1783274.

Eissenberg, J.C. *et al.* (1992) 'The heterochromatin-associated protein HP-1 is an essential protein in Drosophila with dosage-dependent effects on position-effect variegation', *Genetics*.

Evans, R. *et al.* (2022) 'Protein complex prediction with AlphaFold-Multimer'. bioRxiv, p. 2021.10.04.463034. Available at: https://doi.org/10.1101/2021.10.04.463034.

Her, C. *et al.* (2022) 'Molecular interactions underlying the phase separation of HP1 α : role of phosphorylation, ligand and nucleic acid binding', *Nucleic Acids Research*, 50(22), pp. 12702–12722. Available at: https://doi.org/10.1093/nar/gkac1194.

Holehouse, A.S. and Kragelund, B.B. (2024) 'The molecular basis for cellular function of intrinsically disordered protein regions', *Nature Reviews. Molecular Cell Biology*, 25(3), pp. 187–211. Available at: https://doi.org/10.1038/s41580-023-00673-0.

Honda, S. and Selker, E.U. (2008) 'Direct interaction between DNA methyltransferase DIM-2 and HP1 is required for DNA methylation in Neurospora crassa', *Molecular and Cellular Biology*, 28(19), pp. 6044–6055. Available at: https://doi.org/10.1128/MCB.00823-08.

Hoskins, R.A. *et al.* (2007) 'Sequence finishing and mapping of Drosophila melanogaster heterochromatin', *Science (New York, NY)*. Available at:

https://doi.org/10.1126/science.1139816.

Hsu, K.-L., Yen, H.-C.S. and Yeang, C.-H. (2022) 'Cooperative stability renders protein complex formation more robust and controllable', *Scientific Reports*, 12(1), p. 10490. Available at: https://doi.org/10.1038/s41598-022-14362-z.

Hsu, W.-L. *et al.* (2013) 'Exploring the binding diversity of intrinsically disordered proteins involved in one-to-many binding', *Protein Science: A Publication of the Protein Society*, 22(3), pp. 258–273. Available at: https://doi.org/10.1002/pro.2207.

Huang, H.C. and Cole, R.D. (1984) 'The distribution of H1 histone is nonuniform in chromatin and correlates with different degrees of condensation.', *Journal of Biological Chemistry*, 259(22), pp. 14237–14242. Available at: https://doi.org/10.1016/S0021-9258(18)89883-0.

Huang, J. and Alexander D MacKerell, J. (2013) 'CHARMM36 all-atom additive protein force field: Validation based on comparison to NMR data', *Journal of computational chemistry*, 34(25), p. 2135. Available at: https://doi.org/10.1002/jcc.23354.

Humphrey, W., Dalke, A. and Schulten, K. (1996) 'VMD: visual molecular dynamics', *Journal of Molecular Graphics*, 14(1), pp. 33–38, 27–28. Available at: https://doi.org/10.1016/0263-7855(96)00018-5.

Janssen, A., Colmenares, S.U. and Karpen, G.H. (2018) 'Heterochromatin: Guardian of the Genome', *Annual Review of Cell and Developmental Biology*, 34, pp. 265–288. Available at: https://doi.org/10.1146/annurev-cellbio-100617-062653.

Kasinathan, B. *et al.* (2020) 'Innovation of heterochromatin functions drives rapid evolution of essential ZAD-ZNF genes in Drosophila', *eLife*, 9, p. e63368. Available at: https://doi.org/10.7554/eLife.63368.

King, M.R. *et al.* (2024) 'Macromolecular condensation organizes nucleolar sub-phases to set up a pH gradient', *Cell*, 187(8), pp. 1889-1906.e24. Available at: https://doi.org/10.1016/j.cell.2024.02.029.

Kumar, S. and Nussinov, R. (2002) 'Close-Range Electrostatic Interactions in Proteins', *ChemBioChem*, 3(7), pp. 604–617. Available at: https://doi.org/10.1002/1439-7633(20020703)3:7<604::AID-CBIC604>3.0.CO;2-X.

Kyte, J. and Doolittle, R.F. (1982) 'A simple method for displaying the hydropathic character of a protein', *Journal of Molecular Biology*, 157(1), pp. 105–132. Available at: https://doi.org/10.1016/0022-2836(82)90515-0.

Lachner, M. *et al.* (2001) 'Methylation of histone H3 lysine 9 creates a binding site for HP1

proteins.', *Nature*. Available at: https://doi.org/10.1038/35065132.

Larson, A.G. *et al.* (2017) 'Liquid droplet formation by HP1alpha suggests a role for phase separation in heterochromatin', *Nature*. Available at: https://doi.org/10.1038/nature22822.

Lechner, M.S. *et al.* (2005) 'The mammalian heterochromatin protein 1 binds diverse nuclear proteins through a common motif that targets the chromoshadow domain', *Biochemical and Biophysical Research Communications*, 331(4), pp. 929–937. Available at: https://doi.org/10.1016/j.bbrc.2005.04.016.

Li, X. *et al.* (1999) 'Predicting Protein Disorder for N-, C-, and Internal Regions', *Genome Informatics. Workshop on Genome Informatics*, 10, pp. 30–40.

Lin, C.-H. *et al.* (2008) 'Heterochromatin protein 1a stimulates histone H3 lysine 36 demethylation by the Drosophila KDM4A demethylase', *Molecular Cell*. Available at: https://doi.org/10.1016/j.molcel.2008.11.008.

Lindahl *et al.* (2020) 'GROMACS 2020 Manual'. Available at: https://doi.org/10.5281/zenodo.3562512.

Liu, H. and Naismith, J.H. (2008) 'An efficient one-step site-directed deletion, insertion, single and multiple-site plasmid mutagenesis protocol', *BMC Biotechnology*, 8(1), p. 91. Available at: https://doi.org/10.1186/1472-6750-8-91.

Liu, Y. *et al.* (2017) 'Peptide recognition by heterochromatin protein 1 (HP1) chromoshadow domains revisited: Plasticity in the pseudosymmetric histone binding site of human HP1', *Journal of Biological Chemistry*, 292(14), pp. 5655–5664. Available at: https://doi.org/10.1074/jbc.M116.768374.

Madeira, F. *et al.* (2024) 'The EMBL-EBI Job Dispatcher sequence analysis tools framework in 2024', *Nucleic acids research*, 52(W1), pp. W521–W525. Available at: https://doi.org/10.1093/nar/gkae241.

Makunin, I.V. *et al.* (2002) 'The Drosophila suppressor of underreplication protein binds to late-replicating regions of polytene chromosomes', *Genetics*.

Marr, S.K. *et al.* (2014) 'The Metazoan-Specific Mediator Subunit 26 (Med26) Is Essential for Viability and Is Found at both Active Genes and Pericentric Heterochromatin in Drosophila melanogaster', *Molecular and Cellular Biology*, 34(14), pp. 2710–2720. Available at: https://doi.org/10.1128/MCB.01365-13.

Mendez, D.L. *et al.* (2011) 'The HP1a disordered C terminus and chromo shadow domain cooperate to select target peptide partners', *Chembiochem: A European Journal of Chemical Biology*, 12(7), pp. 1084–1096. Available at: https://doi.org/10.1002/cbic.201000598.

Mendez, D.L., Mandt, R.E. and Elgin, S.C.R. (2013) 'Heterochromatin Protein 1a (HP1a) partner specificity is determined by critical amino acids in the chromo shadow domain and C-terminal extension', *The Journal of Biological Chemistry*, 288(31), pp. 22315–22323. Available at: https://doi.org/10.1074/jbc.M113.468413.

Meyer-Nava, S. *et al.* (2020) 'Insights into HP1a-Chromatin Interactions', *Cells*, 9(8), p. 1866. Available at: https://doi.org/10.3390/cells9081866.

Muchardt, C. *et al.* (2002) 'Coordinated methyl and RNA binding is required for heterochromatin localization of mammalian HP1alpha.', *EMBO reports*. Available at: https://doi.org/10.1093/embo-reports/kvf194.

Müller, M.M. *et al.* (2016) 'A two-state activation mechanism controls the histone methyltransferase Suv39h1', *Nature Chemical Biology*, 12(3), pp. 188–193. Available at: https://doi.org/10.1038/nchembio.2008.

Páll, S. *et al.* (2015) 'Tackling Exascale Software Challenges in Molecular Dynamics Simulations with GROMACS', in S. Markidis and E. Laure (eds) *Solving Software Challenges for Exascale*. Cham: Springer International Publishing (Lecture Notes in Computer Science), pp. 3–27. Available at: https://doi.org/10.1007/978-3-319-15976-8_1.

Perrin, L. *et al.* (1998) 'Dynamics of the sub-nuclear distribution of Modulo and the regulation of position-effect variegation by nucleolus in Drosophila.', *Journal of cell science*.

Pindyurin, A.V. *et al.* (2008) 'Interaction between the Drosophila heterochromatin proteins SUUR and HP1', *J Cell Sci*. Available at: https://doi.org/10.1242/jcs.018655.

Pronk, S. *et al.* (2013) 'GROMACS 4.5: a high-throughput and highly parallel open source molecular simulation toolkit', *Bioinformatics (Oxford, England)*, 29(7), pp. 845–854. Available at: https://doi.org/10.1093/bioinformatics/btt055.

Pylaeva, S., Brehm, M. and Sebastiani, D. (2018) 'Salt Bridge in Aqueous Solution: Strong Structural Motifs but Weak Enthalpic Effect', *Scientific Reports*, 8(1), p. 13626. Available at: https://doi.org/10.1038/s41598-018-31935-z.

Rajshekar, S. *et al.* (2023) 'Affinity hierarchies and amphiphilic proteins underlie the co-assembly of nucleolar and heterochromatin condensates', *bioRxiv: The Preprint Server for Biology*, p. 2023.07.06.547894. Available at: https://doi.org/10.1101/2023.07.06.547894.

Romero, P. *et al.* (2001) 'Sequence complexity of disordered protein', *Proteins: Structure, Function, and Bioinformatics*, 42(1), pp. 38–48. Available at: https://doi.org/10.1002/1097-0134(20010101)42:1<38::AID-PROT50>3.0.CO;2-3.

Schotta, G. *et al.* (2002) 'Central role of Drosophila SU(VAR)3-9 in histone H3-K9

methylation and heterochromatic gene silencing', *The EMBO journal*. Available at: https://doi.org/10.1093/emboj/21.5.1121.

Schwendemann, A. *et al.* (2008) 'Hip, an HP1-interacting protein, is a haplo- and triplo-suppressor of position effect variegation', *Proceedings of the National Academy of Sciences of the United States of America*, 105(1), pp. 204–209. Available at: https://doi.org/10.1073/pnas.0705595105.

Seller, C.A. and O'Farrell, P.H. (2018) 'Rif1 prolongs the embryonic S phase at the Drosophila mid-blastula transition', *PLoS biology*, 16(5), p. e2005687. Available at: https://doi.org/10.1371/journal.pbio.2005687.

Shaffer, C.D. *et al.* (2002) 'Heterochromatin protein 2 (HP2), a partner of HP1 in Drosophila heterochromatin', *Proceedings of the National Academy of Sciences of the United States of America*. Available at: https://doi.org/10.1073/pnas.212458899.

Shakya, A. *et al.* (2020) 'Liquid-Liquid Phase Separation of Histone Proteins in Cells: Role in Chromatin Organization', *Biophysical Journal*, 118(3), pp. 753–764. Available at: https://doi.org/10.1016/j.bpj.2019.12.022.

Smothers, J.F. and Henikoff, S. (2000) 'The HP1 chromo shadow domain binds a consensus peptide pentamer', *Current biology: CB*, 10(1), pp. 27–30. Available at: https://doi.org/10.1016/s0960-9822(99)00260-2.

Stephens, G.E. *et al.* (2005) 'Interaction of heterochromatin protein 2 with HP1 defines a novel HP1-binding domain', *Biochemistry*, 44(40), pp. 13394–13403. Available at: https://doi.org/10.1021/bi051006+.

Strom, A.R. *et al.* (2017) 'Phase separation drives heterochromatin domain formation', *Nature*. Available at: https://doi.org/10.1038/nature22989.

Swenson, J.M. *et al.* (2016) 'The composition and organization of Drosophila heterochromatin are heterogeneous and dynamic', *eLife*, 5, p. e16096. Available at: https://doi.org/10.7554/eLife.16096.

Thiru, A. *et al.* (2004) 'Structural basis of HP1/PXVXL motif peptide interactions and HP1 localisation to heterochromatin', *The EMBO journal*, 23(3), pp. 489–499. Available at: https://doi.org/10.1038/sj.emboj.7600088.

Vector Graphics Software – Adobe Illustrator (no date). Available at: https://www.adobe.com/products/illustrator.html (Accessed: 23 October 2024).

Wang, L., Friesner, R.A. and Berne, B.J. (2010) 'Competition of electrostatic and hydrophobic interactions between small hydrophobes and model enclosures', *The journal of physical*

chemistry. B, 114(21), pp. 7294–7301. Available at: https://doi.org/10.1021/jp100772w.

Wang, T. *et al.* (2012) 'Crystal Structure of the Human SUV39H1 Chromodomain and Its Recognition of Histone H3K9me2/3', *PLoS ONE*, 7(12), p. e52977. Available at: https://doi.org/10.1371/journal.pone.0052977.

Weiler, K.S. and Wakimoto, B.T. (1995) 'Heterochromatin and gene expression in Drosophila.', *Annual review of genetics*. Available at: https://doi.org/10.1146/annurev.ge.29.120195.003045.

Xie, N.-Z. *et al.* (2015) 'Exploring Strong Interactions in Proteins with Quantum Chemistry and Examples of Their Applications in Drug Design', *PLOS ONE*, 10(9), p. e0137113. Available at: https://doi.org/10.1371/journal.pone.0137113.

Yamada, T. *et al.* (2017) 'Drosophila Dalmatian combines sororin and shugoshin roles in establishment and protection of cohesion', *The EMBO journal*, 36(11), pp. 1513–1527. Available at: https://doi.org/10.15252/embj.201695607.

Zhou, H.-X. and Pang, X. (2018) 'Electrostatic Interactions in Protein Structure, Folding, Binding, and Condensation', *Chemical Reviews*, 118(4), pp. 1691–1741. Available at: https://doi.org/10.1021/acs.chemrev.7b00305.